NAVAL POSTGRADUATE SCHOOL

MONTEREY, CALIFORNIA

THESIS

AN EMPIRICAL STUDY OF A PIN FIN HEAT EXCHANGER IN LAMINAR AND TURBULENT FLOW

by

Jeffrey W. Summers
December 2003

Thesis Advisor: Ashok Gopinath

Approved for public release; distribution is unlimited

THIS PAGE INTENTIONALLY LEFT BLANK

REPORT DOCUMENTATION PAGE

Form Approved OMB No. 0704-0188

Public reporting burden for this collection of information is estimated to average 1 hour per response, including the time for reviewing instruction, searching existing data sources, gathering and maintaining the data needed, and completing and reviewing the collection of information. Send comments regarding this burden estimate or any other aspect of this collection of information, including suggestions for reducing this burden, to Washington headquarters Services, Directorate for Information Operations and Reports, 1215 Jefferson Davis Highway, Suite 1204, Arlington, VA 22202-4302, and to the Office of Management and Budget, Paperwork Reduction Project (0704-0188) Washington DC 20503.

1. AGENCY USE ONLY *(Leave blank)*	2. REPORT DATE December 2003	3. REPORT TYPE AND DATES COVERED Master's Thesis	
4. TITLE AND SUBTITLE: **An Empirical Study of a Pin Fin Heat Exchanger in Laminar and Turbulent Flow**			**5. FUNDING NUMBERS**
6. AUTHOR(S) Jeffrey W. Summers			
7. PERFORMING ORGANIZATION NAME(S) AND ADDRESS(ES) Naval Postgraduate School Monterey, CA 93943-5000			**8. PERFORMING ORGANIZATION REPORT NUMBER**
9. SPONSORING /MONITORING AGENCY NAME(S) AND ADDRESS(ES) Naval Air Systems Command Patuxent River, MD			**10. SPONSORING/MONITORING AGENCY REPORT NUMBER**
11. SUPPLEMENTARY NOTES The views expressed in this thesis are those of the author and do not reflect the official policy or position of the Department of Defense or the U.S. Government.			
12a. DISTRIBUTION / AVAILABILITY STATEMENT Approved for public release; distribution is unlimited			**12b. DISTRIBUTION CODE**

ABSTRACT *(maximum 200 words)*

This study concentrates on the empirical characterization of a staggered array pin fin compact heat exchanger placed in a modular, rectangular wind tunnel. A full analysis of the heat transfer and pressure drop behavior was conducted on various pin-fin shapes, sizes, and configurations. The study was based on airflow over a range of low Reynolds numbers in the laminar and low turbulent flow, as well as higher turbulent flow regimes. The empirical data gathered can be used to corroborate and develop better numerical models to characterize the performance of such compact heat exchangers.

14. SUBJECT TERMS compact heat exchanger, experimental study, pin-fin array			**15. NUMBER OF PAGES** 121
			16. PRICE CODE
17. SECURITY CLASSIFICATION OF REPORT Unclassified	**18. SECURITY CLASSIFICATION OF THIS PAGE** Unclassified	**19. SECURITY CLASSIFICATION OF ABSTRACT** Unclassified	**20. LIMITATION OF ABSTRACT** UL

NSN 7540-01-280-5500

Standard Form 298 (Rev. 2-89)
Prescribed by ANSI Std. 239-18

i

THIS PAGE INTENTIONALLY LEFT BLANK

AN EMPIRICAL STUDY OF A PIN FIN HEAT EXCHANGER IN LAMINAR AND TURBULENT FLOW

Jeffrey W. Summers
Lieutenant, United States Navy
B.S.H.R.M., New School University, 1994

Submitted in partial fulfillment of the
requirements for the degree of

MASTER OF SCIENCE IN MECHANICAL ENGINEERING

from the

**NAVAL POSTGRADUATE SCHOOL
December 2003**

Author: Jeffrey W. Summers

Approved by: Ashok Gopinath
                                 Thesis Advisor

                                 Anthony J. Healey
                                 Chairman, Department of Mechanical Engineering

THIS PAGE INTENTIONALLY LEFT BLANK

ABSTRACT

This study concentrates on the empirical characterization of a staggered array pin fin compact heat exchanger placed in a modular, rectangular wind tunnel. A full analysis of the heat transfer and pressure drop behavior was conducted on various pin-fin shapes, sizes, and configurations. The study was based on airflow over a range of low Reynolds numbers in the laminar and low turbulent flow, as well as higher turbulent flow regimes. The empirical data gathered can be used to corroborate and develop better numerical models to characterize the performance of such compact heat exchangers.

THIS PAGE INTENTIONALLY LEFT BLANK

TABLE OF CONTENTS

LIST OF FIGURES

THIS PAGE INTENTIONALLY LEFT BLANK

LIST OF TABLES

THIS PAGE INTENTIONALLY LEFT BLANK

ACKNOWLEDGMENT

THIS PAGE INTENTIONALLY LEFT BLANK

I.   INTRODUCTION

Compact heat exchangers have been widely studied and have numerous applications such as gas turbine blade cooling and microelectronics.   A common heat exchanger design for these types of applications consists of a short pin fin staggered array assembly. It is time consuming and expensive to design, develop and test just one type of pin fin arrangement. The solution is to develop an accurate numerical model that can optimize a pin fin arrangement to save time and resources. However a numerical model can only be proven against reliable empirical data.

Ramthun (2003) designed and built a rectangular shaped, short pin-fin compact heat exchanger consisting of ten rows. The main purpose of the test assembly was to validate numerical models. Initial testing showed that results from the compact heat exchanger correlated well with 3-D numerical models constructed by Hamilton (2003) and Boulares (2003).

The motivation of this thesis is to expand the experimental database of the staggered array pin fin compact heat exchanger designed by Ramthun. A full analysis of heat transfer and pressure drop characteristics for various pin shapes, sizes and configurations will be explored in both the laminar and turbulent flow regions. With the expansion of the empirical database more accurate numerical models will be developed to include all ranges of flow. This will lead to enhanced optimization for the design and development of future micro heat exchangers.

THIS PAGE INTENTIONALLY LEFT BLANK

II.   BACKGROUND AND OBJECTIVES

A.   BACKGROUND DISCUSSION

The heat transfer area per unit volume determines if a heat exchanger is compact. Shah and Kraus (1990) indicate that the heat transfer per unit volume needed to exceed $600 - 700$ m^2/m^3 to be considered compact. Along with the ratio stated above, a defining characteristic of compact heat exchangers is the pin height to diameter ratio (H/D). Long and short pins are commonly referred to in the literature, with short pins corresponding to H/D ratios of less than five. The CHE used in this research will consist of a short pin staggered array configuration.

The CHE is an important design for modern applications due to its smaller size and weight while providing an increased heat transfer rate per unit volume density. Extensive research in pin shape selection and placement has been conducted to optimize the compact heat exchanger. As technology advances it has become more time and cost efficient to build numerical computer models to represent a CHE. With the collection of empirical data from the past and present, numerical models can be refined and improved too further enhance the simulation of actual CHE conditions.

B.   PREVIOUS WORK

Research concerning compact heat exchanger began approximately thirty years ago with the two major pioneers being Van Fossen and Metzger. Van Fossen (1982) studied how the heat transfer coefficient varied over an array of four rows of pins. His work compared the heat transfer coefficients of short pins versus long pins. He concluded that the pin-fin heat transfer coefficient was 35% greater than the end wall. Sparrow, et al. in 1984, later verified this result. Van Fossen also showed that short pins do not perform similarly to long pins therefore calling for more research in the short pin-fin area. Metzger, et al. (1982) furthered the research by experimenting with a ten row staggered short pin-fin compact heat exchanger. Where Van Fossen took an overall approach Metzger compiled a row-by-row heat transfer coefficient analysis of the rectangular CHE. He mainly worked with H/D = 1.0, S/D =2.5, and X/D varying from 1.5 to 2.5. His results showed that heat transfer coefficients peaked within the first three

3

to five rows of the array as well as with the higher X/D ratio of 2.5. His results showed that heat transfer coefficients peaked within the first three to five rows of the array as well as with the higher X/D ratio of 2.5.

After the initial research Metzger, et al. (1984) researched the effects of varying pin geometry. The pins were oblong and orientated with the major axis parallel to the direction of flow. The results showed that the differential pressure and heat transfer rates were higher for the new oblong pin-fins. Earlier Metzger, et al. (1982) valued the difference between pin-fin heat transfer and end wall coefficients to be 10% however now updated the number to be closer to 50% higher for the pin surfaces. In 1984 Yao Peng completed further studies of heat transfer, differential pressure and friction loss for various pin-fin configurations. It was Arora (1989) that continued the analysis of various pin-fin geometrical shapes and arrangements. His research showed that with elliptical fins in rectangular channels the heat transfer rates were greater and the friction loss was smaller than associated circular pins. This advantage was only true if the pins were aligned perfectly in the stream wise flow direction.

Research conducted by Chyu (1989) and Chyu and Goldstein (1991) utilized a naphthalene sublimation mass transfer technique. Naphthalene sublimation measures the heat transfer of various points in a pin-fin array based on the erosion of the naphthalene. The fillets were accurate however produced the undesirable effects of higher differential pressures and lower heat transfer rates. The research was able to verify the row averaged heat transfer rates determined by Metzger, et al. (1982).

Al Dabagh, et al. (1992) evaluated the difference between pin surface and end wall heat transfer coefficients and determined that the end wall coefficients were 50% higher. This contradicted the previous work by Van Fossen (1982) and Metzger, et al. (1982, 1984). Chyu, et al. (1999) analyzed the discrepancy and determined that the heat transfer coefficient for the pin surfaces was 10 to 20 percent greater than the end wall. This supported the earlier work by Van Fossen.

Jubran, et al. (1993) and Tahat, et al. (1994) concentrated on the optimal pin-fin configuration that would give the maximum heat transfer rate per unit area. The first found that the optimum configuration for all flows tested was X/D =2.5 and S/D = 2.5.

The data, however, was attained from a long pin-fin array (H/D =9.5). The second team also used a long pin-fin array (9.5) and came up with the optimal configuration of X/D = 1.23 and S/D between 0.16 and 0.48. The way the heat exchanger was setup coupled with the long pin-fin geometry makes comparison to earlier work by Van Fossen (1982) and Metzger, et al. (1982, 1984) difficult.

Qingling, et al. (1997) performed research that was able to confirm much of the research conducted in the 1980's. In rectangular channels the heat transfer rates increased and the differential pressure decreased for the elliptical pins as compared to equivalent cylindrical pins. Also noted was that the elliptical pins had a reduced Nusselt number. In the following year Chen, et al. (1998) and Li, et al. (1998) conducted research in reference to drop-shaped and elliptical pin-fin arrays respectively. The results were desirable and similar to Qingling, et al. (1997) showing an increase in heat transfer rates while reducing differential pressure as compared to circular pin-fin configurations. O'Brien, et al. (2001) continued the research of changing pin shapes. He experimented with a finned-tube heat exchanger that incorporated oval tubes and delta winglets that served as vortex generators.

With the advancement in computer technology numerical modeling became a useful tool in the design of compact heat exchangers. Shah, et al. (2001) was instrumental in the incorporation of computer modeling to more efficiently design compact heat exchangers. Donahoo, et al (2001) used numerical models to optimize a 2-D staggered pin-fin array. The model showed that the maximum heat transfer did occur between rows four and five. This result agreed with Metzger, et al. (1982). The numerical model showed evidence of increased fluid velocity between the pins and wall. The model also provided a detailed row-by-row analysis that demonstrated actual flow patterns and the effectiveness of each row. The 2-D model was promising however did not account for the height of the flow passage. A 3-D model would be needed.

Adametz (2002) developed a 3-D numerical model to simulate the heat transfer and differential pressure characteristics in a rectangular, staggered short pin-fin array compact heat exchanger. The results showed fluid acceleration between the passage walls and neighboring pin-fins to be 5-6 times the inlet velocity. Adametz also found that the heat transfer coefficient of the end wall was 20-100% greater than that of the pin fins.

This supports Qingling, et al. (1997) while opposing results from earlier studies. He also found that the maximum heat transfer coefficient occurred at X/D = 1.5 and S/D between 1.75 and 2.0. Using Adametz' work along with the CHE Ramthun (2003) built Hamilton (2003) was able to successfully simulate the pin-fin staggered array compact heat exchanger with a 3-D numerical model and manipulate it to investigate a wide range of configurations and pin shapes. Errors for the heat transfer calculations were within 18% however the model had difficulties predicting friction factor.

Boulares (2003) used a 3-D numerical model to simulate and evaluate the performance of a compact heat exchanger made of teardrop shaped pin fins. The pin spacing was varied in the span wise and stream wise directions to determine the optimum configuration. The arrangement that gave the highest heat transfer for a certain pressure drop was X/D = 1.5 and S/D = 1.5. The teardrop shaped pins displayed enhanced heat transfer characteristics as compared to circular pin-fins due to the delay of flow separation off of the pin surface. As with Hamilton (2003) numerical and experimental friction factors did not agree.

C. OBJECTIVES

Numerical models are an efficient means for the development, testing and analysis of various pin-fin shapes and configurations to optimize compact heat exchangers. However it is imperative that numerical results be corroborated with empirical data. To achieve this goal a laboratory scale CHE has been built with the following objectives in mind:

1. **Obtain Extensive Empirical Data Regarding Various Pin-Fin Geometries. Pin-Fin Geometries Will Include:**

   a. 10, 16.5, 33, and 66 mm circular pins.

   b. Teardrop shaped pins.

2. **Obtain Empirical Data Concerning Various Configurations. Configurations Will Include:**

   a. Full ten-row analysis with no missing pins.

   b. Pins removed to double X/D and leave S/D unchanged.

   c. Pins removed to double S/D and leave X/D unchanged.

d.   Pins removed to double X/D and S/D.

e.   H/D will change as pin geometry changes.

3.   **Quantify The Heat Transfer Characteristics And Perform A Differential Pressure Analysis For The Various Pin Shapes And Configurations Mentioned Above.**

4.   **Validate 3-D Numerical Models While Providing Evidence That Correlations Based On Hydraulic Diameter Allow An Extension Of The Data To Include Micro-Scale Heat Exchangers.**

5.   **To Determine Optimal Pin-Fin Array Configurations Based On Suitably Defined Measures Of Heat Exchanger Effectiveness.**

THIS PAGE INTENTIONALLY LEFT BLANK

III. EXPERIMENTAL SETUP

A. OVERVIEW

The original design (figure 1) by Ramthun (2003) was a wind tunnel that provided a fully developed, turbulent velocity profile entering a heat transfer section. The compact heat exchanger and inlet ducting were rectangular with the downstream piping being circular. A blower drew air through the system and bypass valves were positioned down stream of the CHE to control flow. With the expansion of the system to include laminar and low turbulent flow regions certain conversions had to be performed. A new throttle valve was added to the inlet of the system to accurately control flow for experiments in the low turbulent region. With the smaller flow rates associated with the lower turbulent region leak detection and removal were extremely important. This required minor alterations to the inlet section and compact heat exchanger. Also associated with lower turbulent flow regions were significant changes in CHE exit pressure and differential pressure. This resulted in the addition of two manometers to cover the various pressure ranges achieved. For testing in the laminar flow range the system setup was similar to figure (1) except a new mass flow meter and throttle valve were installed in place of the turbine airflow meter shown.
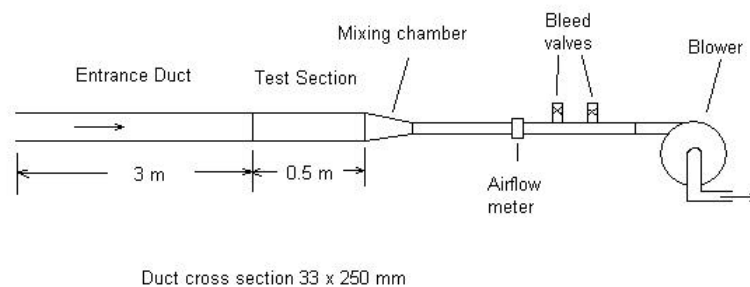
Figure 1.   Original design of test apparatus

B. SYSTEM COMPONENTS
1. Inlet Section

The inlet section was designed to accommodate both laminar and turbulent flow conditions. It had to be flexible to shift through the varying flow regimes. Reynold's numbers in the range of 10 – 50 thousand defined the upper turbulent flow region and

9

Reynold's numbers in the range of 100 – 2000 define the laminar flow region. For experiments in these two regions the inlet (Figure 2) section was rectangular and comprised of half-inch thick Plexiglas. Plexiglas was chosen for it's smooth surface minimizing friction and thermal losses. The inlet section was modular and measured three meters in length. The length was sufficient to produce either a turbulent or laminar velocity profile. The ducting was rectangular (33 mm x 250 mm) to provide a smooth transition to the heat transfer section. Reynold's numbers between three and ten thousand defined the lower turbulent flow region. For this region an air manifold (Figure 3) was designed to provide an air source at five points to the inlet. The goal was to avoid a point source for air into the inlet duct. The idea was later abandoned due to the large pressure drop associated with the device. The higher differential pressure led to increased system leakage.
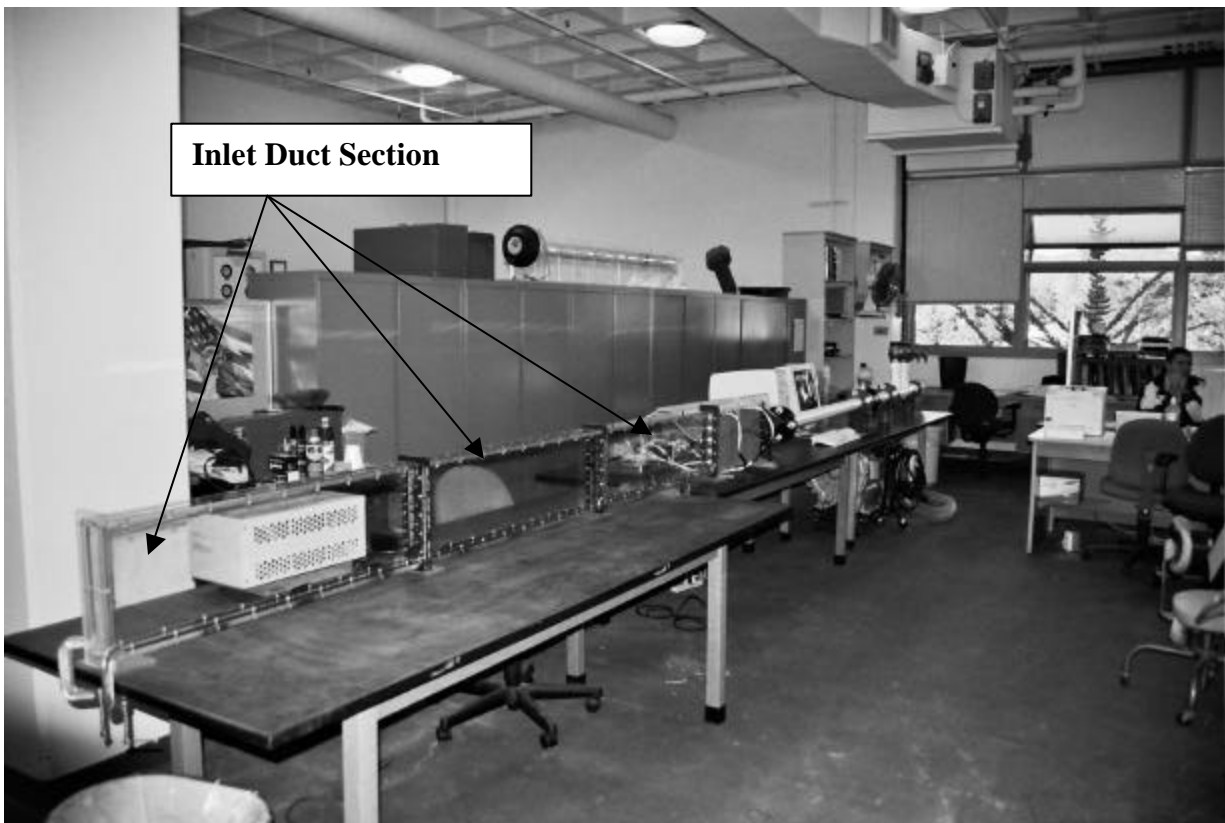
Figure 2.   Inlet duct section for laminar and upper turbulent flow

Figure 3.   Air manifold section

Figure (4) shows the actual inlet section used for testing in the lower turbulent flow region. An air throttle valve controls the amount of air entering the system. The throttle valve and transition ducting were connected using 0.5 inch, outside diameter, piping. The transition ducting was connected to the inlet by eight spring-compressed clamps (figure 5). The compression springs along with a rubber gasket were designed to prevent system leakage.
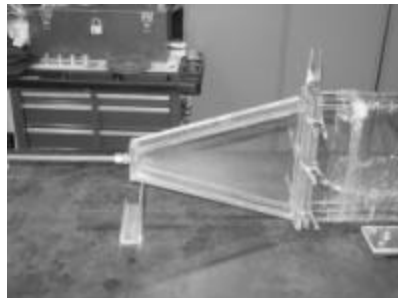
Figure 4.   Inlet section for lower turbulent flow region

11
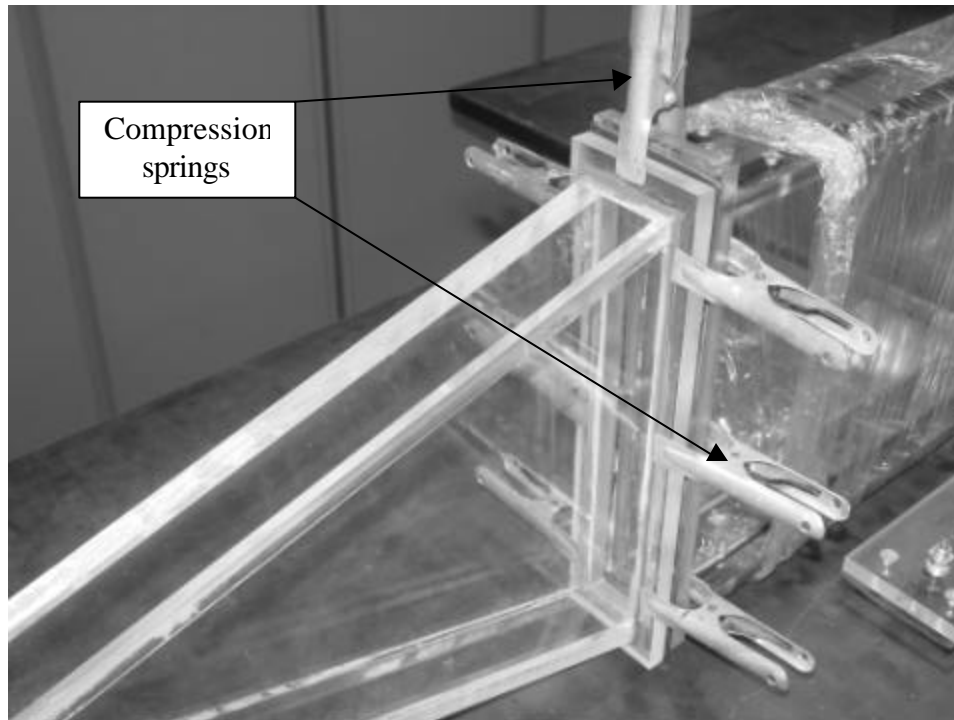
Figure 5.   Inlet transition connection

2.   Heat Transfer Test Section

The test section (Figure 6) was comprised of ten separate rows pin-fins and heating elements. Each row consisted of two corrosion resistant 6061 T6 aluminum plates measuring 12 mm x 50 mm. Between the plates inter-changeable aluminum pin-fins were mounted. One 50-watt heating element and one type E thermocouple was mounted on each aluminum plate (Figure 7) to provide a system heat input (1000 watt maximum) and temperature control.   Each row was physically and thermally isolated from one other by 1 mm Plexiglas strips. Neoprene seals were utilized around the perimeter of each aluminum plate to prevent air leakage. The top and bottom sidewalls of the section were also made of Plexiglas, which provided a smooth, adiabatic surface. The original sidewalls were slightly modified to increase strength and minimize leakage. This was done by increasing the width from 85-110 mm and removing the beveled portion of the sidewall (Figure 8).

10-row staggered pin fin array compact heat exchanger
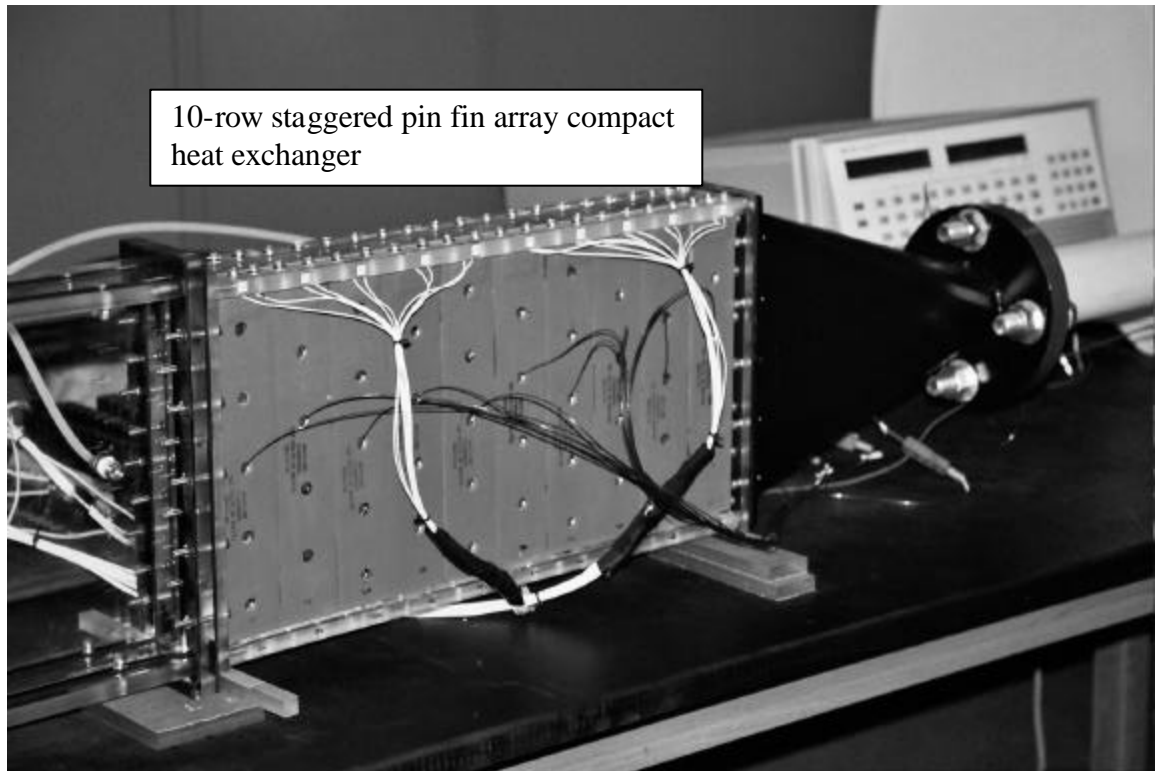
Figure 6. Heat transfer test section
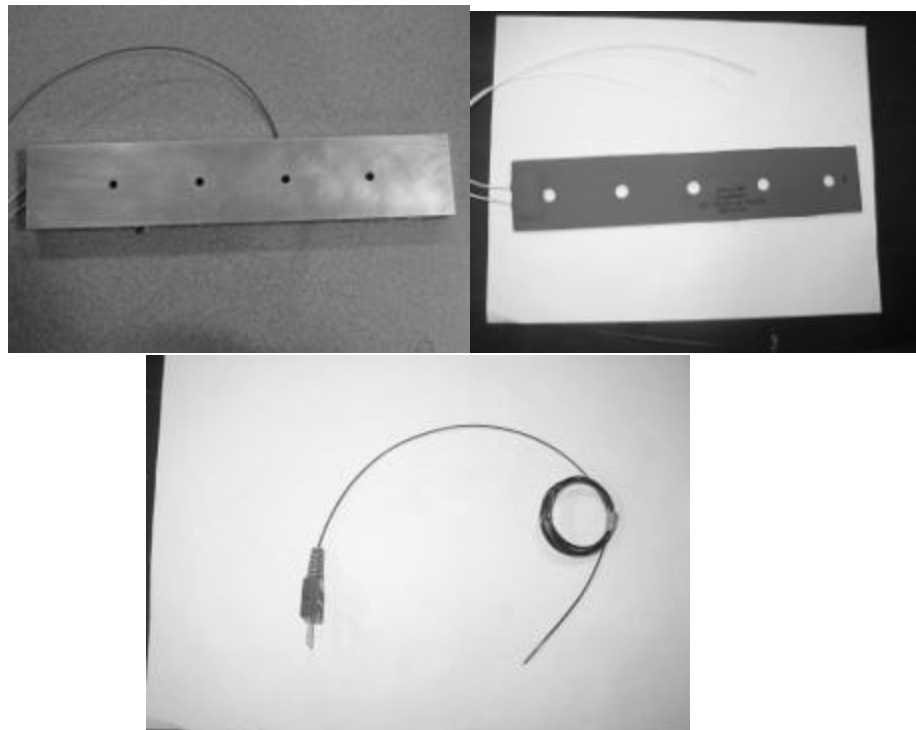
Figure 7. Aluminum base plate, heating element and type E thermocouple
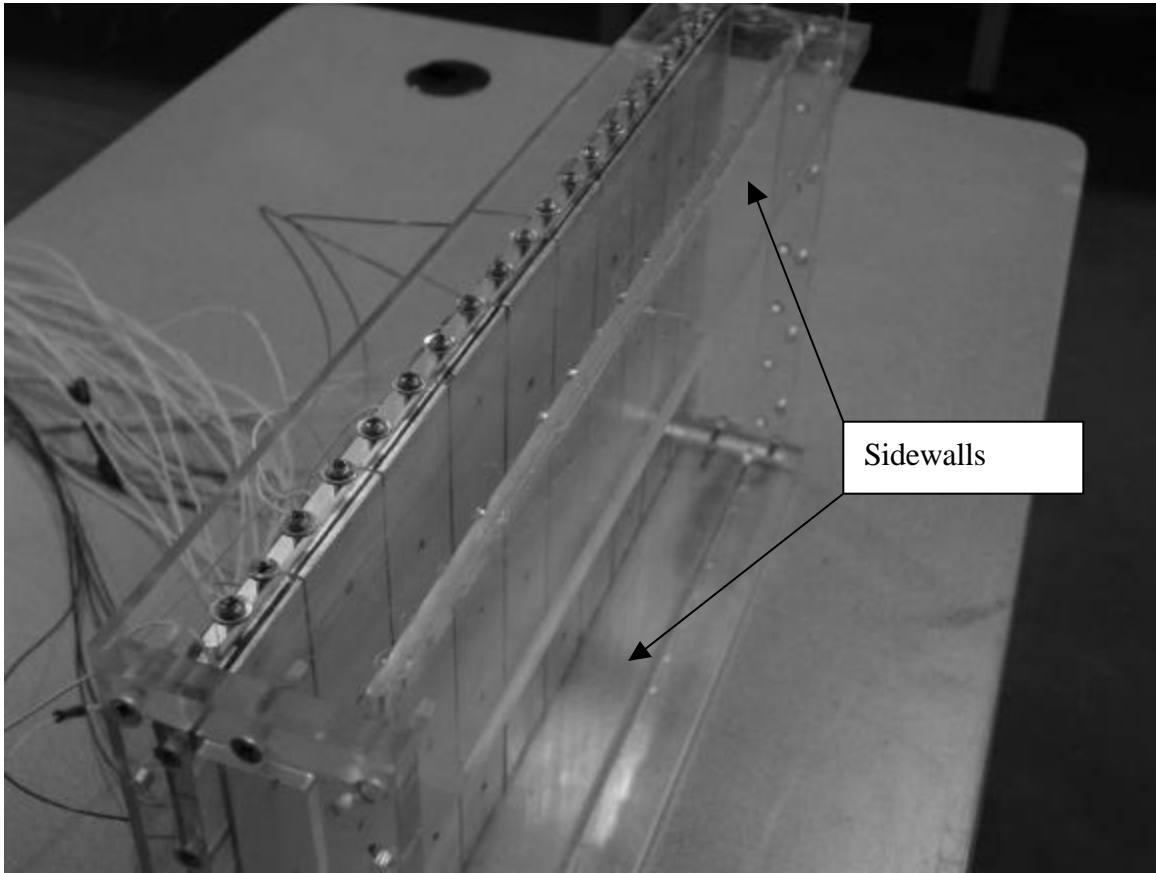
Figure 8.   Sidewall of heat transfer section

3.   Compact Heat Exchanger Pin-Fins

As discussed earlier the pin-fins were mounted between the two aluminum plates of the test section. As with the base plates, the pins were constructed of the same corrosion resistant aluminum. The geometry of the pins varied including four different cylindrical shapes and a teardrop design. The four cylindrical pin (Figure 9) diameters were 10 mm, 16.5 mm, 33 mm, and 66 mm. The teardrop (Figure 10) shape was non-cylindrical however it was the same height as the cylindrical pins (33 mm).
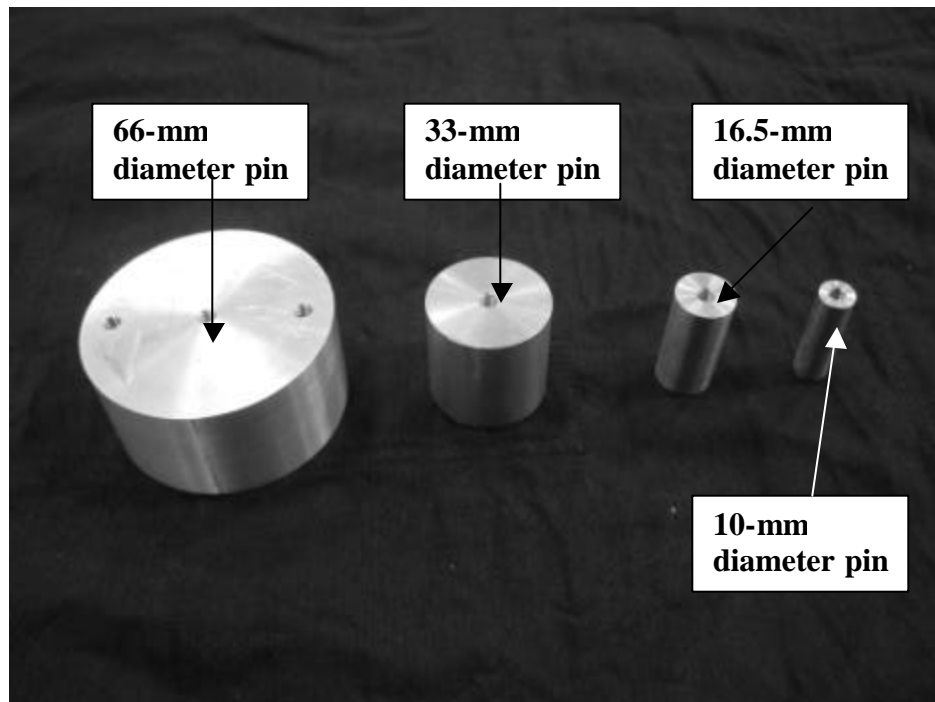
Figure 9.   Cylindrical shaped pin-fins
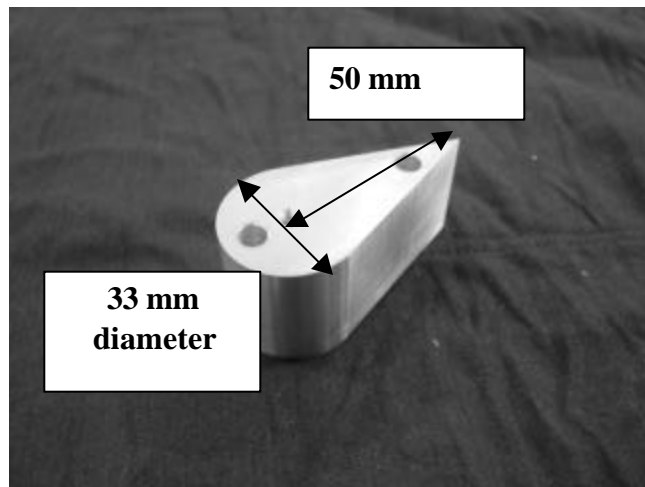
Figure 10.   Teardrop shaped pin fin

Various pins would have to be removed to accommodate the different S/D, X/D and H/D dimensions as defined in figure (11). For this research X/D, S/D, and H/D will vary from 1.5 – 20, 0.75-10, and 0.5-3.3 respectively. Non-fluted wooden dowel (figure 12) was used to block the holes in the plates due to the vacated pin and it's associated screw. The end of the dowel was smoothed by sandpaper and made flush with the airflow side of the plate to prevent any flow disruption. The wooden dowels were used

15

for their poor heat conduction characteristics as well as ease of insertion and removal while providing system airtight integrity.
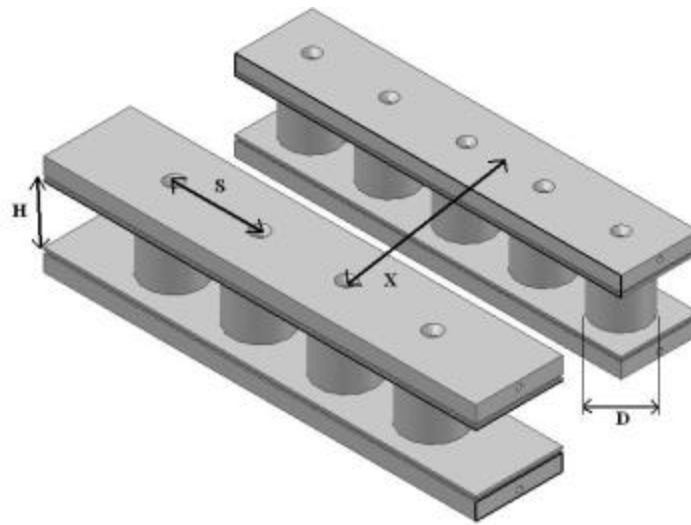
Figure 11.   Schematic of a staggered pin-fin array
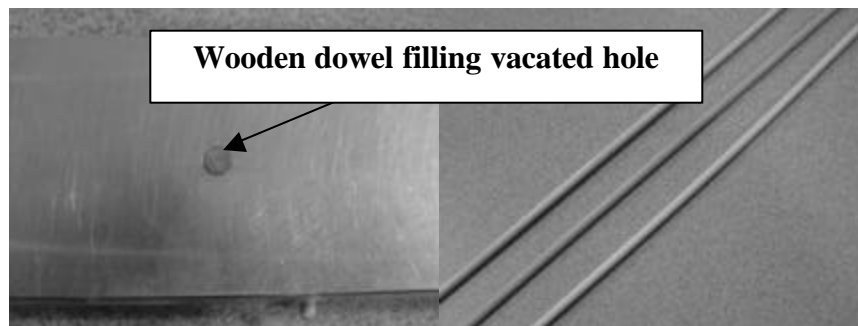
Figure 12.   Non-fluted wooden dowel

4.   Exit Duct

As with the inlet the exit duct had to be changed to accommodate the varying flow regions. For the upper and lower turbulent regions the exit duct consisted of a transition piece, turbine flow meter, bypass valves and blower. The transition piece (Figure 13) converted the rectangular shaped heat transfer section to the 2.5-inch exit piping. At this connection point four type E thermocouples were installed to measure the outlet temperature of the heat exchanger.   The thermocouples were installed in a staggered pattern (Figure 14) to give a thorough indication of temperature leaving the heat transfer section. The turbine flow meter or FTB-940 (Figure 15) exhibits linear

characteristics in its normal operating range of 21.4 – 468.7 ACFM. The transmitter portion of the flow meter converts frequency to a DC voltage output proportional to volumetric flow.
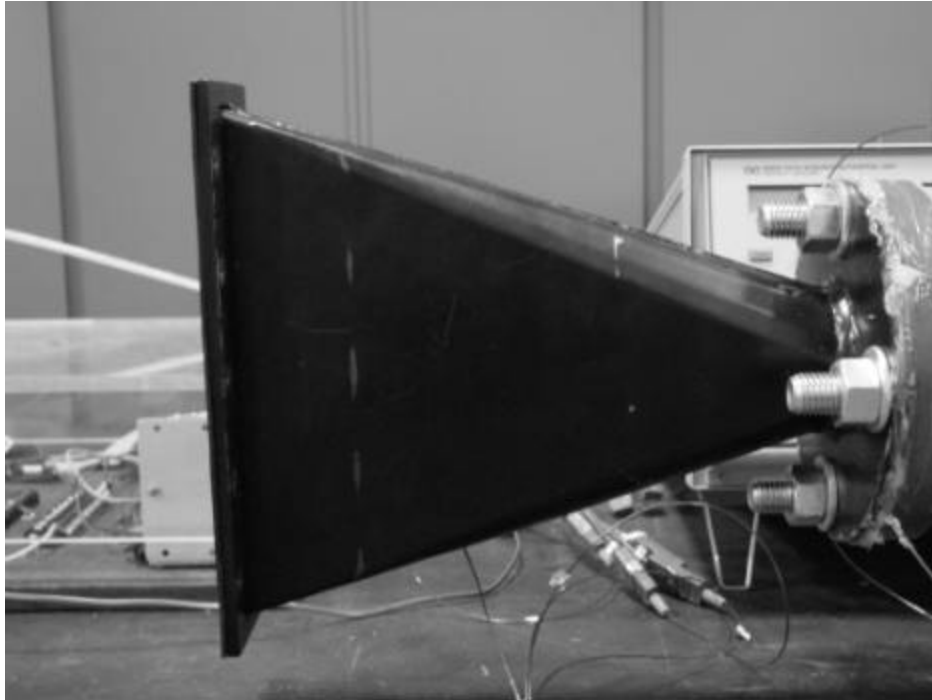
Figure 13.   Exit duct transition piece
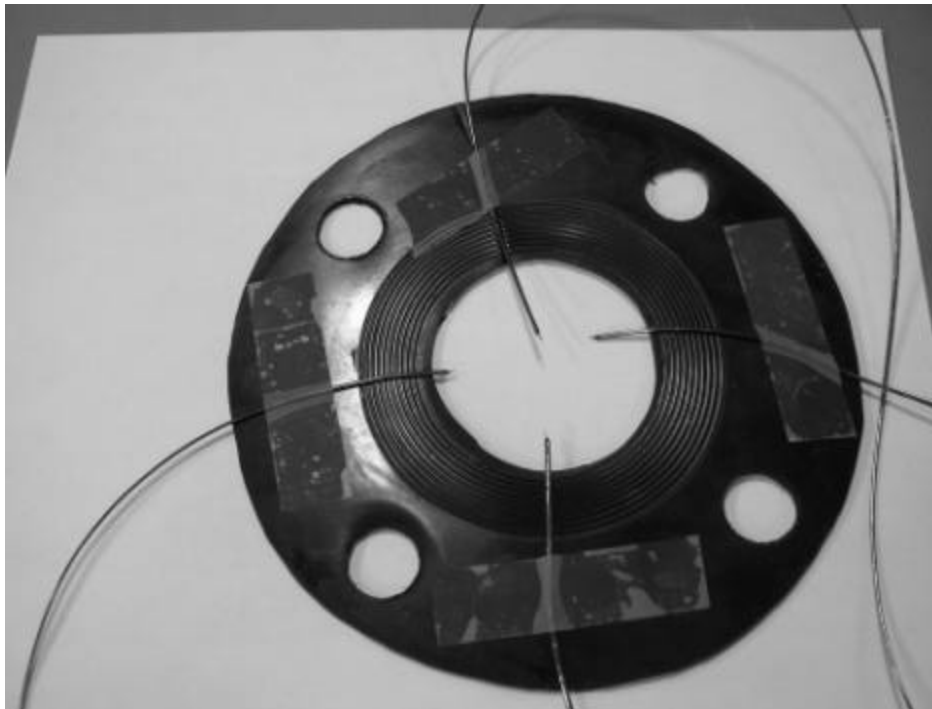
Figure 14.   Exit duct thermocouple arrangement

17
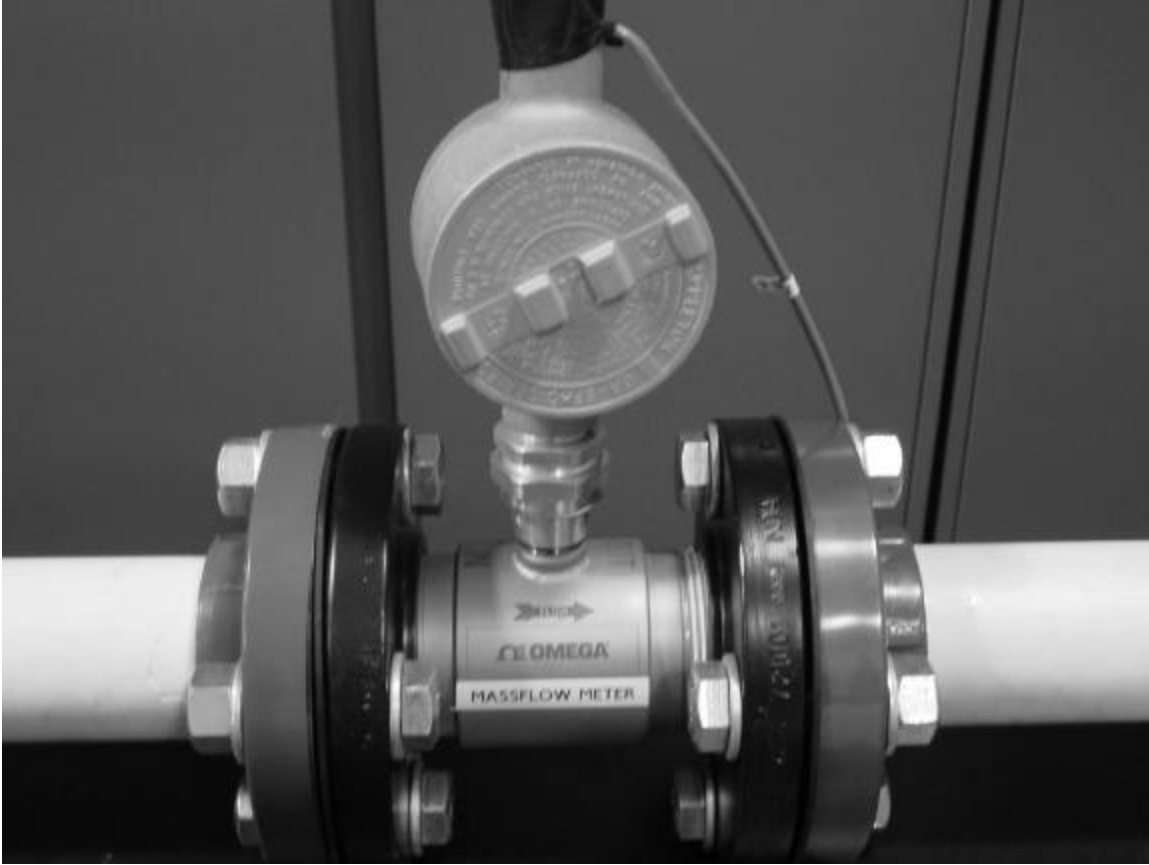
Figure 15.   Omega FTB-940 turbine flow meter

For laminar flow regions the turbine flow meter and supporting 2.5-inch ducting was removed and a new mass flow meter and throttle valve were installed. This was done to maintain a large opened inlet as well as minimize the pressure drop in the system to better minimize leakage. Figures (16) and (17) show the new setup to support laminar testing. The original rectangular to 2.5-inch diameter transition piece housing the four exit thermocouples remained unchanged. The new configuration has a four foot section of 2.5-inch diameter PVC piping followed by a 2.5-inch to 0.5-inch reduction section followed by 18 inches of 0.5 inch diameter PVC piping and 12 inches of 0.5 inch diameter stainless steel piping. The stainless steel piping was connected to a new mass flow meter, Omega model FMA-1844 (Figure 18). The new mass flow meter was required to accurately read the lower volumetric flow rates associated with laminar flow. The flow meter was selected for its accuracy, 1.5 percent of full scale, as well as its range. The range of the mass flow meter is 0-500 SLPM (0-17.657 ACFM) and was perfect for Reynold's numbers, based on hydraulic diameters, from 0 – 2000.

Exit duct transition
(2.5" PVC to 0.5"
PVC)

Exit duct transition
piece (rectangular to
2.5" PVC)
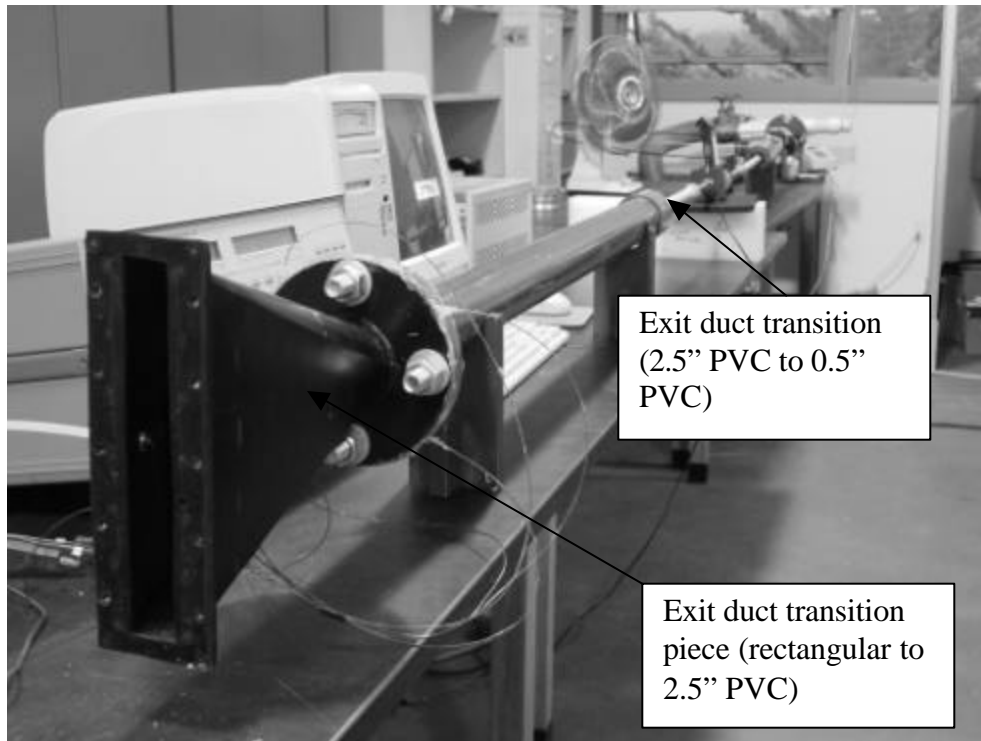
Figure 16.   Exit section for laminar flow

Throttle valve to control system
airflow
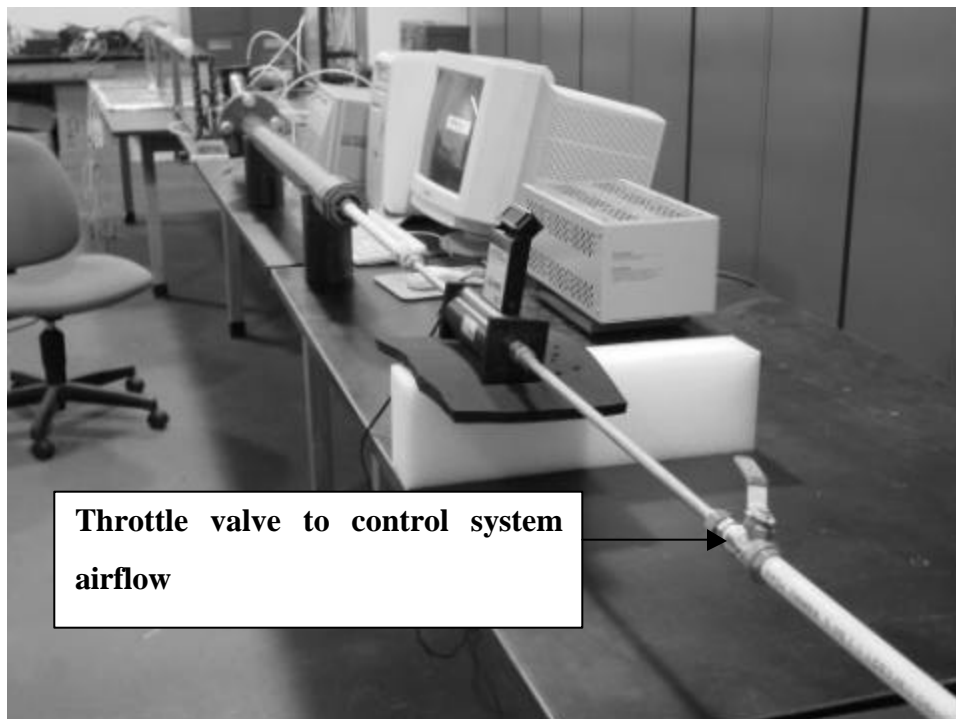
Figure 17.   Exit section for laminar flow

Figure 18.   Omega FMA-1844 mass flow meter

The three bypass valves (Figure 19) located in the exit duct were used to vary the flow rates for each flow region and eliminated the need for a variable speed blower. Two of the bypass valves were globe valves the last a simple capped end connection. The blower (Figure 20) was chosen based on an early differential pressure and turbulent flow analysis (Ramthun 2003). The blower was connected to draw air through the system based on inlet temperature monitoring concerns, cleanliness and most important to ensure a fully developed flow prior to the heat transfer section.

Figure 19.   Exit duct bypass valves

Figure 20.   System blower

5.   Monitoring Equipment

The experiments conducted in this research required monitoring equipment that could record a wide range of parameters. Twenty-five thermocouples, two manometers, one pressure transmitter and the two flow meters were used to collect data. Twenty of the thermocouples were used to monitor and control the cycling of the heaters for the heat transfer test section. There was one thermocouple designated for each heater installed. Of the remaining five thermocouples four were used, as discussed earlier, to measure heat exchanger outlet temperature.   The last thermocouple was used to measure heat exchanger inlet temperature.

Due to the various ranges of heat exchanger outlet pressure as well as heat exchanger differential pressure three different measuring devices were used. All three were chosen to provide some overlap for calibration and redundancy purposes. For small pressure values an inclined micro-manometer was used (Figure 21). The range for the manometer was zero to four inches of water readable in 0.001 increments. Another manometer (Figure 22) was chosen to cover a wide range of pressures ranging from zero to forty inches of water readable in 0.01 increments. The last pressure-monitoring device

21

was a pressure transmitter (Figure 23) that converted pressure to a DC voltage output. A digital power meter (Figure 24) was used to determine power delivered by the group of heaters. The power was compared to heat transfer calculations for reasons of accuracy and confidence.
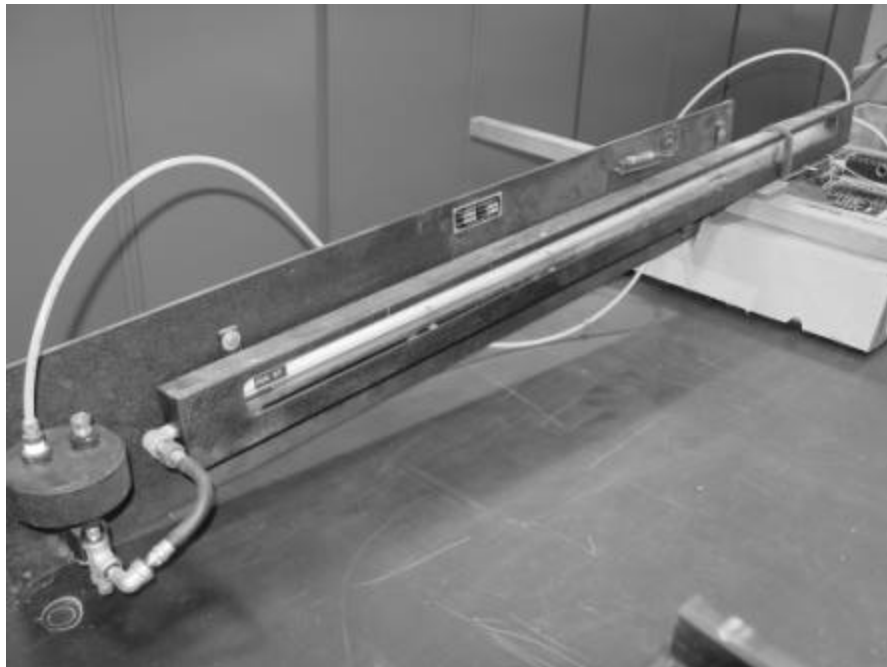
Figure 21.   0 – 4 inch inclined micro- manometer
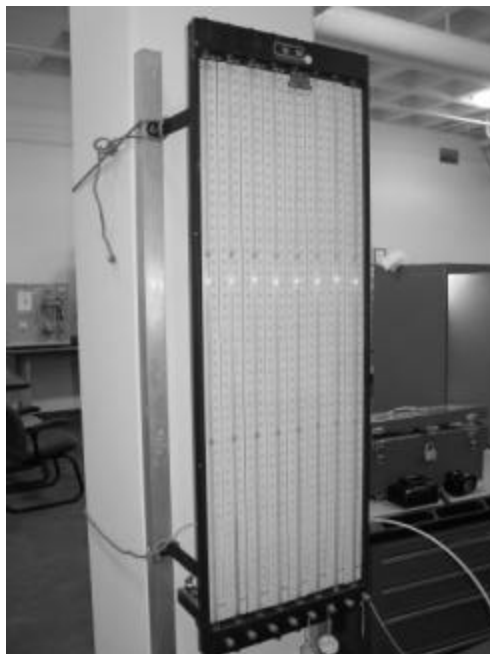
Figure 22.   0 – 50 inch vertical manometer

Figure 23.   Pressure transmitter (VDC)

Figure 24.   Digital power meter

The electronics board (Figure 25) housed the pressure transmitter as well as the relays used by the individual heater thermocouples to control temperature. A Hewlett Packard 3852A Data Acquisition/Control Unit (Figure 26) was used to record and deliver the thermocouple, turbine flow meter and pressure transmitter data to a computer program called LabVIEW written by National Instruments. LabVIEW cycles through each data channel provided by the HP 3852A and records the information in a Microsoft Excel file. The desired temperature of the system is controlled by user input to LabVIEW. The rate of channel cycling can be varied as well as graphical or numerical

monitoring of each channel's value.   The data captured by Excel could be analyzed manually or by MATLAB using the "XLSREAD" command.
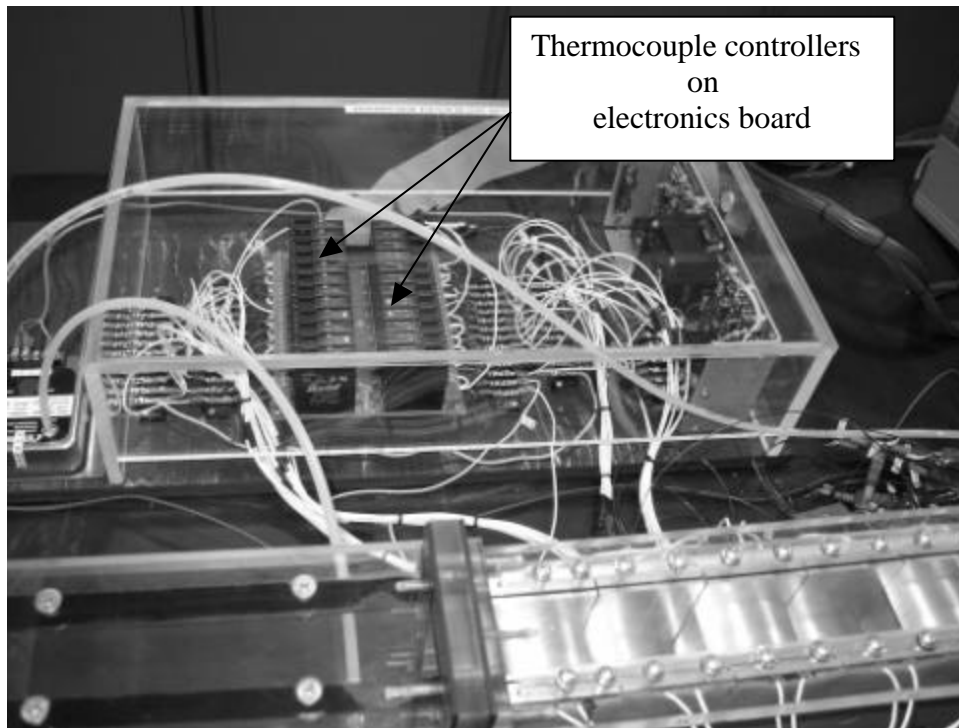
Figure 25.   Electronics Board

Figure 26.   HP 3852A Data Acquisition/Control Unit

IV.   EXPERIMENTAL TESTING

A.   TESTING PROCEDURE

1.   Test Matrix - Pin Configuration Table

Various pin sizes, shapes, and configurations were tested in multiple flow regions. Table (1) shows the four sets of data taken for each pin configuration based on S/D and X/D. H is fixed for the compact heat exchanger therefore H/D can only be varied by changing pin diameter. For set number one the compact heat exchanger has its full complement of 45-pins. For set number two 22 pins were removed to double S/D and stagger X/D. Set number three required the removal of 18 pins resulting in the doubling of X/D between two sets of rows while S/D remained the same. For set number four 20 pins were removed to double S/D and leave X/D the same. These four sets of data were performed on the 10mm, 16.5 mm, 33 mm, and teardrop pins. A minor adjustment was made for the teardrop pins. The tenth row had to be filled with 33 mm pins to prevent the teardrop pins from protruding into the exit ducting. The 66 mm pin experiments were conducted with set number one and three. Set number one involved 12 pins and set number three contained only six to double X/D and leave S/D unchanged. The 66 mm pins could not occupy the first or last rows due to the increased pin size. Appendix B contains pictures of each set.

Table 1.   Pin configuration table

	Set 1	Set 2	Set 3	Set 4
10 mm	S/D = 5.0 X/D = 5.0 H/D = 3.3	S/D = 10.0 X/D = 10.0 H/D = 3.3	S/D = 5.0 X/D = 10.0 H/D = 3.3	S/D = 10.0 X/D = 5.0 H/D = 3.3
16.5 mm	S/D = 3.0 X/D = 3.0 H/D = 2.0	S/D = 6.1 X/D = 6.0 H/D = 2.0	S/D = 3.0 X/D = 6.1 H/D = 2.0	S/D = 6.1 X/D = 3.0 H/D = 2.0
33 mm	S/D = 1.5 X/D = 1.5 H/D = 1.0	S/D = 3.0 X/D = 3.0 H/D = 1.0	S/D = 1.5 X/D = 3.0 H/D = 1.0	S/D = 3.0 X/D = 1.5 H/D = 1.0
66 mm	S/D = 1.89 X/D = 0.76 H/D = 0.5	Not Possible	S/D = 1.89 X/D = 1.5 H/D = 0.5	Not Possible
Tear Drop	S/D = 1.5 X/D = 1.5 H/D = 1.0	S/D = 3.0 X/D = 3.0 H/D = 1.0	S/D = 1.5 X/D = 3.0 H/D = 1.0	S/D = 3.0 X/D = 1.5 H/D = 1.0
Two configurations were completed with the 66mm pins. CHE cannot accommodate set number two or four. An empty run was completed with zero pins for baseline data.				

2. Test Matrix – Data Runs

A full data run was conducted for each set of each pin listed in table (1). Full data runs consisted of 15 sub-data runs that took twenty minutes each. Volumetric flow rate was increased for each time period to adequately cover the laminar, low turbulent and high turbulent regions. Table (2) shows that six of the sub-runs examined laminar flow while four covered the lower turbulent region and five the upper turbulent region. The only exception is that the teardrop data was performed in the laminar range only due to time constraints associated with thesis completion.

Table 2. Test Matrix – Typical full data run

Pin	Set	#1	#2	#3	#4	#5	#6	#7	#8	#9	#10	#11	#12	#13	#14	#15
Size	No.	L	L	L	L	L	L	LT	LT	LT	LT	UT	UT	UT	UT	UT
		Re = 100-2000						Re = 2500–10,000				Re = 10,000 – 50,000				
L = Laminar flow region LT = Lower turb. flow region UT = Upper turb. flow region																

B. PROCEDURE

1. Initial Setup

The first step was to physically prepare the system based on the type of flow desired. The experimental setup section of this paper explains the system layout and pin configuration was established per the table (1) test matrix. The next action was to prepare the system for operation. For laminar flow ranges the Omega FMA-1844 mass flow meter required a 15-minute warm-up period and was energized first. The circuit board, HP Data Acquisition Unit (HP3852) and heater power supply were started as well as the program LabVIEW. Microsoft's Excel program was setup to collect and analyze data.

Prior to drawing air through the system baseline or no-flow data was recorded. The differential pressure transmitter, two manometers, turbine flow meter (turbulent operations) and FMA-1844 mass flow meter (laminar operations) were all recorded prior to system initiation. Also, the National Oceanic and Atmospheric Administration (NOAA) provided the reference atmospheric pressure. After system startup these values were used as offset reference points to compare with experimental data. After these initial values were taken the heaters were energized to 12 degrees Kelvin greater than ambient. System response time had to be analyzed to ensure that the system was in steady state prior to collecting any data. From a cold start the normal system response

time for low flow conditions was approximately 30 minutes and for turbulent conditions 20 minutes. After starting, transition time from one flow setting to another decreased significantly. Times to reach a steady state condition were approximately three minutes for turbulent flow and approximately 5 minutes for laminar. Once the heat transfer section was in a steady state condition a 20-minute data sub-run was recorded. This was done to determine the losses of the heat transfer section with no airflow to be compared with heat transfer rate data obtained from future full data runs. The zero flow heat loss determination was completed before every full data run as described in table (2).

2.   Full Data Run

After collecting the required baseline data the blower was energized. Volumetric airflow was controlled based on which flow region was being tested. For laminar conditions the airflow was controlled by an inline throttle valve located downstream of the FMA-1844 mass flow meter as well as the three exit duct bypasses shown in figure (19). The valves were manipulated to obtain a desired reading on the FMA-1844's LCD display. For the six 20-minute data collection events the targeted volumetric flow rates were 25, 75, 125, 175, 225 and 275 SLPM respectively. In the lower turbulent region an inline throttle valve along with the exit duct bypasses controlled airflow. For the upper turbulent region the exit duct bypasses alone controlled airflow. In both turbulent cases flow was measured by the FTB-940 turbine flow meter. An attached transmitter (Omega FLSC-61) converted the turbine's output frequency to a VDC output. The output is sent to LabVIEW were it was monitored and recorded. Calibration data concerning flow meters and other equipment is located in appendix F.

Once the desired flow was obtained and the system reached a steady state operating condition, data was collected by pressing the record button in LabVIEW. During the recording period data was collected by both the operator and the computer program LabVIEW (figure 27). LabVIEW operates in cycles averaging approximately 8.35 seconds each. During each cycle LabVIEW records the value of each data point along with its time into an Excel file. After twenty minutes the recording was complete and the next desired flow rate was established. This process was repeated until all of the data for that pin set was obtained. The CHE was then disassembled and rebuilt with the new pin-fin shape and configuration and the process was started all over again.
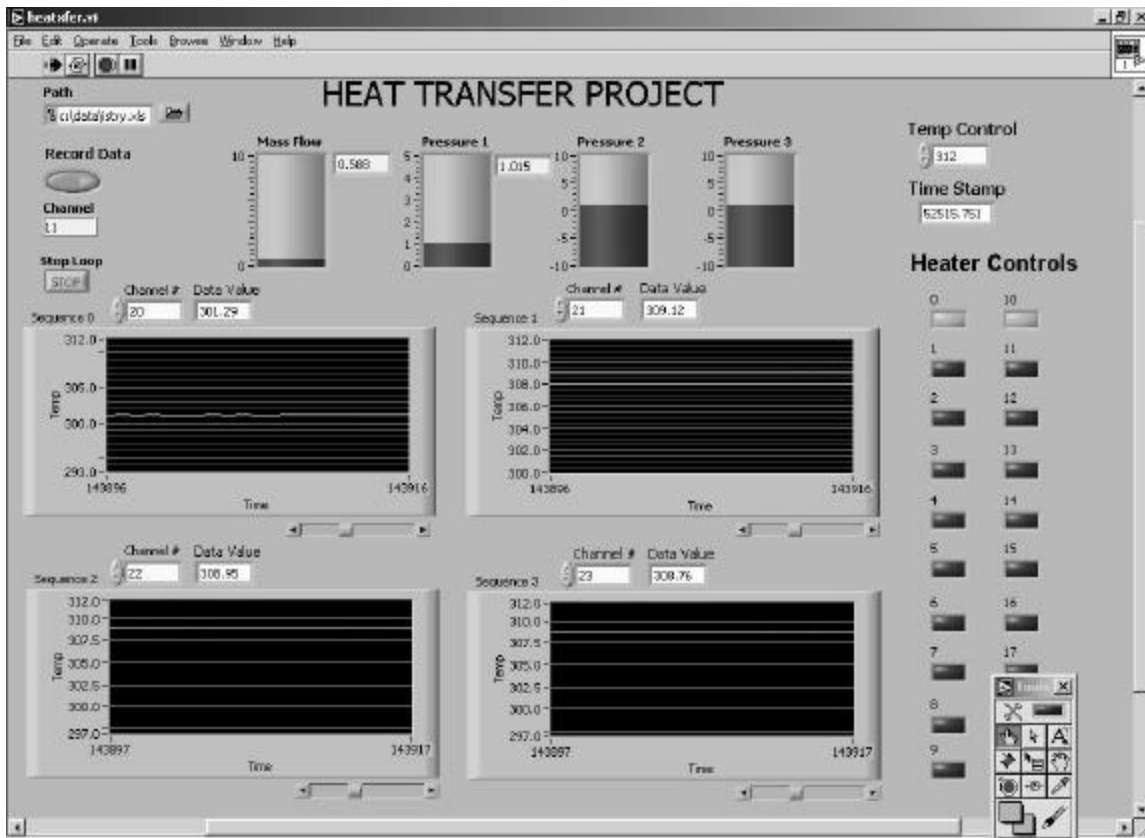
Figure 27.   LabVIEW control window

C.   DATA COLLECTION

Data collection was briefly explained during the baseline establishment discussion however table (3) shows in greater detail the various parameters monitored. Included are how the data was collected and what the information was used for. Appendix C shows the equations used for calculations and appendix A defines the nomenclature.

Table 3.   Data collection

Parameter	Data Collection Source	How Used
Individual heater temperatures, 0-19 (k)	LabVIEW channels 0-19 respectively	Row by row analysis of heat transfer rate, T_{wall}, ΔT_{lm}, h, and Nu_{Dh}
Inlet temperature (k)	LabVIEW channel 20	ΔT, ΔT_{lm}, q, h, and Nu_{Dh}.
Four outlet temperatures (k)	LabVIEW channels 21-24	ΔT, ΔT_{lm}, Hx exit density, f, viscosity, P_{turb}, $\dot{m}$, Re_{Dh}, q, h, Nu_{Dh}, and E.

28

Volumetric flow rate – Turbine flow meter (VDC)	LabVIEW channel 40	P_{turb}, f, $\bar{U}$, $\dot{m}$, Re_{Dh}, q, h, Nu_{Dh}, and E.
Differential pressure Transmitter (VDC) Turbulent regions only	LabVIEW channel 41	Hx dp, Hx exit density, f, P_{turb}, $\dot{m}$, Re_{Dh}, q, h, Nu_{Dh}, and E.
Total heater power output (watts)	Read directly from digital wattmeter	Total heater output - Compare with q for each sub-run.
Manometer 0-40 inches water	Read directly off manometer	Hx dp, Hx exit density, f, P_{turb}, $\dot{m}$, Re_{Dh}, q, h, Nu_{Dh}, and E.
Manometer 0-4 inches water	Read directly off manometer	Hx dp, Hx exit density, f, P_{turb}, $\dot{m}$, Re_{Dh}, q, h, Nu_{Dh}, and E.
FMA-1844 gas mass flow meter (SLPM) Laminar region only	Read directly off meter	P_{turb}, f, $\bar{U}$, $\dot{m}$, Re_{Dh}, q, h, Nu_{Dh}, and E.
Atmospheric pressure Inches of mercury	www.noaa.com	Reference pressure compared with manometer and pressure transmitter values.
Thermocouple bistable	LabVIEW records when heater is on or off	LabVIEW gives value of 1 for on and 0 for off for each sub-run. Used to determine how many heaters were on each sub-run to calculate q (electric).
Time stamp (seconds)	LabVIEW records time for each data point	Every data point from LabVIEW received a time stamp. Used to calculate q (electric).
Pin diameter (D)	Recorded by data taker	X/D, S/D, V_{open}, A_{wf}, A_{wh}, D_h, and A_{duct}.
Number of pins	Recorded by data taker	V_{open}, A_{wf}, A_{wh}, and D_h.
Value of X in flow direction	Recorded by data taker	X/D determination.

Value of S in span wise direction	Recorded by data taker	S/D determination
LabVIEW Channels 25-39, 42, 43 are reserved for future use.		

D. DATA ANALYSIS

The main goal of data collection is to be as accurate as possible. This involved using multiple pressure monitoring devices as well as calibrated flow meters and thermocouples. System leakage detection and removal was paramount for accurate heat transfer and differential pressure analysis. Calculated heat transfer rates were compared with the digital wattmeter monitoring total heater input. Any deviation greater than 15% required an investigation and the data to be retaken. A typical sub-run could generate approximately 2,600 data points in an Excel file. Usually there were no anomalies in the data collection phase however data scatter did occur. The amount of data scatter was rare however LabVIEW could generate erroneous data into the Excel file. This required review of all the data and statistical analysis to ensure that any errors were found and eliminated. An uncertainty analysis was performed and is located in Appendix D.

V.   RESULTS AND DISCUSSION

A.   INTRODUCTION

The first two objectives emphasized the attainment of empirical data regarding various pin-fin geometries and configurations. The goals were met and will be presented in both the laminar and turbulent flow regions. The third objective was to quantify the empirical data collected and perform a detailed analysis of heat transfer and pressure drop characteristics of a short pin-fin staggered array compact heat exchanger. The Nusselt number and heat transfer coefficient will be the main heat transfer characteristics discussed.   This will include the comparison of these values to various Reynolds numbers. With the ultimate goal being the maximum heat transfer with the minimal pressure drop, a differential pressure analysis will also be conducted by comparing friction factors to various Reynolds numbers. To meet the fourth objective the data collected was compared with previously developed numerical models. The last goal is to determine the optimal pin-fin array configuration by comparing the heat transfer coefficient to fluid friction power expenditure.

All research was conducted on the premise that both Reynolds and Nusselt numbers are based on hydraulic diameter. The hydraulic diameter is an important length scale that characterizes the entire compact heat exchanger. Therefore results non-dimensionalized with respect to hydraulic diameter are valid over all length scales. This allows the study to be conducted at both the macro and micro level.   Appendix C contains the equations used for calculations. Table (1) is re-introduced as table (4) to aid in the reading of this section's graphs.

Table 4.   Pin configuration table

	Set 1	Set 2	Set 3	Set 4
10 mm	S/D = 5.0 X/D = 5.0 H/D = 3.3	S/D = 10.0 X/D = 10.0 H/D = 3.3	S/D = 5.0 X/D = 10.0 H/D = 3.3	S/D = 10.0 X/D = 5.0 H/D = 3.3
16.5 mm	S/D = 3.0 X/D = 3.0 H/D = 2.0	S/D = 6.1 X/D = 6.0 H/D = 2.0	S/D = 3.0 X/D = 6.1 H/D = 2.0	S/D = 6.1 X/D = 3.0 H/D = 2.0
33 mm	S/D = 1.5 X/D = 1.5 H/D = 1.0	S/D = 3.0 X/D = 3.0 H/D = 1.0	S/D = 1.5 X/D = 3.0 H/D = 1.0	S/D = 3.0 X/D = 1.5 H/D = 1.0
66 mm	S/D = 1.89 X/D = 0.76 H/D = 0.5	Not Possible	S/D = 1.89 X/D = 1.5 H/D = 0.5	Not Possible
Tear Drop	S/D = 1.5 X/D = 1.5 H/D = 1.0	S/D = 3.0 X/D = 3.0 H/D = 1.0	S/D = 1.5 X/D = 3.0 H/D = 1.0	S/D = 3.0 X/D = 1.5 H/D = 1.0
Two configurations were completed with the 66mm pins. CHE cannot accommodate 66 mm sets number two or four. An empty run was completed with zero pins for baseline data.				

B.   HEAT TRANSFER COEFFICIENT

1.   Laminar Region

The heat transfer coefficient was calculated based on the heat transfer wetted surface area as well as system heat transfer rate flow and bulk differential log mean temperature.   Figures (28-32) display the heat transfer coefficient versus Reynolds results for the different pins and configurations in the laminar flow region.
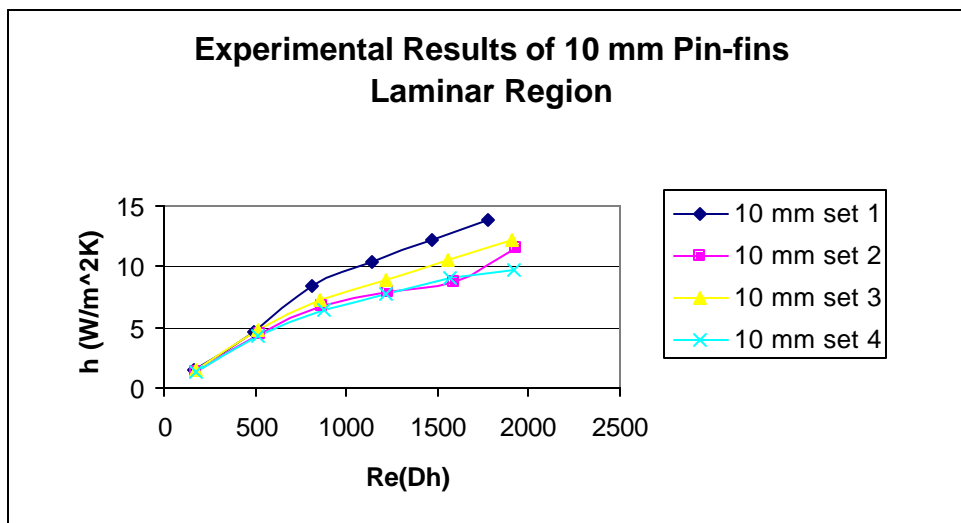
Figure 28.   Laminar 10 mm pin-fin experimental results, h vs. Re_{Dh}

32
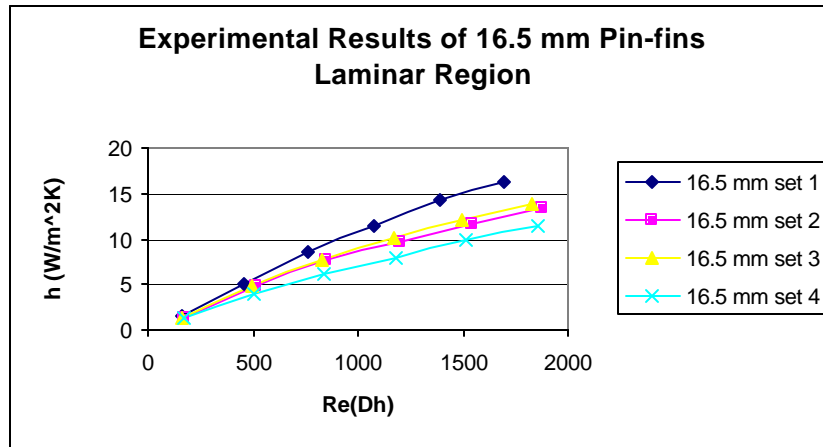
Figure 29.   Laminar 16.5 mm pin-fin experimental results, h vs. Re$_{Dh}$
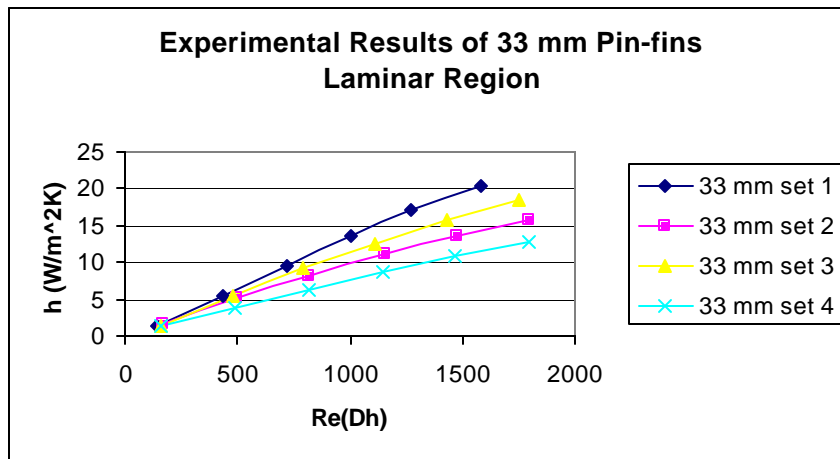
Figure 30.   Laminar 33 mm pin-fin experimental results, h vs. Re$_{Dh}$
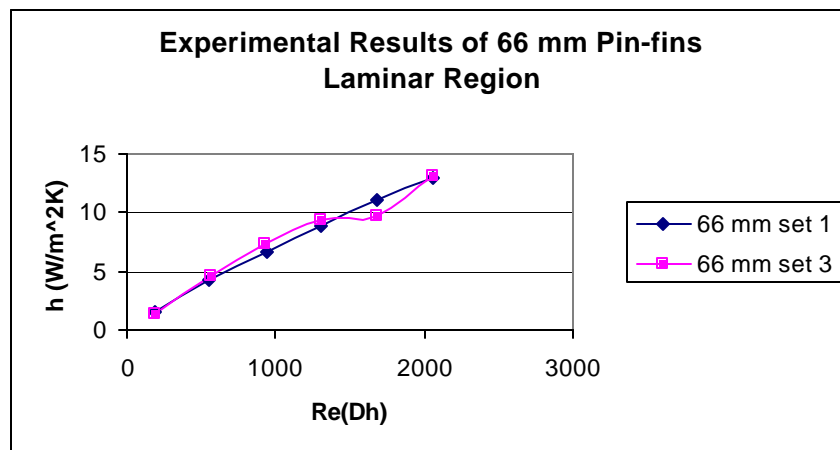
Figure 31.   Laminar 66 mm pin-fin experimental results, h vs. Re$_{Dh}$
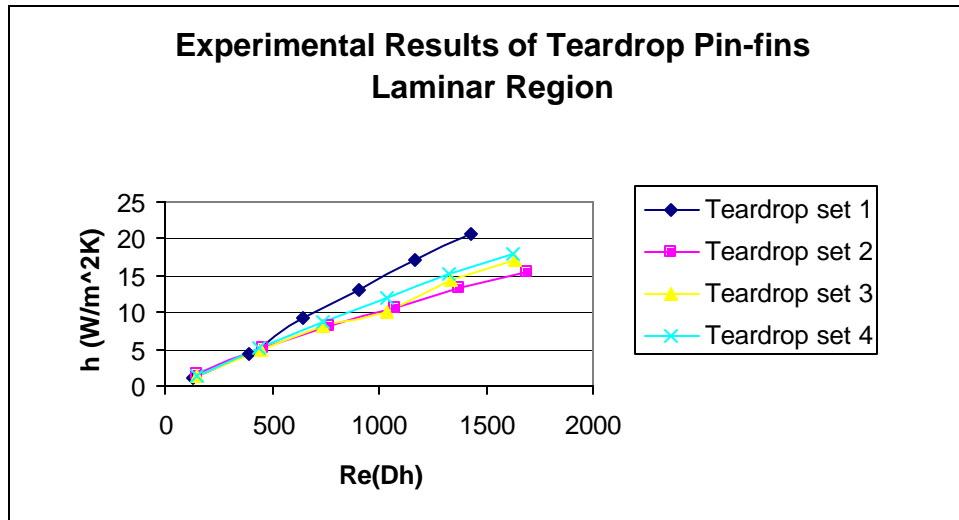
Figure 32.   Laminar teardrop pin-fin experimental results, h vs. Re_{Dh}

With the exception of the 66 mm pin-fins the set one configuration led to the highest heat transfer coefficient in each case. Set one had the full complement of pin-fins, which would give the maximum heat transfer rate therefore supporting the experimental results. The 66 mm pin-fin results showed that for both cases the heat transfer coefficient was relatively the same. This can be attributed to while doubling X/D the heat transfer wetted surface area decreased enough to offset the decrease in heat transfer rate.

Figure (33) shows the results of each leading pin-fin plotted together. The set one teardrop pin-fin displayed the highest heat transfer coefficient followed second by the set one 33 mm pin-fin.   From Re_{Dh} 500 – 1500 the teardrop set one configuration performed 5–8% better than the 33 mm pins.   The 66 mm pin-fins performed the worst.   The teardrop shaped pin performed the best due to its geometry. The geometry accounted for the rise in the heat transfer coefficient due to the increase in heat transfer area as well as minimizing flow separation.
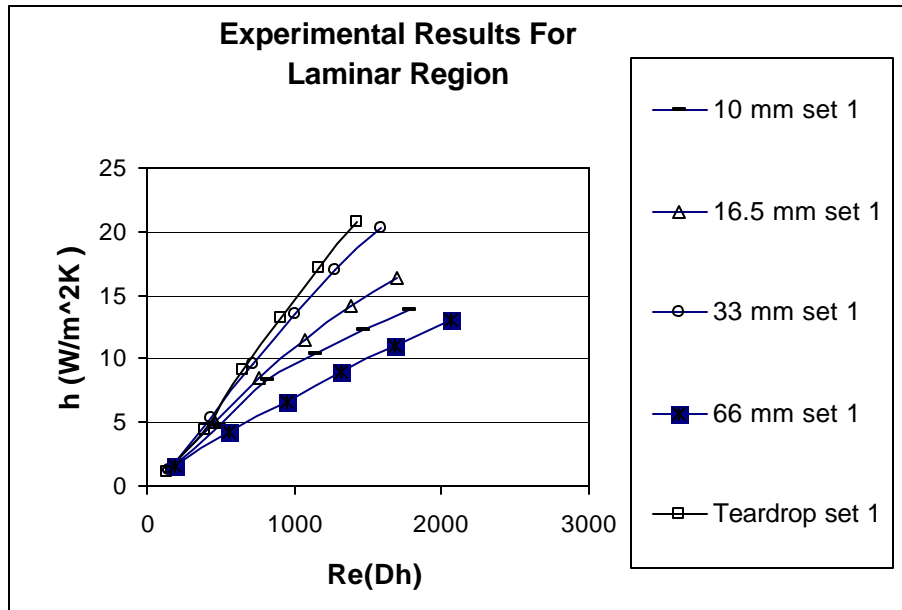
Figure 33.   Laminar leading pin-fin experimental results, h vs. Re_{Dh}
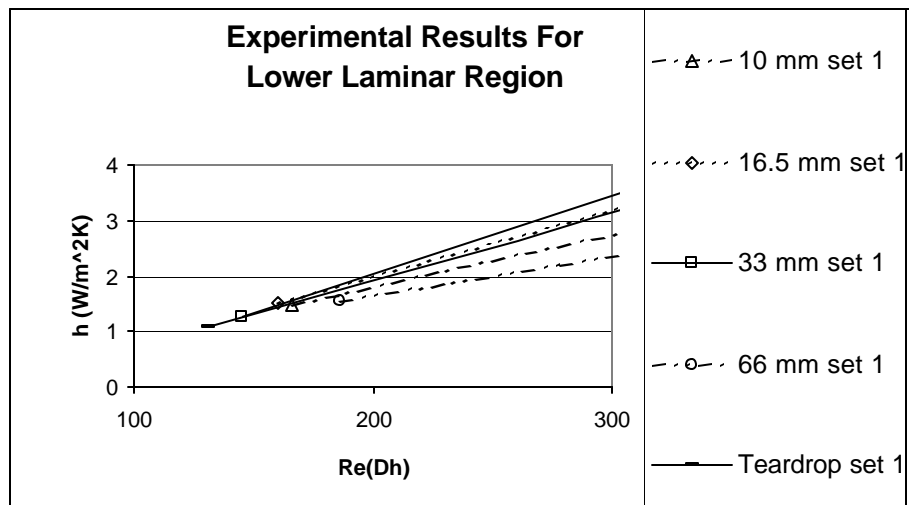
Figure 34.   Leading experimental results, h vs. Re_{Dh}, lower laminar region

Figure (34) shows that with Reynolds numbers less than 200 the various pins performed similarly with the advantage offered by the 33 mm and 16.5 mm pin-fin geometries. This may be attributed to the decrease in significance of flow separation at very low flow rates. The graph does represent trend lines therefore more data points are needed to properly analyze this region.

2.   Turbulent Region

The turbulent flow region offered similar results with the set one configuration providing the highest heat transfer coefficients.   These results can be seen in figures (35-38). With the increase in pin-fin numbers the heat transfer area increases resulting in a larger heat transfer coefficient.   Removing pin-fins resulted in the reduction of heat transfer coefficients by 5-20%. For heat exchangers not requiring high heat flux removal sets 2-4 could be a cost effective alternative.
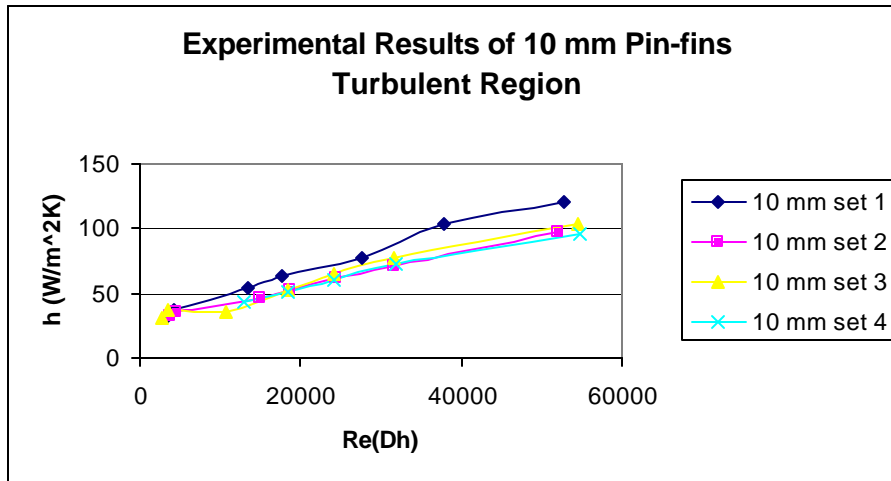

Figure 35.   Turbulent 10 mm pin-fin experimental results, h vs. Re_{Dh}
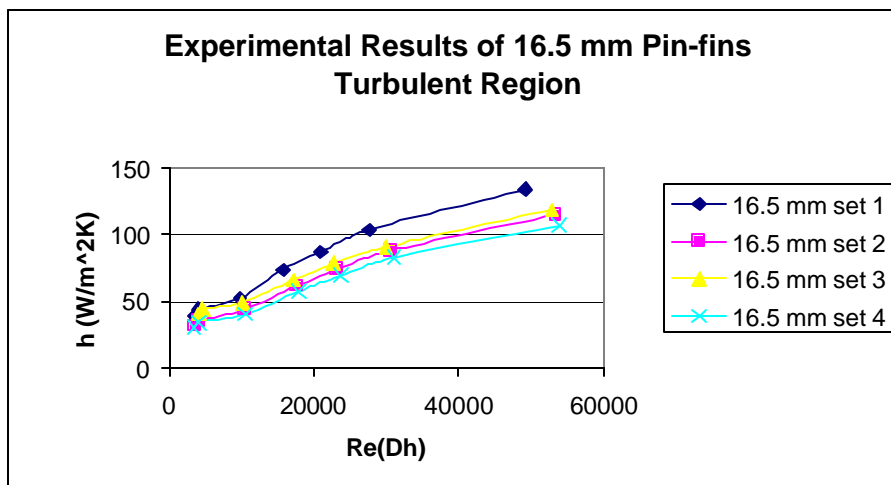
Figure 36.   Turbulent 16.5 mm pin-fin experimental results, h vs. Re_{Dh}
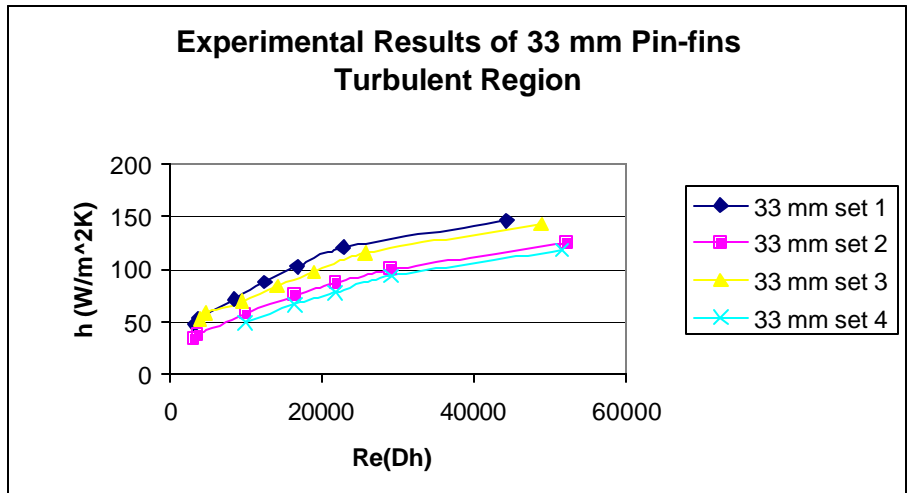
Figure 37.   Turbulent 33 mm pin-fin experimental results, h vs. Re_{Dh}
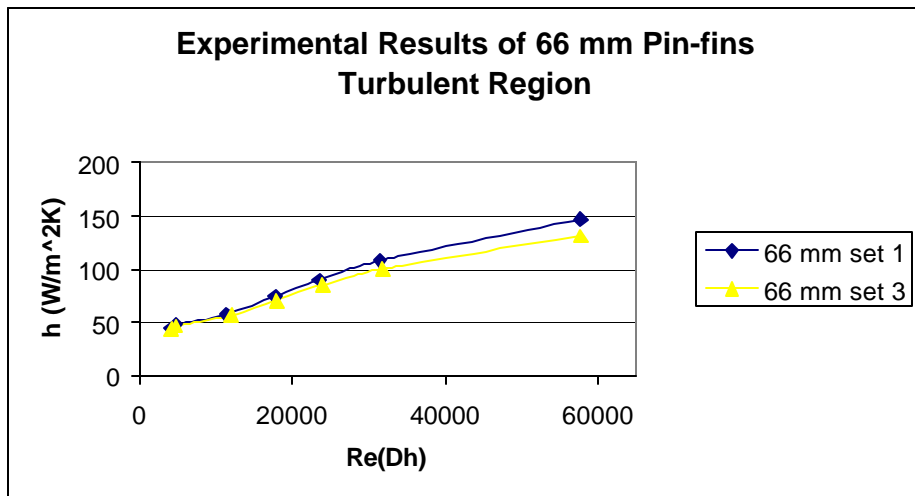
Figure 38.   Turbulent 66 mm pin-fin experimental results, h vs. Re_{Dh}

Figure (39) displays the results of all the cylindrical pin sets together. As can be seen in figure (39) the 33 mm pins performed the best with the 66 mm pins performing better than in laminar flow. The teardrop shaped pins were not completed due to time constraints of research work. Numerical and experimental research on the teardrop shaped pin fins (set one only) was conducted by Boulares (2003) and is depicted in figure (97) of appendix B as "teardrop set one." It shows that the teardrop shaped pins performed better in this region due to the increase in heat transfer area and the decrease in flow separation from the pins themselves. This increase performance was reported in Boulares (2003) as an increase of 18-33%. This research found the increase over the respective 33 mm pin-fin configuration to be similar at 18-36%.

37
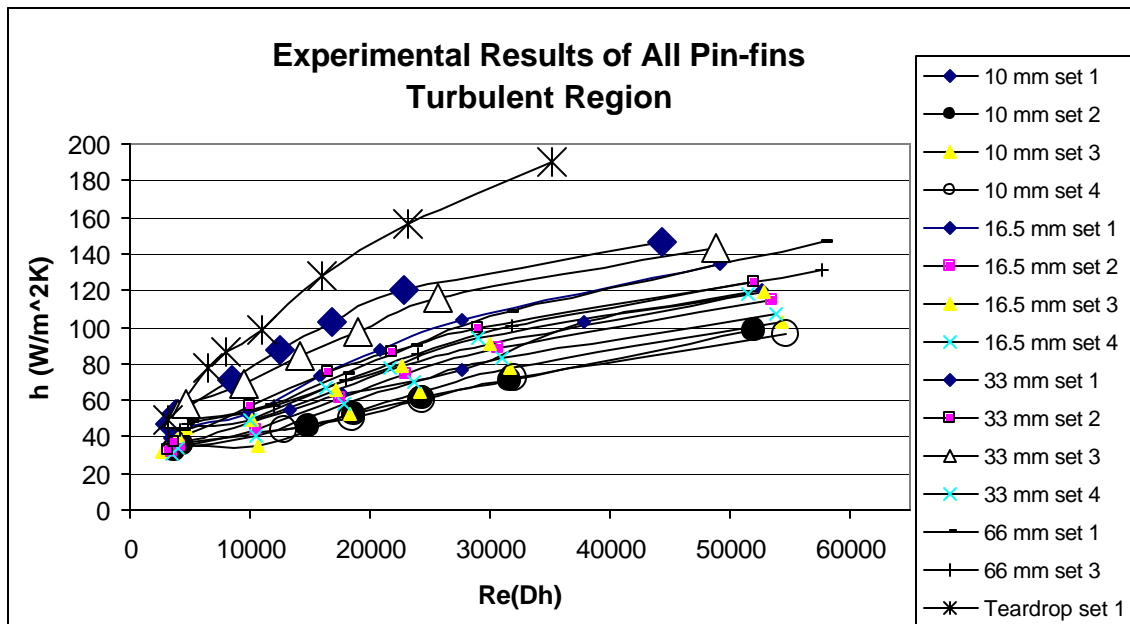
Figure 39.   Turbulent total pin-fin experimental results, h vs. Re$_{Dh}$

C.   NUSSELT NUMBER (NU$_{DH}$)

1.   Laminar Region

The Nusselt number is a dimensionless temperature gradient that details the convective heat transfer in the CHE. The larger the Nusselt number the more productive the convective heat transfer process is. It describes the thermal boundary layer and is applicable to varying types of fluids, hydraulic diameters, and flow rates provided the boundary conditions have not changed. The Nusselt number is proportional to the heat transfer coefficient and hydraulic diameter and inversely proportional to the thermal conductivity of the system. Figures (40-44) show how the Nusselt number varied with the Reynolds number in the laminar range.

For the 10 mm and 16.5 mm pins the results were similar to the heat transfer coefficient with set number one being the highest. However with the larger shapes (33 mm, 66 mm, teardrop) this was not the case. The 33 mm data showed that set number three (X/D doubled) provided an increase of heat transfer of 12%. This was the same case for the 66 mm pins. The teardrop set four configuration showed better heat transfer results over the entire laminar range with an average increase of 3-5%. With the Nusselt number being directly proportional to the heat transfer coefficient the expected results

38

should have been similar to the heat transfer coefficient data. The change in order is attributed to the increase in hydraulic diameter as pins are removed. This event has more of an effect on the larger pins than the 10 mm and 16.5 mm pins. When moving out of the full set one configuration the average increase in hydraulic diameter is 27% for the 33 mm pins and 7% for the 10 mm pins. This larger increase in hydraulic diameter offsets the decrease in the heat transfer coefficient causing the sets 2-4 Nusselt numbers to be higher than set one for the larger pins.
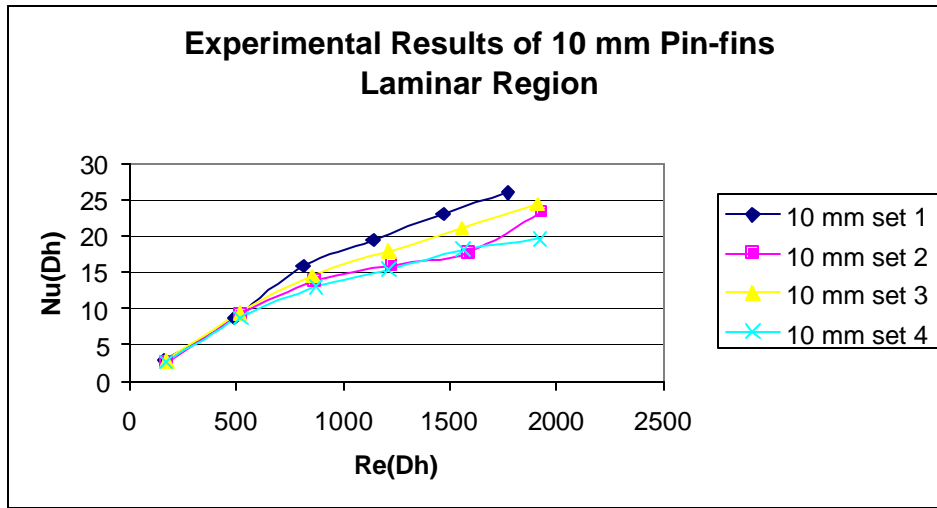
Figure 40.　　　Laminar 10 mm pin-fin experimental results, Nu_{Dh} vs. Re_{Dh}
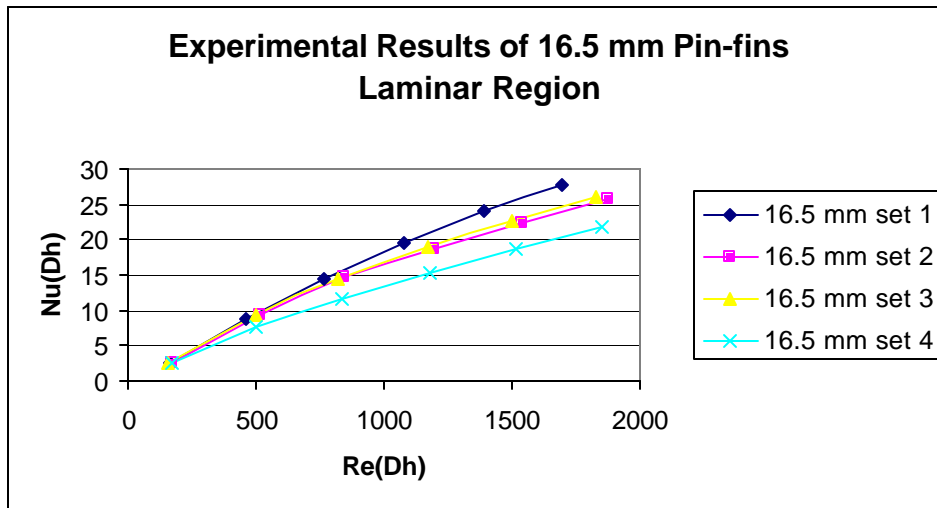
Figure 41.　　　Laminar 16.5 mm pin-fin experimental results, Nu_{Dh} vs. Re_{Dh}
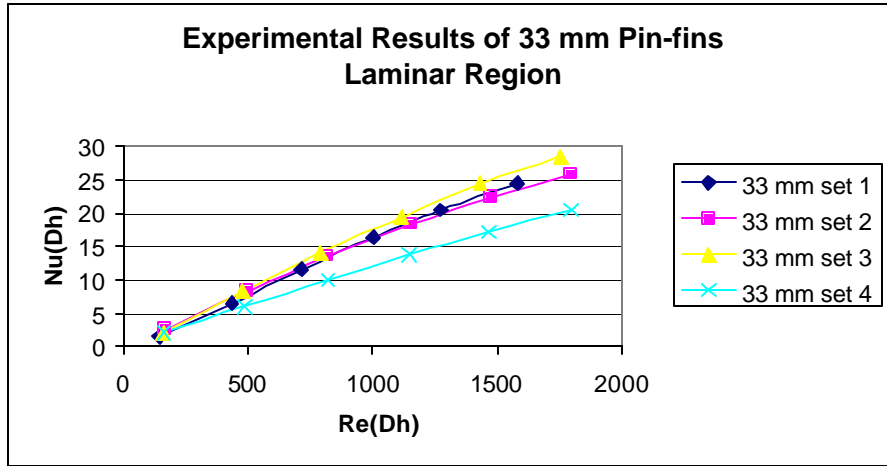
Figure 42.　　　　　Laminar 33 mm pin-fin experimental results, Nu_{Dh} vs. Re_{Dh}
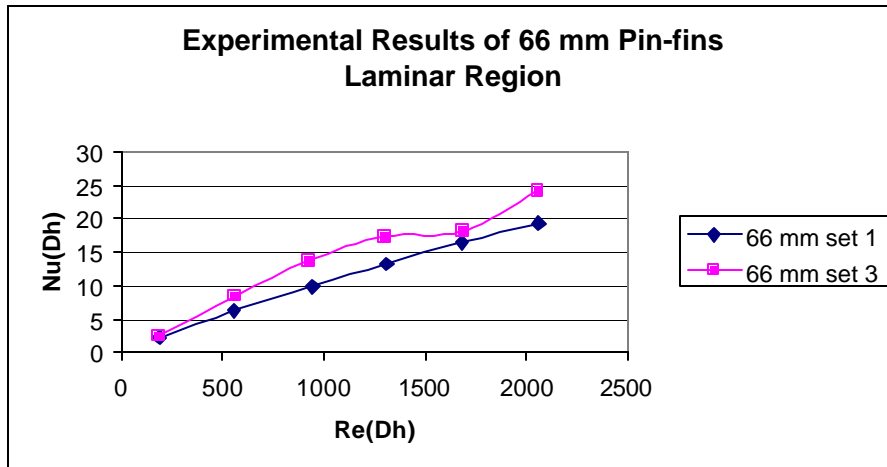
Figure 43.　　　　　Laminar 66 mm pin-fin experimental results, Nu_{Dh} vs. Re_{Dh}
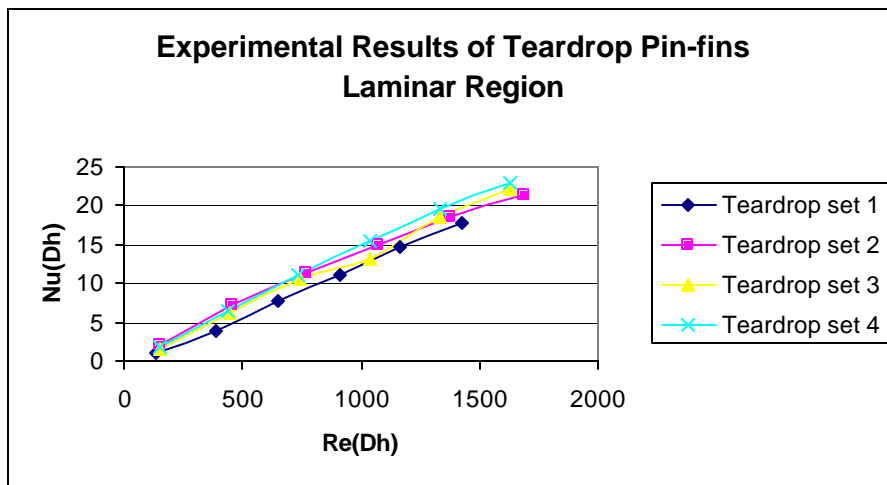
Figure 44.　　　　　Laminar teardrop pin-fin experimental results, Nu_{Dh} vs. Re_{Dh}

Figure (45) shows how the best pins from each group compared to one another. The 16.5 mm set one pins and the 33 mm set three pins were the overall top performers. They were nearly identical with an average of less than 5% difference. Whichever configuration would be the cheapest to construct while providing adequate structural strength would be the best decision.
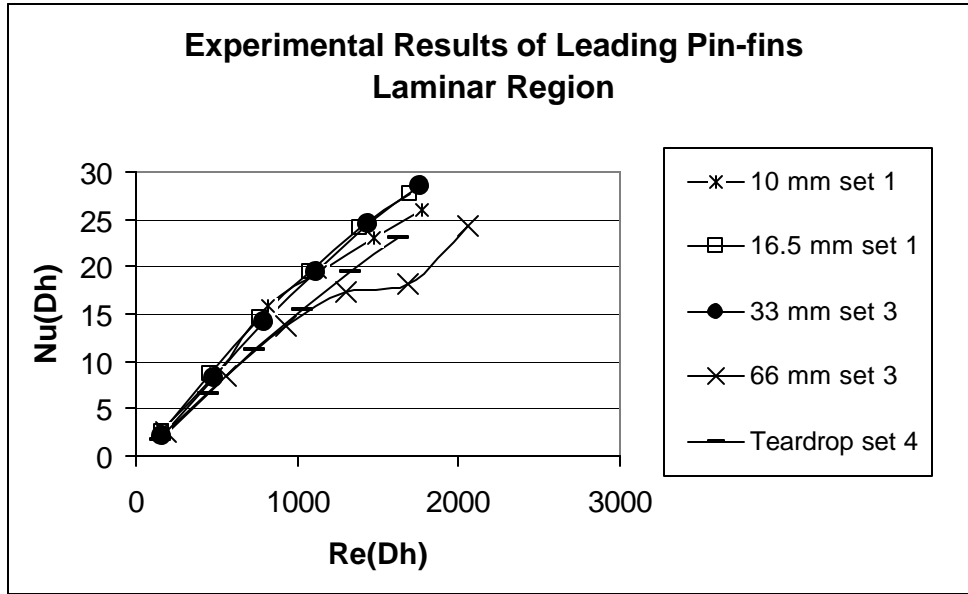
Figure 45.   Laminar leading pin-fin experimental results, Nu_{Dh} vs. Re_{Dh}
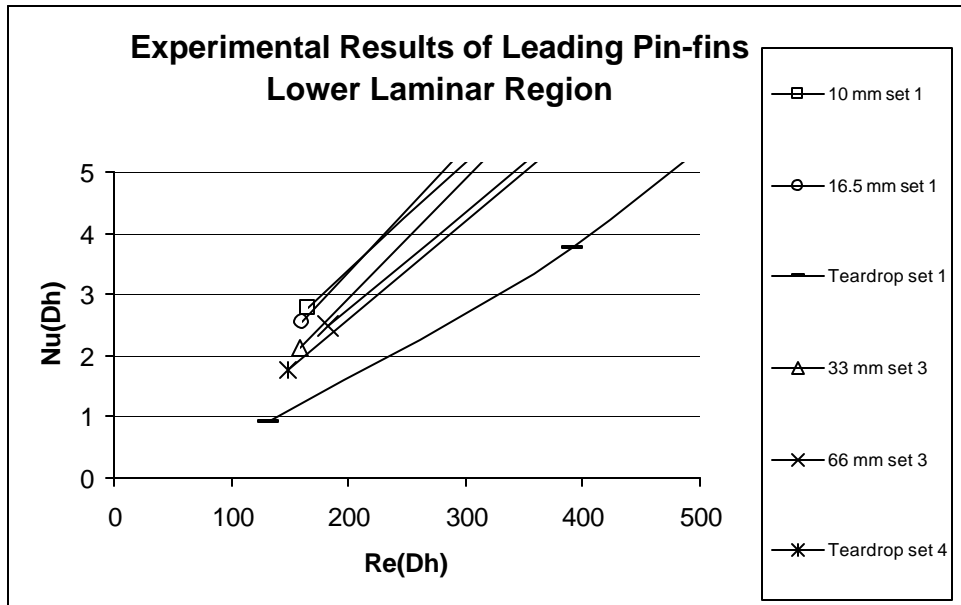
Figure 46.   Leading experimental results, Nu_{Dh} vs. Re_{Dh}, lower laminar region

41

Figure (46) shows the performance of the leading pins tested at low Reynolds numbers of 100 – 300. Again these are just trend lines with the top performing pins being the 10 mm and 16.5 mm pins in the set one configuration. The teardrop set one pins performed poorly in this range with the Nusselt number decreasing 50% from the mentioned 10 mm and 16.5 mm pins. This can be attributed to the smaller hydraulic diameters associated with the larger pins outweighing the increase of their heat transfer coefficients over the smaller pins.

2. Turbulent Region

The turbulent region results can be seen in Figures (47-50). The graphs coincide with past numerical and experimental results showing the expected similar trend in heat transfer coefficients. The same phenomenon that occurred in the laminar region occurred here as well. This was due to the smaller pins having a larger open volume coupled with a relatively smaller change in wetted surface area for flow. This lead to the hydraulic diameter and heat transfer coefficient comparison that explained the lesser performance of the larger diameter pin-fin set one configurations.
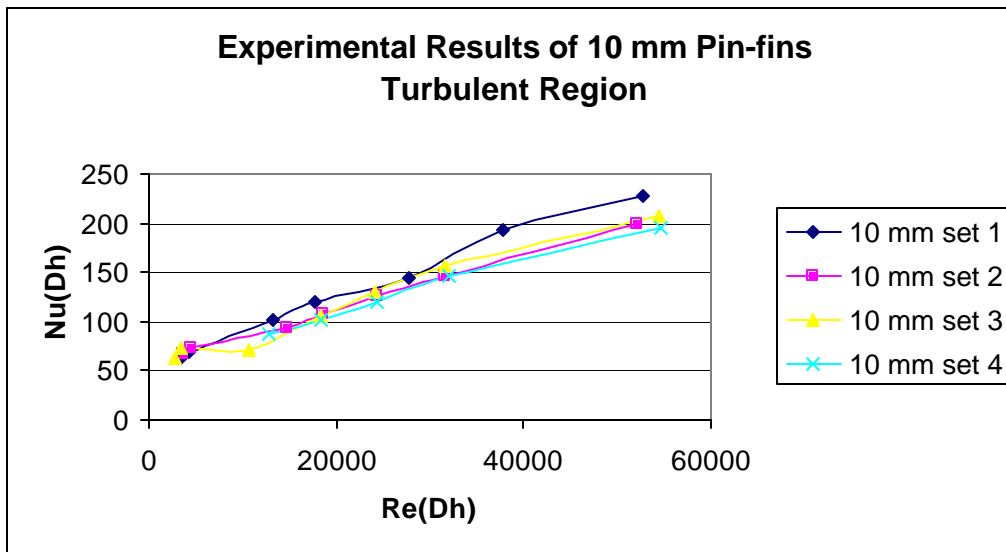
Figure 47.   Turbulent 10 mm pin-fin experimental results, Nu_{Dh} vs. Re_{Dh}
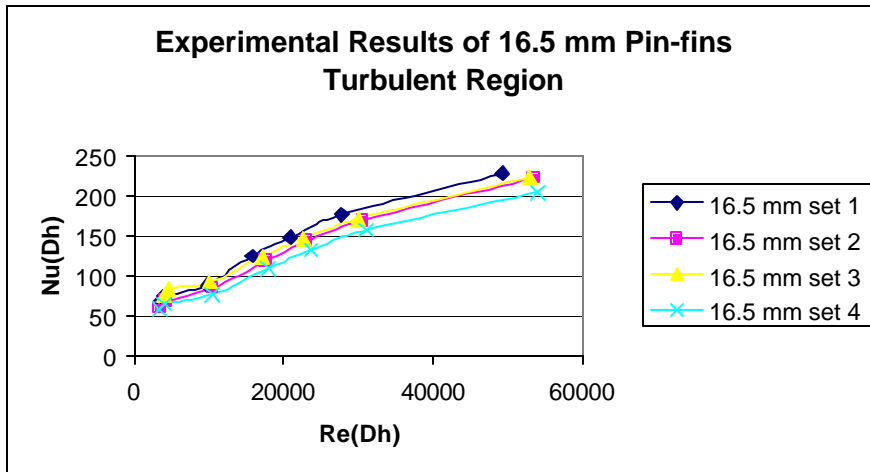
Figure 48.　　　Turbulent 16.5 mm pin-fin experimental results, Nu_{Dh} vs. Re_{Dh}
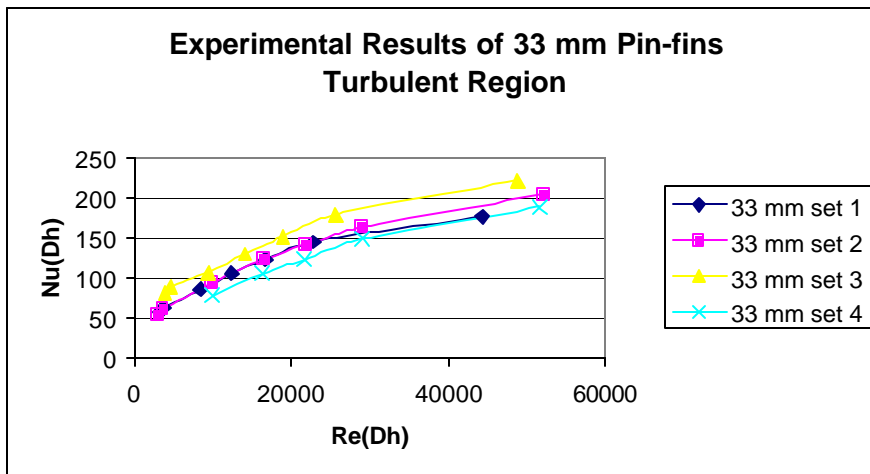
Figure 49.　　　Turbulent 33 mm pin-fin experimental results, Nu_{Dh} vs. Re_{Dh}
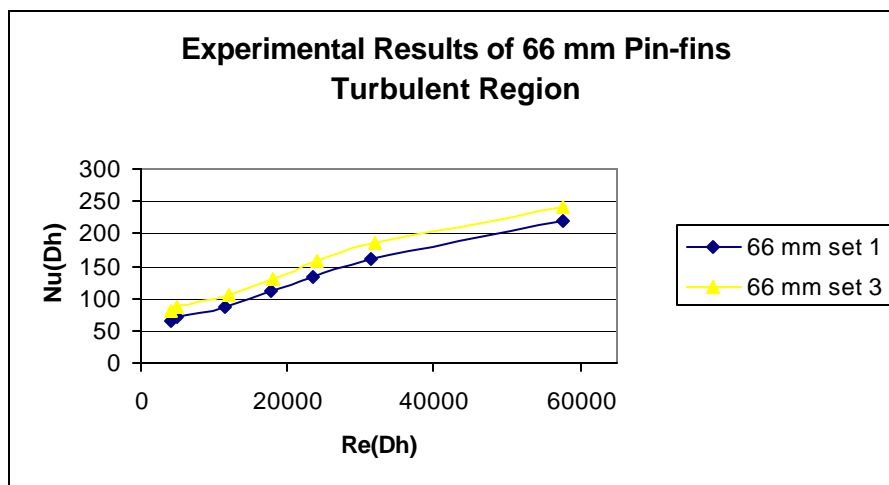
Figure 50.　　　Turbulent 66 mm pin-fin experimental results, Nu_{Dh} vs. Re_{Dh}

43

Figure (51) displays the Nusselt versus Reynolds numbers for the leading cylindrical pin-fins including the teardrop data collected by Boulares (2003). The data is labeled as "teardrop set 1." The 33 mm set three performed well however the set one 16.5 mm pins-fins performed best over the entire spectrum. In the lower turbulent range the 16.5 mm pins performed 15-20% better than the other leading pins however at the high turbulent range all of the pins performed within 5% of each other. As the Reynolds number increased the changes in the heat transfer coefficient offset the changes in hydraulic diameter resulting in the data convergence.

There should be a numerical analysis performed to see how the set three teardrop configuration would perform. With the increase in hydraulic diameter and relatively smaller decrease in the heat transfer coefficient it could possibly be the top pin configuration.
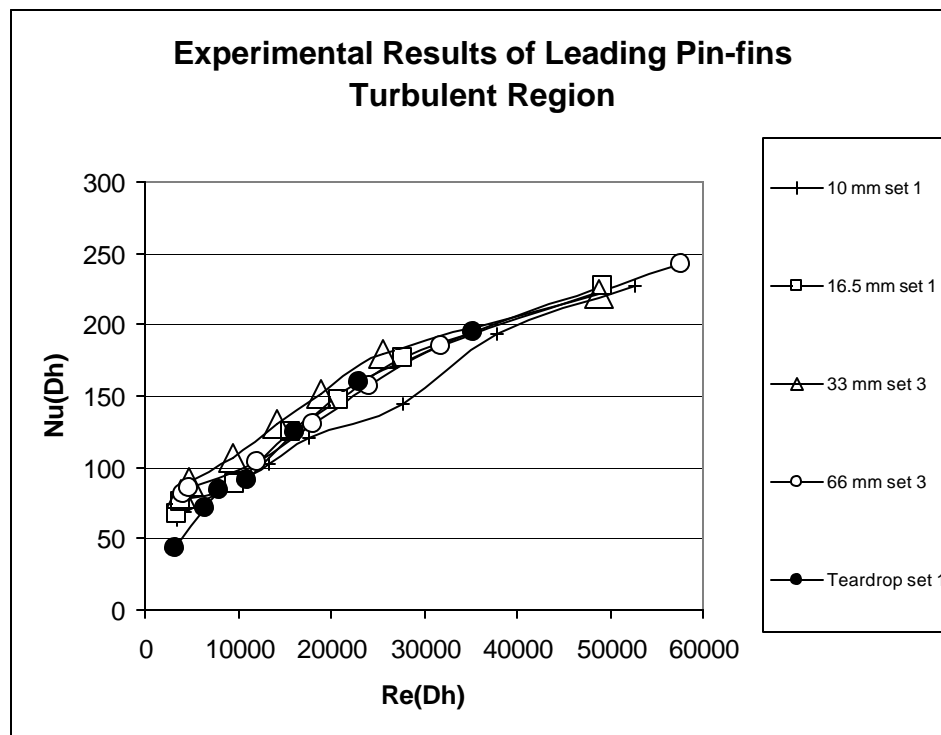
Figure 51.   Turbulent leading pin-fin experimental results, Nu_{Dh} vs. Re_{Dh}

The previously shown graphs provide an indicator of the best performing pin configurations however heat transfer characteristics alone cannot completely describe a CHE. A differential pressure analysis must be conducted to provide a real comprehensive assessment of heat exchanger performance.

D.   FRICTION COEFFICIENT ANALYSIS

1.   Laminar Region

The friction factor is an important parameter because it tells how much power was required to achieve the heat transfer results. Friction factor is directly proportional to the differential pressure across the CHE and hydraulic diameter, while being inversely proportional to density and average fluid velocity. Figures (52-56) show the results of friction factor versus Reynolds number in the laminar region. As can be derived from the graphs usually as pins were removed the differential pressure across the heat exchanger decreased causing friction factor to decrease. The friction factor values for Reynolds numbers less than 800 were unstable. This could be attributed to the data collection method. The 0-5 inch inclined manometer could be read to 0.001 inches of water (0.249 Pa). In the lower laminar region differential pressure changes across the CHE were extremely small and difficult to measure. Parallax errors coupled with manometer resolution made data collection a challenge. With the exception to the 66 mm (not tested) and teardrop pins, set number four was the configuration that offered the lowest differential pressure and friction factor.
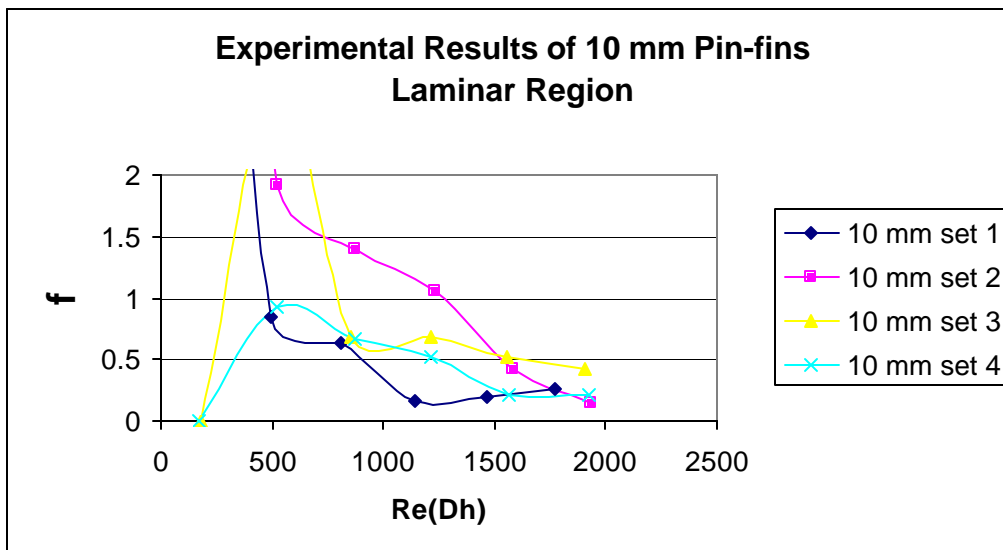
Figure 52.   Laminar 10 mm pin-fin experimental results, f vs. Re_{Dh}
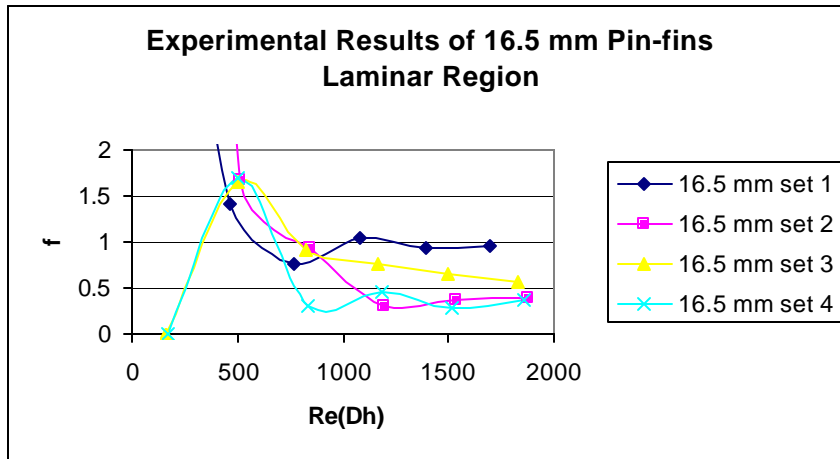
Figure 53.   Laminar 16.5 mm pin-fin experimental results, f vs. Re$_{Dh}$
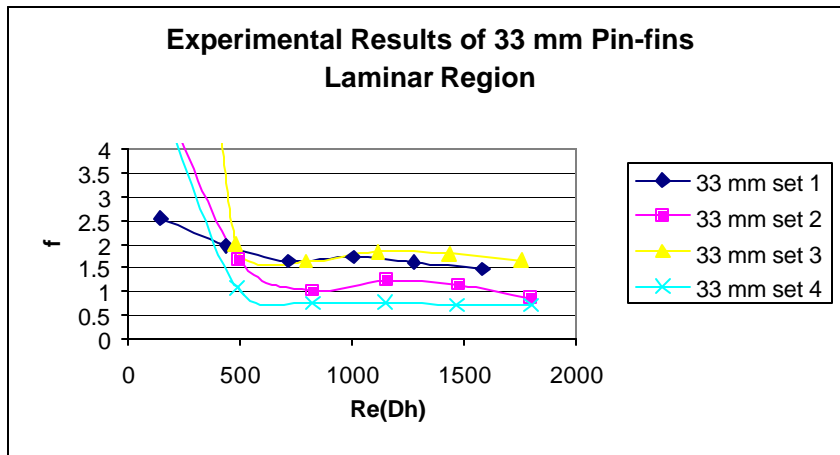
Figure 54.   Laminar 33 mm pin-fin experimental results, f vs. Re$_{Dh}$
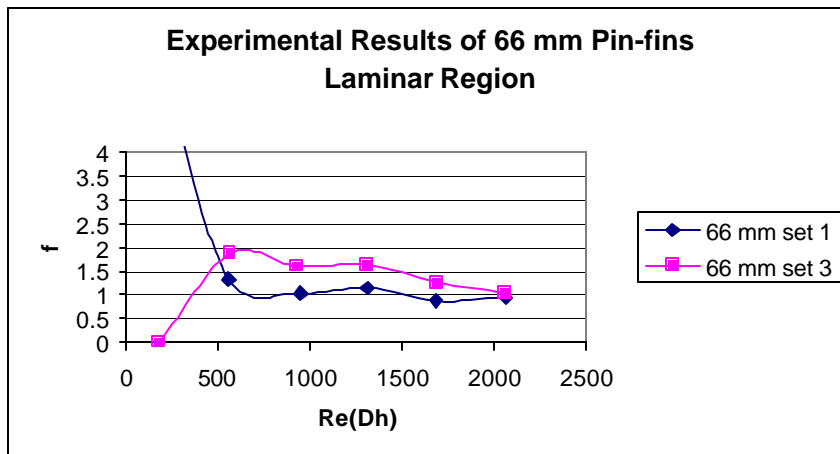
Figure 55.   Laminar 66 mm pin-fin experimental results, f vs. Re$_{Dh}$
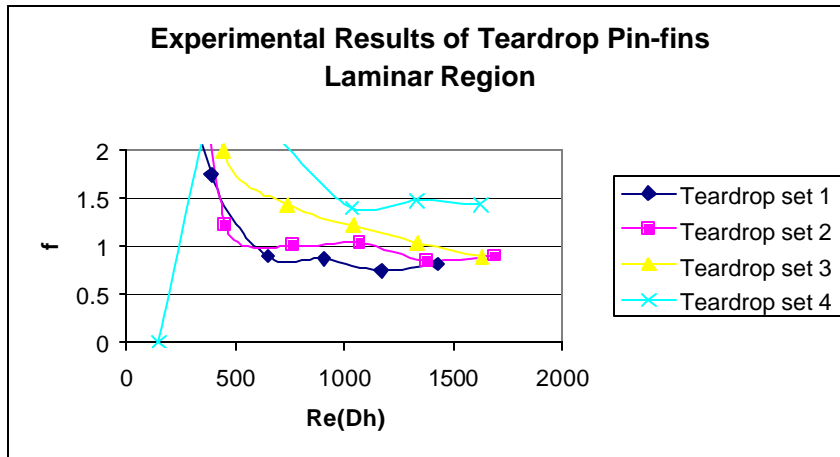
Figure 56.　　　　　Laminar teardrop pin-fin experimental results, f vs. Re_{Dh}

Figure (57) displays the lowest friction factor from each group for comparison. The 10 mm and 16.5 mm pins performed the best due to their relatively small diameters leading to smaller differential pressures. The upper laminar region showed the set four 10 mm pins performing approximately 15% better than it 16.5 mm counterpart. The lower laminar range was unstable for reasons mentioned before however the graph shows the 16.5 mm pins performing the best at around $Re_{Dh} = 800$.
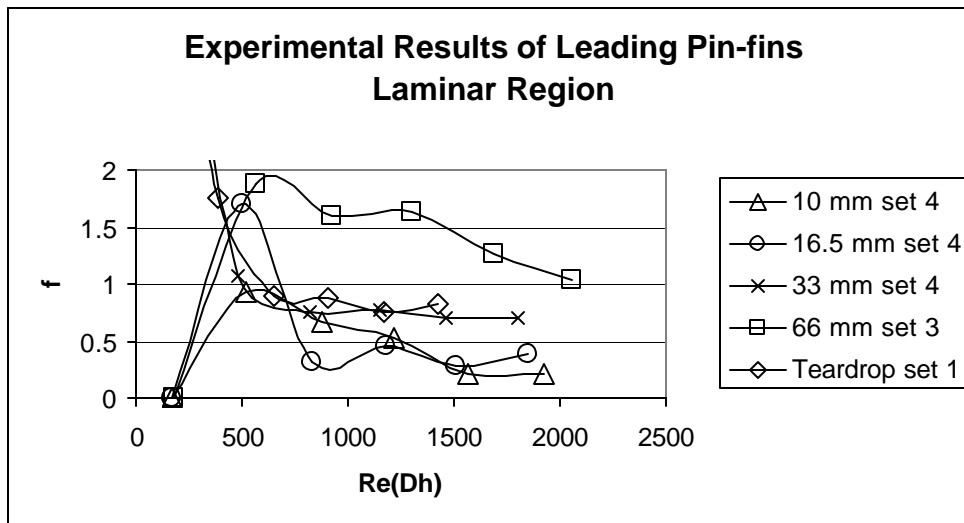
Figure 57.　　　　　Laminar leading pin-fin experimental results, f vs. Re_{Dh}

2. Turbulent Region

The turbulent region friction factor versus Reynolds number is displayed in figures (58-61). They show the similar trends depicted in the graphs for the laminar region. In general the set four configurations performed the best. This was expected since this configuration offered the least resistance to airflow.
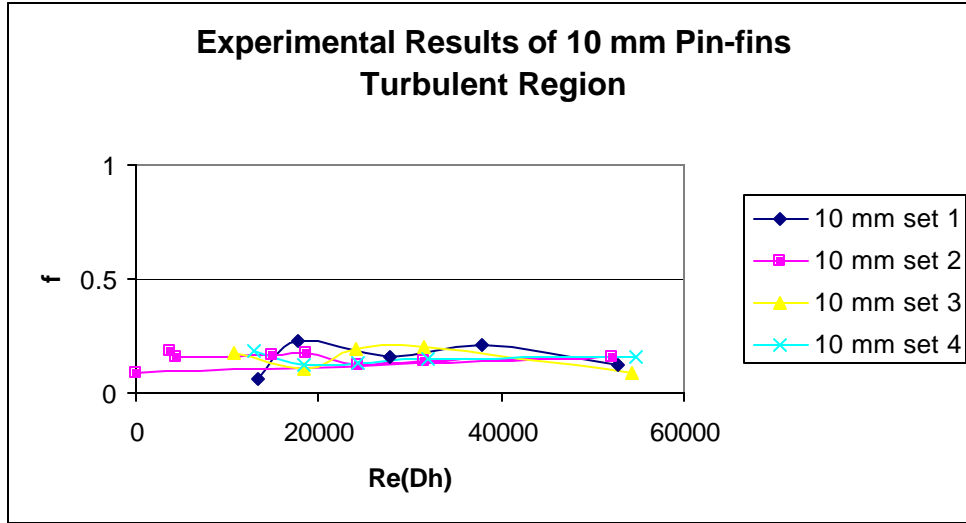
Figure 58.   Turbulent 10 mm pin-fin experimental results, f vs. Re_{Dh}
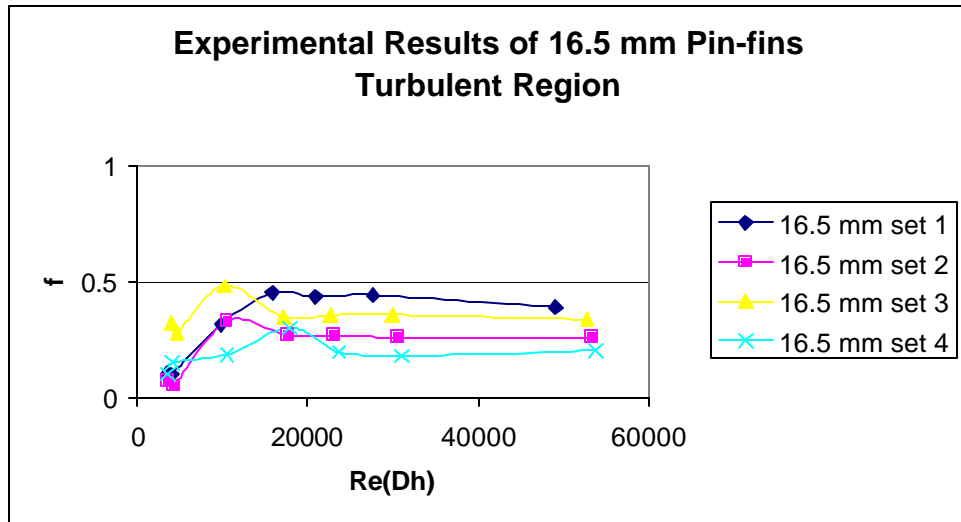
Figure 59.   Turbulent 16.5 mm pin-fin experimental results, f vs. Re_{Dh}
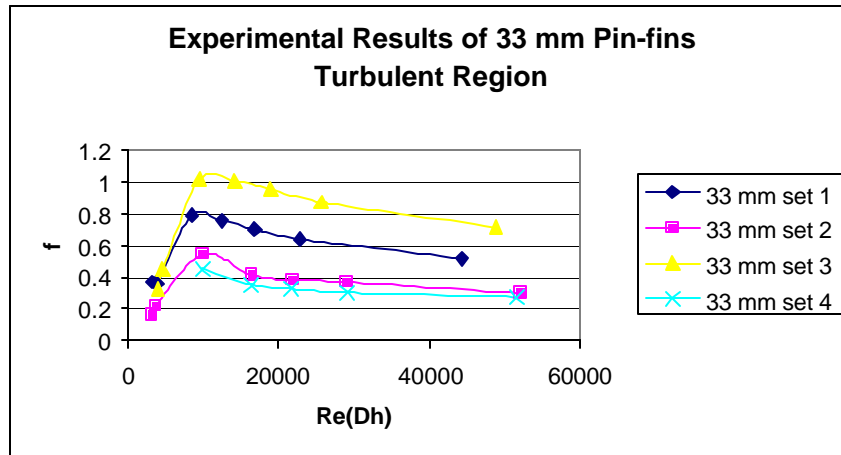
Figure 60.   Turbulent 33 mm pin-fin experimental results, f vs. Re_{Dh}
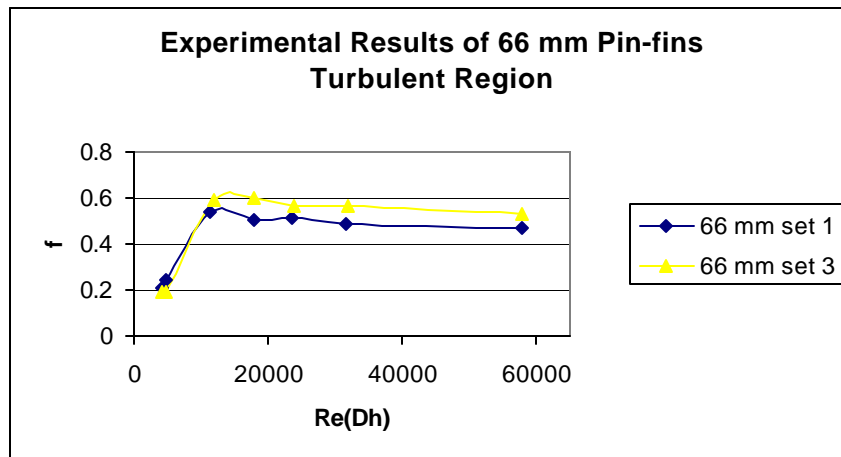
Figure 61.   Turbulent 66 mm pin-fin experimental results, f vs. Re_{Dh}

Figure (62) shows the result of the leading pin-fins including the teardrop set one data collected by Boulares (2003).   The 10 mm pin-fins performed the best providing the smallest pressure drop and subsequently friction factor. They performed nearly 30-40% better than the nearest rival, the set four 16.5 mm pin set. This again was expected since the pin size and configuration offered the smallest pressure drop.

The lower turbulent region is described as Re_{Dh} = 2500 – 10,000. Some of the data in this range was unreliable and is attributed to the method of collection. In order to obtain the flow rates necessary a throttle valve was placed on the CHE duct inlet. The throttle valve worked well when allowing small volumetric flow rates (15 – 20 SCFM) however when larger airflows were desired certain challenges occurred. Operation of the throttle valve at flow rates greater than 20 SCFM resulted in large system pressure drops.

The increased differential pressures placed on the system resulted in leaks that corrupted the heat transfer data as well as masked the true differential pressure of the system. As a result sub-run numbers nine and ten were considered invalid for each experiment.
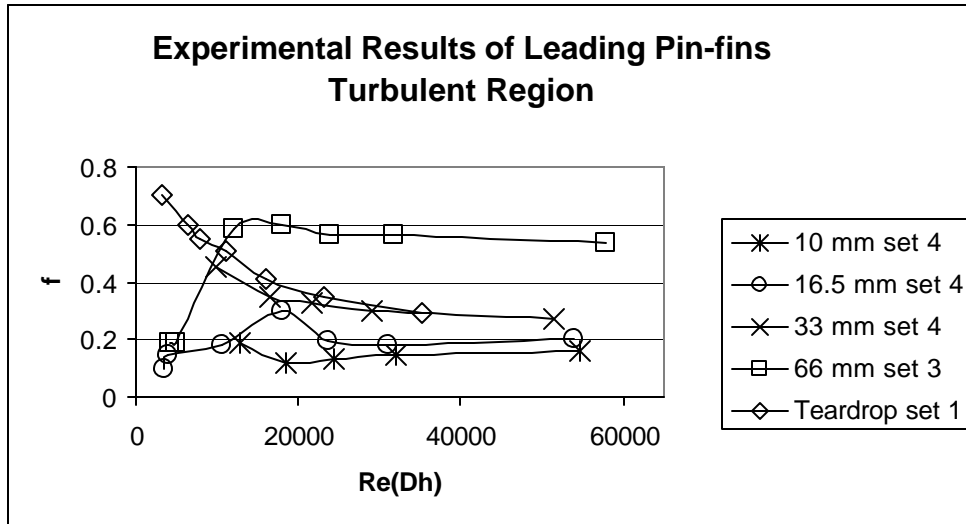
Figure 62.   Turbulent leading pin-fin experimental results, f vs. Re$_{Dh}$

E.   HEAT TRANSFER COEFFICIENT VS. FRICTION POWER (E)

By comparing the heat transfer coefficient with the friction power the optimum pin geometry and configuration can be determined.   Neither the heat transfer characteristics nor friction factor alone can determine the overall CHE performance. The heat transfer coefficient represents heat transfer as friction power represents the power required to overcome the friction of the fluid.

1.   Laminar Region

Figures (63-67) represent the heat transfer coefficient versus friction power for all tested pins and configuration in the laminar flow region. Except for the 10 mm pin set the best performing pin configurations were set number two.
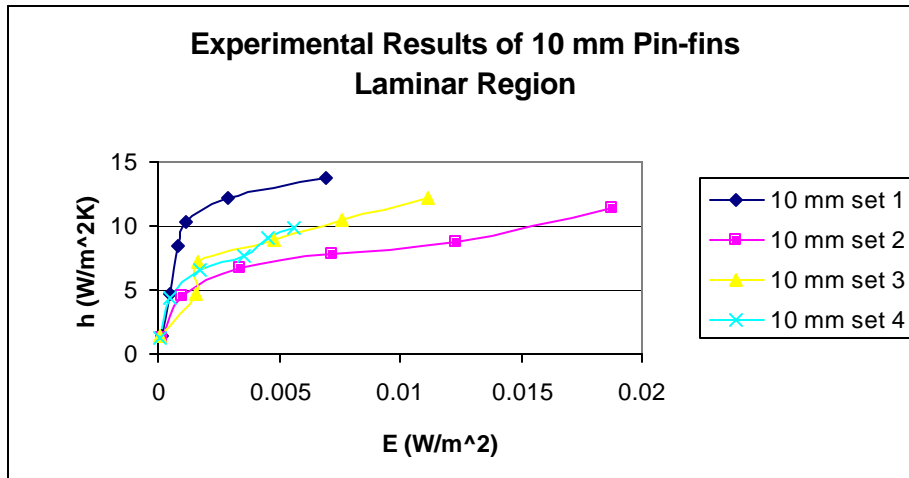
Figure 63.   Laminar 10 mm pin-fin experimental results, h vs. E
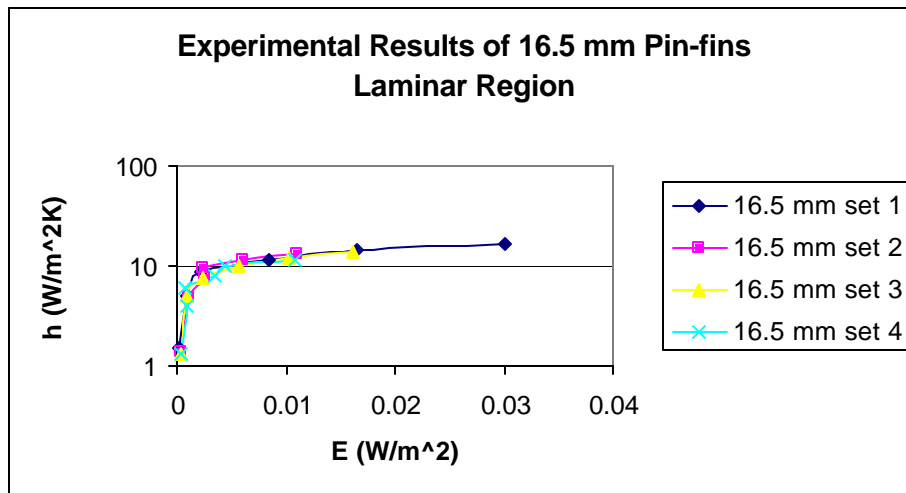

Figure 64.   Laminar 16.5 mm pin-fin experimental results, h vs. E
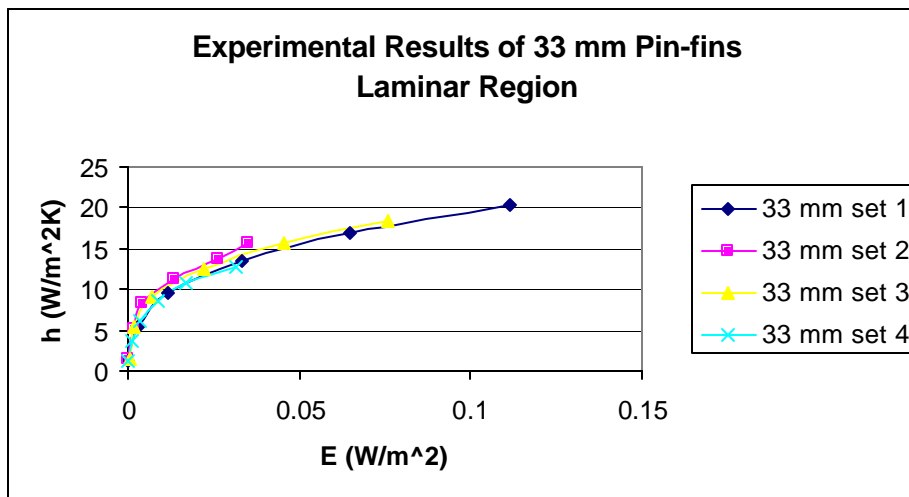

Figure 65.   Laminar 33 mm pin-fin experimental results, h vs. E
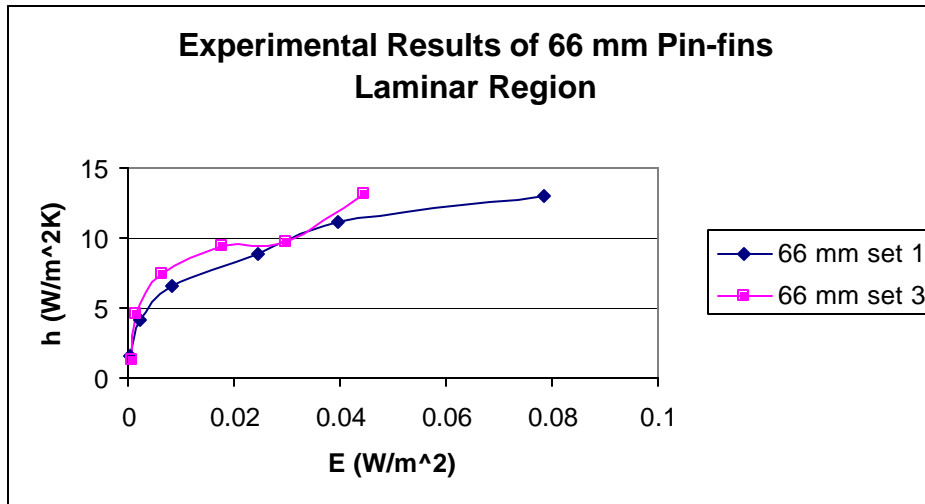
Figure 66.   Laminar 66 mm pin-fin experimental results, h vs. E
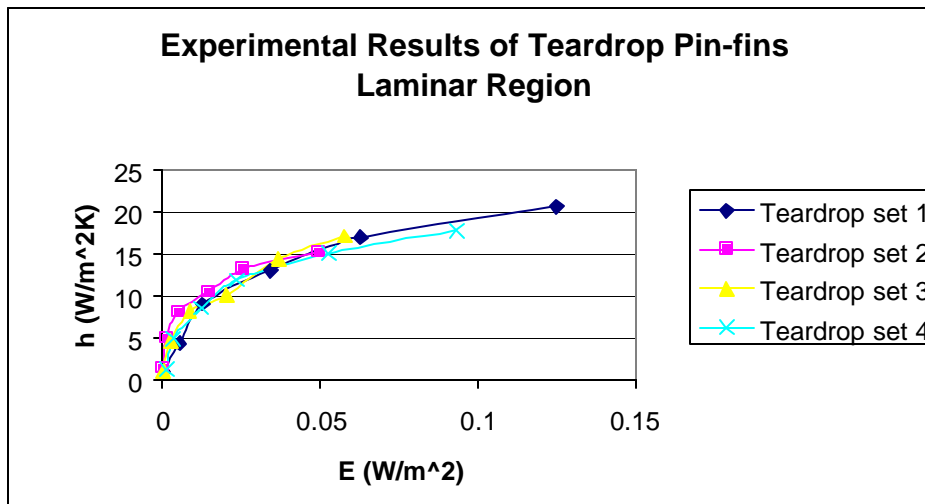
Figure 67.   Laminar teardrop pin-fin experimental results, h vs. E

Figure (68) shows how the leading pin-fin from each set compared to one another. The figure shows that the set one 10 mm pin-fins provided the best performance from the beginning however had more heat transfer limitations. To obtain the same h vs. E value the teardrop configuration required 50% less volumetric airflow. Therefore the 10 mm pin-fins offer more heat transfer per pressure drop however they may not be desirable for higher heat flux removal applications. This emphasizes the trade-off between heat transfer and pressure drop across a heat exchanger and the need for a strong optimization process.
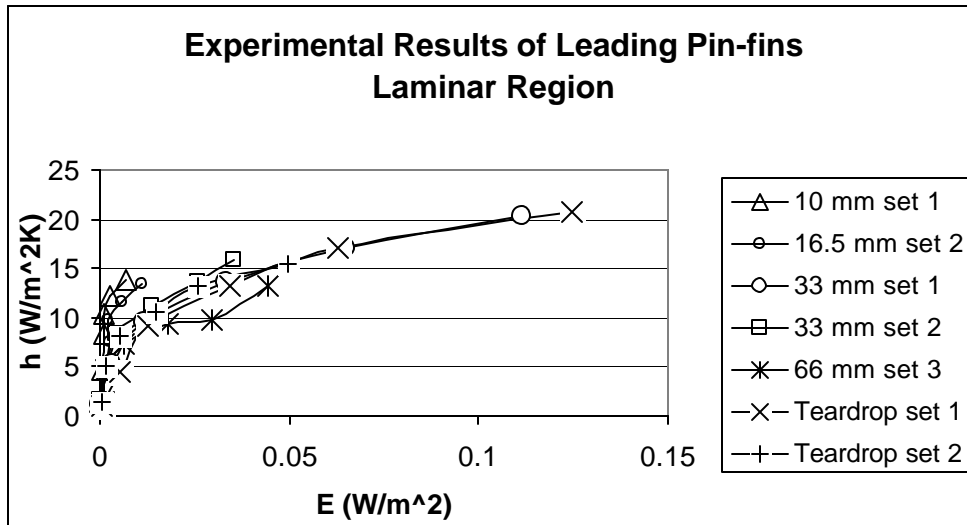
Figure 68.   Laminar leading pin-fin experimental results, h vs. E

2.   Turbulent Region

Figures (69-72) represent the heat transfer coefficient versus friction power for the various pin-fin geometries and configuration in the turbulent flow region. The value of E was plotted in the logarithmic scale to provide better clarity for relatively close values. Contrary to the laminar flow conditions set one performed the best in each case. This can be attributed to the rise in heat transfer associated with turbulent flow conditions.
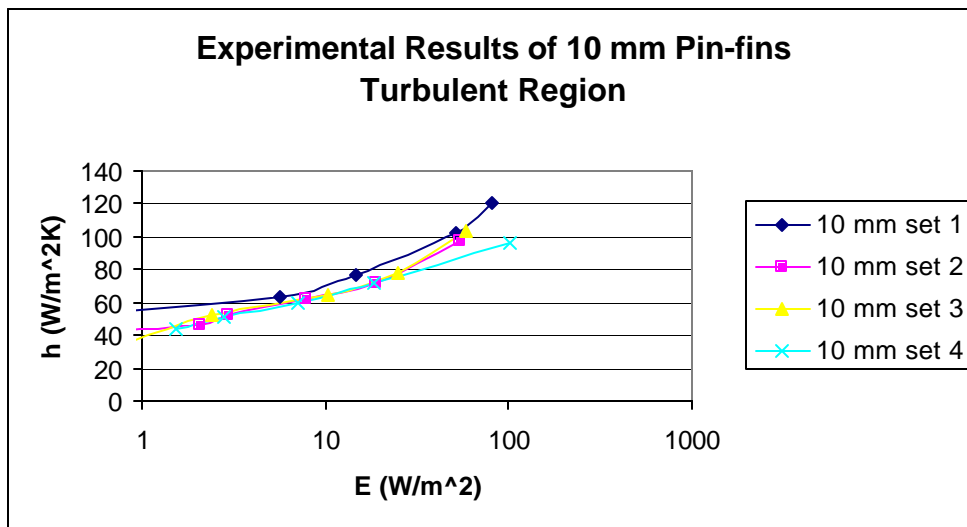

Figure 69.   Turbulent 10 mm pin-fin experimental results, h vs. E
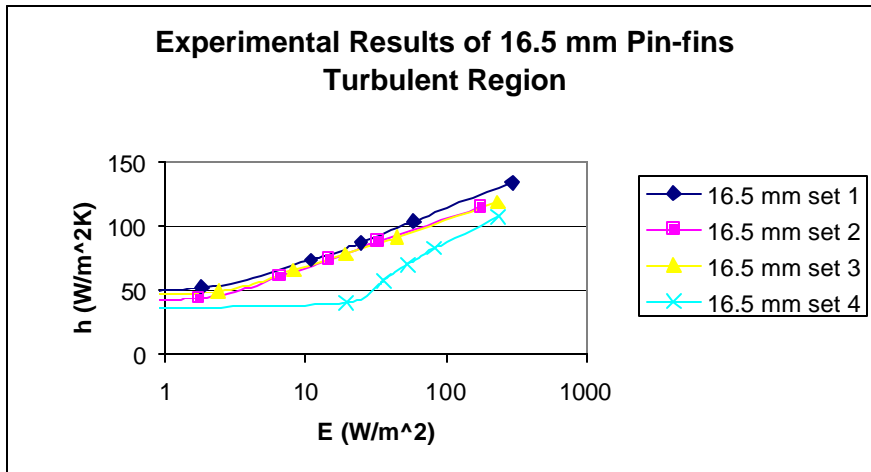
Figure 70.   Turbulent 16.5 mm pin-fin experimental results, h vs. E
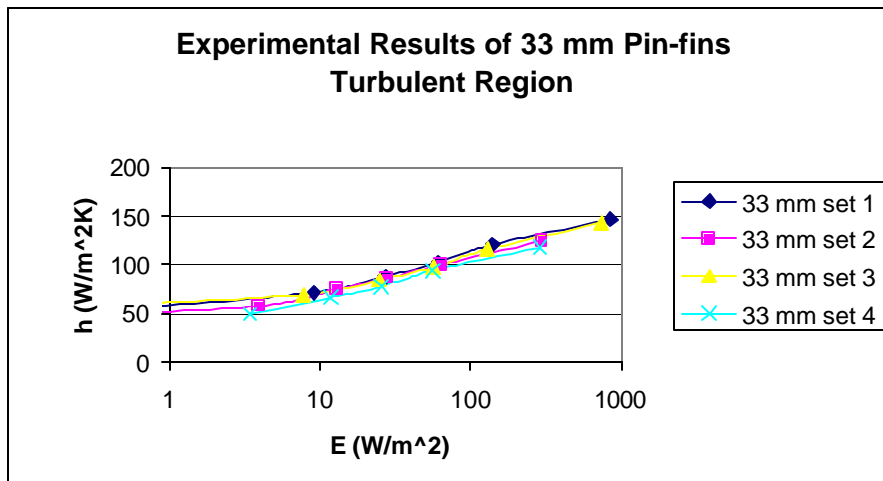

Figure 71.   Turbulent 33 mm pin-fin experimental results, h vs. E
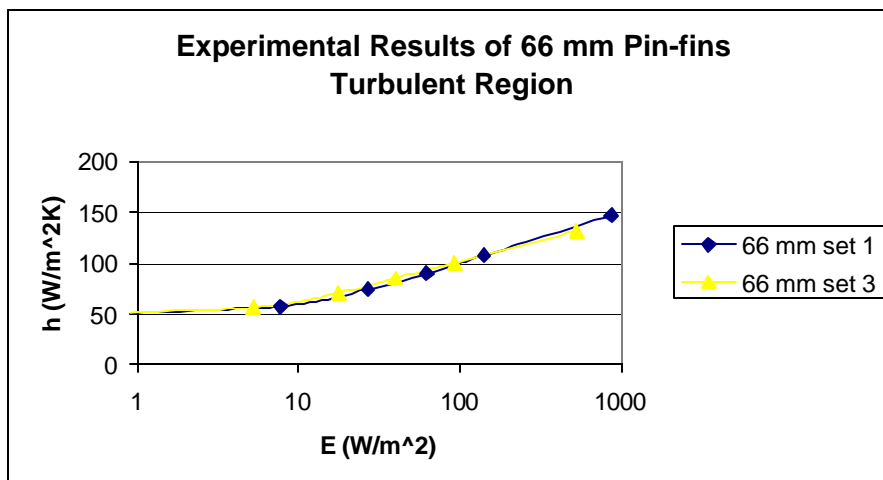
Figure 72.   Turbulent 66 mm pin-fin experimental results, h vs. E

Figure (73) compares set one from each case including the set one teardrop data from Boulares' research in 2003. As can be seen by the graph for turbulent conditions the set one teardrop configuration was the top performer and the 66 mm set one was the worst. The teardrop pin-fins performed any where from 10 to 25 percent better than its 33 mm counterpart.
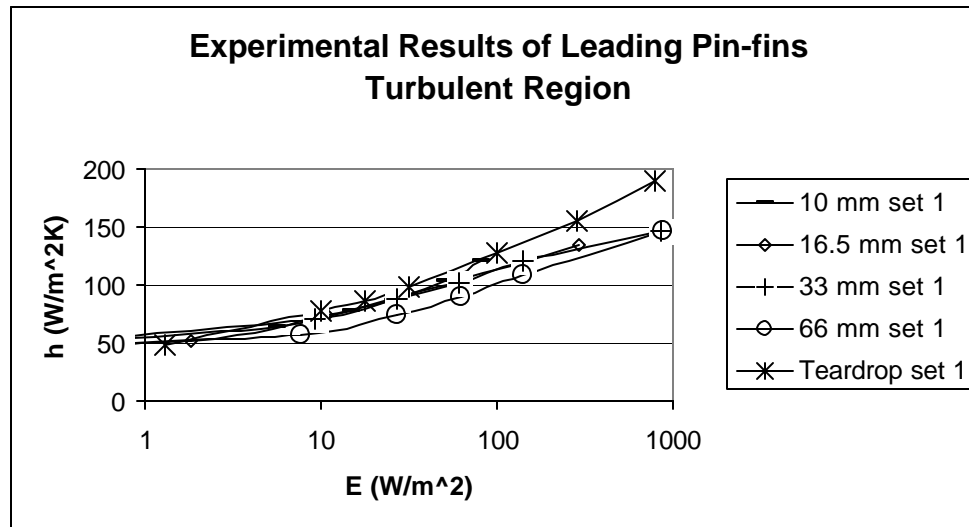
Figure 73.   Turbulent leading pin-fin experimental results, h vs. E

F.   NUMERICAL VS. EXPERIMENTAL

The fourth objective of this research was to build an experimental database to help improve numerical models. Extensive data was collected with about 5% repeating past numerical and experimental research. This was done to compare present work with past research to provide evidence of consistency in research methodology.

1.   Turbulent Range

Past work by Ramthun (2003) and Hamilton (2003) resulted in experimental and numerical data that can be compared to this research for validation. The 10 mm, 16.5 mm, and 33 mm set one turbulent data was repeated to provide some overlap in the research. Figure (74), heat transfer coefficient versus Reynolds number, displays the numerical and experimental results for the 10 mm pins. The max difference between Summers (2003) and the numerical data was 9%, which was acceptable.

Figure (75-76) provided the same comparison for the heat transfer coefficient versus Reynolds number regarding the 16.5 and 33 mm pin-fins. For both sets of pins there was excellent correlation between Re_{Dh} 7.5 – 25,000. All three sources of data were within 10%, which was acceptable. Above Re_{Dh} = 25,000 there was a maximum divergence of 12% for the 16.5 mm pins and 23% for the 33 mm pins. The divergence as the pins become larger could be attributed to limits of the numerical model specified by Hamilton (2003). The numerical model however does provide reliable heat transfer characteristics from Reynolds numbers of 3500 to 25, 000.
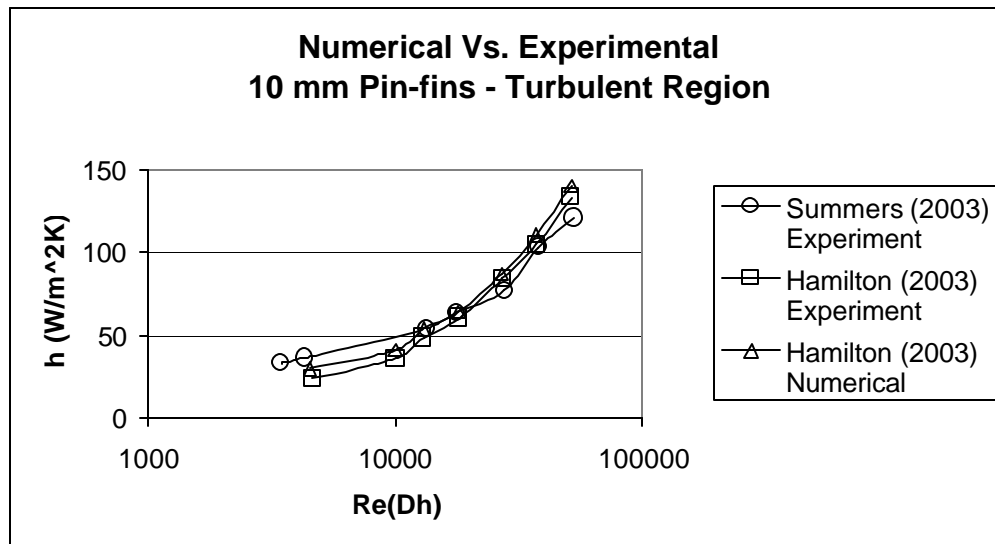
Figure 74.   Turbulent 10 mm set one comparative analysis, h vs. Re_{Dh}
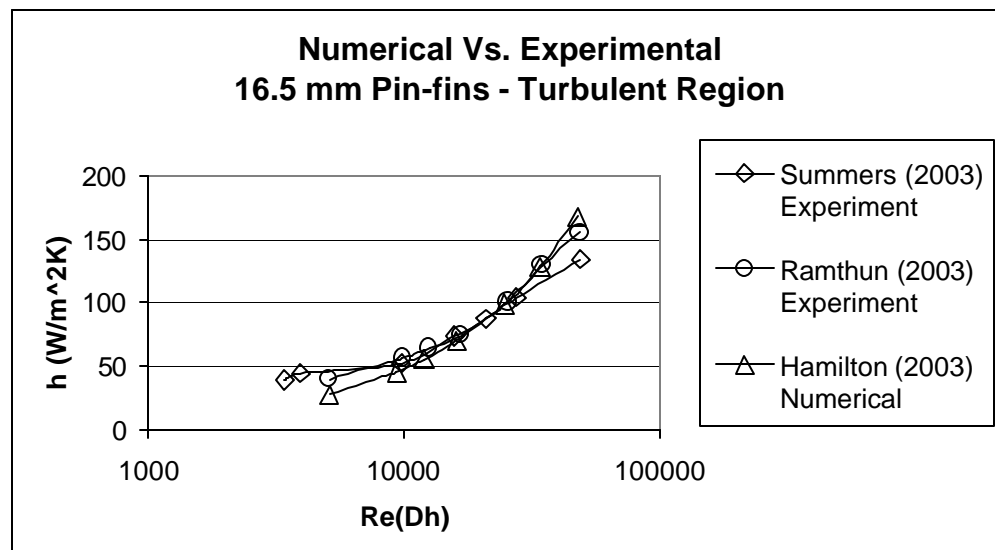
Figure 75.   Turbulent 16.5 mm set one comparative analysis, h vs. Re_{Dh}
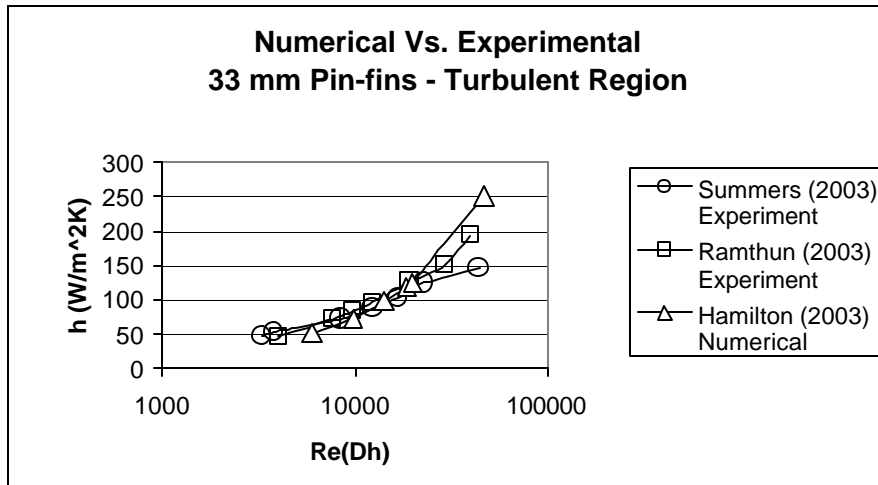
Figure 76.   Turbulent 33 mm set one comparative analysis, h vs. Re_{Dh}

Figures (77-79) compare the turbulent friction factor versus Reynolds numbers for the 10 mm, 16.5 mm, and 33 mm pin-fin configuration one data. The 16.5 mm and 33 mm data showed reasonable correlation (10-15%) however both were significantly different then the numerical data. This could be related to the flow separation from the pins resulting in large recirculation zones behind the pins not realized by the numerical model. The 10 mm pin data showed a greater error (25 %) between the more recent experiment and the past numerical and empirical data. The differential pressure measurement continues to be an issue and will be discussed in the recommendations portion of this thesis.
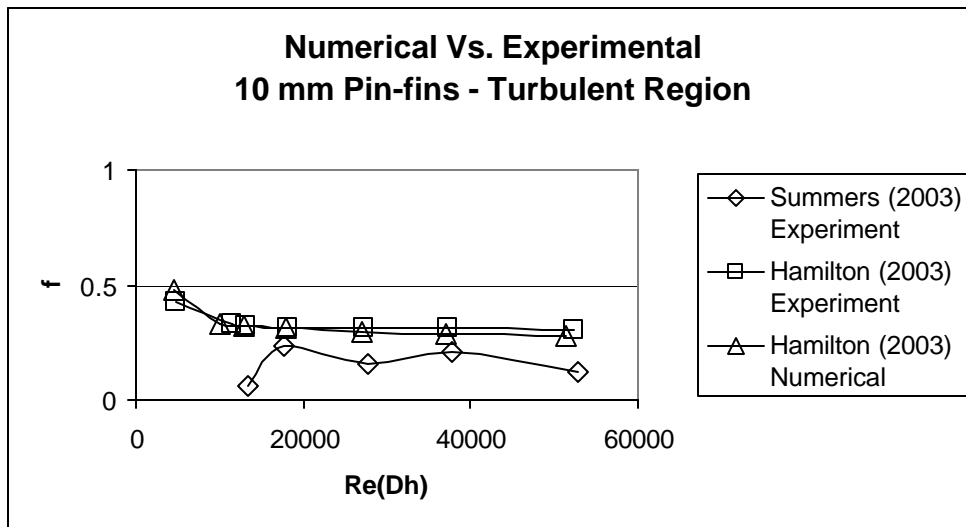
Figure 77.   Turbulent 10 mm set one comparative analysis, f vs. Re_{Dh}
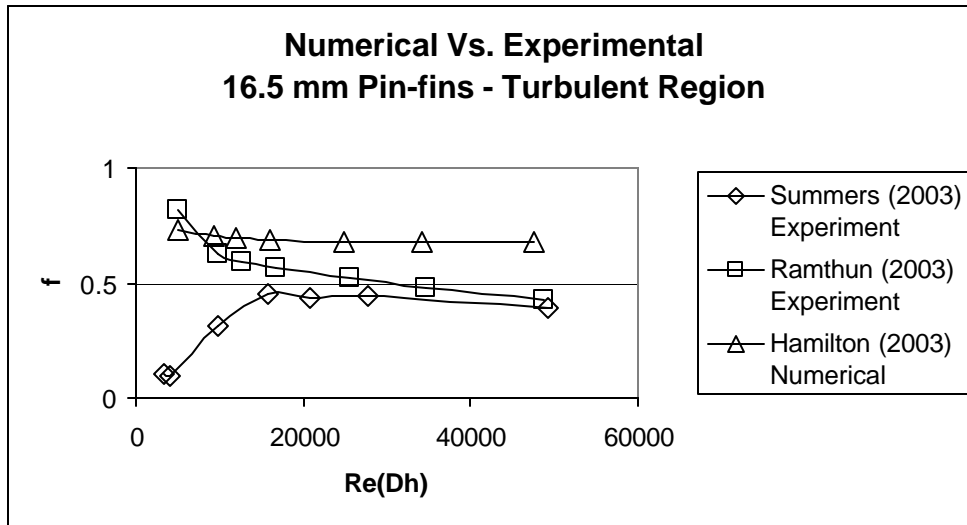
Figure 78.   Turbulent 16.5 mm set one comparative analysis, f vs. Re_{Dh}
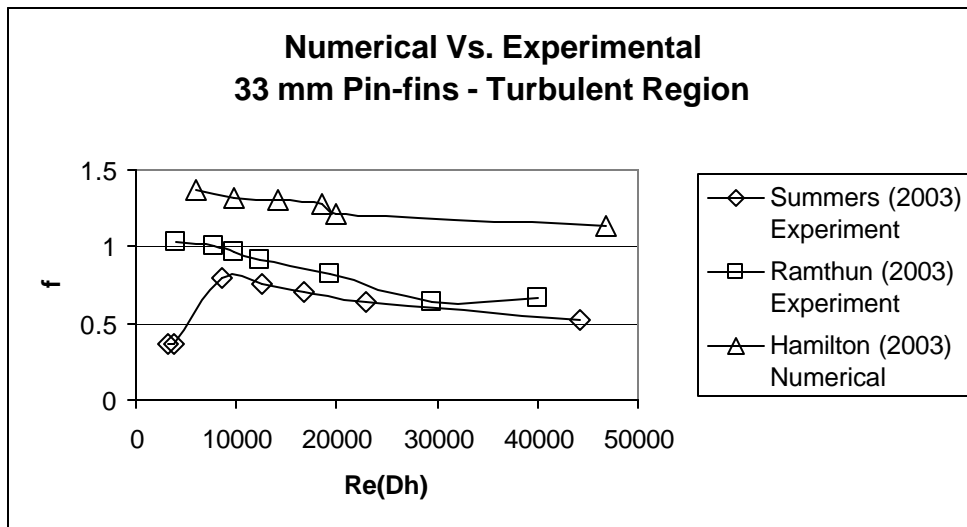
Figure 79.   Turbulent 33 mm set one comparative analysis, f vs. Re_{Dh}

As mentioned earlier the lower turbulent region was unstable due to the placement of the throttle valve at the inlet of the system inlet duct. To prevent this in the future all flow limiting devices should be maintained at the exit duct to prevent similar challenges.

2.   Laminar Range

Boulares (2003) performed a numerical analysis of a teardrop shaped pin-fin in the laminar and turbulent flow spectrums. There was a significant amount of turbulent data collected from the numerical runs however only the X/D, S/D and H/D of 1.5, 1.5, and 1.0 were performed in the laminar range. Figure (80) compares the numerical and experimental result for the Nusselt number versus Reynolds number. The data correlates

well with minor deviation of less than five percent in the mid-laminar range and larger errors of nearly 50 percent in the low laminar ranges. The experimental data was linear and the numerical model appeared less stable. This could be associated with the flow characteristics associated with very low velocity airflow over a cylindrical surface.

**Experimental Results of Teardrop Pin-fins
Laminar Region
Set 1 (1.5, 1.5,1.0)**
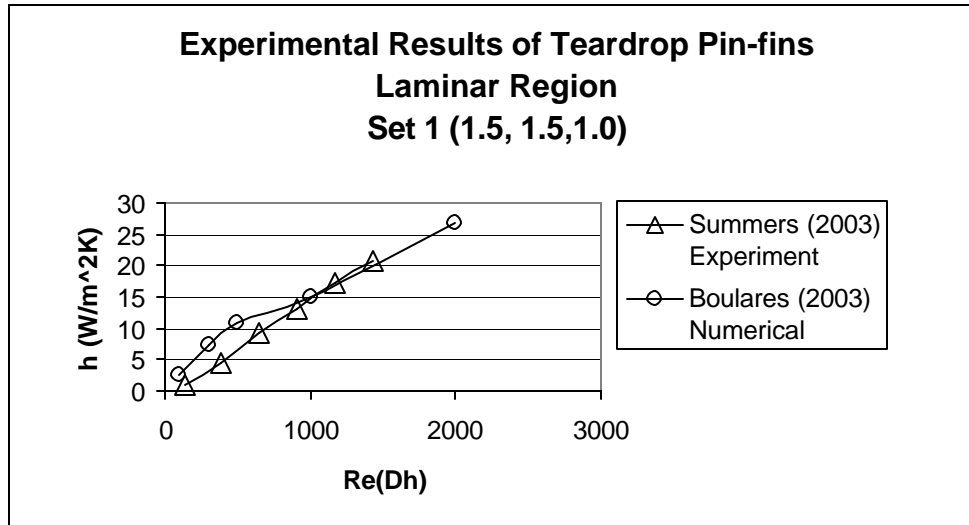
Figure 80.　　　Laminar teardrop set one comparative analysis, h vs. Re_{Dh}

**Experimental Results of Teardrop Pin-fins
Laminar Region
Set 1 (1.5, 1.5,1.0)**
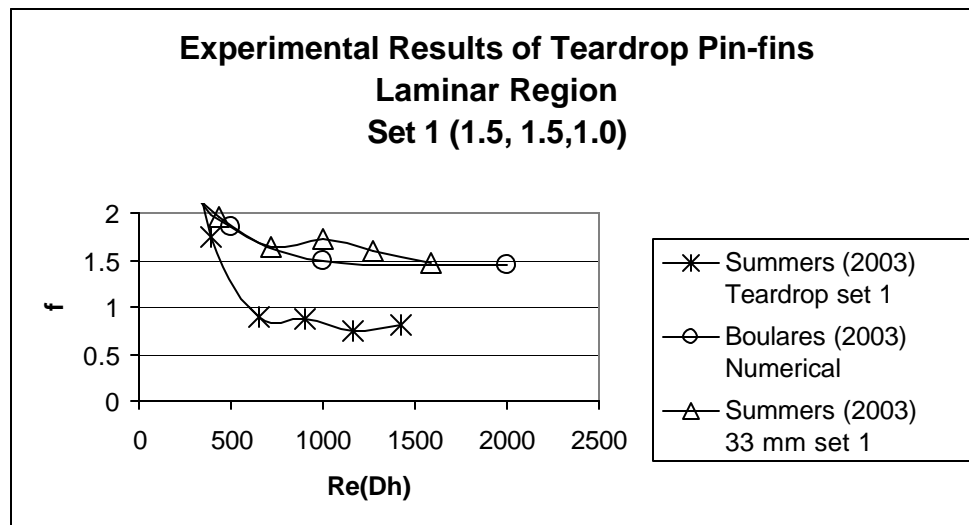
Figure 81.　　　Laminar teardrop set one comparative analysis, f vs. Re_{Dh}

Figure (81) shows the relationship between friction factor and Reynolds numbers in the laminar flow range. The teardrop friction factor was nearly one half that of the numerical. The 33 mm set one configurations was plotted to show that the numerical model resembled it more than the teardrop. Both pins appear the same to oncoming flow however the teardrop pin-fin has a tail to prevent flow separation. This should cause the

59

friction factor to decrease from the 33 mm pin-fin reading. The differential pressure analysis for Reynolds numbers less than 500 was unstable. The resolution of the differential pressure-monitoring device was not accurate enough.

Currently there is no numerical data available concerning cylindrical pin-fins in the laminar range. However research at the Naval Post-Graduate School is ongoing to develop such a model. Data from this thesis will help develop and validate that model.

VI. CONCLUSIONS AND RECOMMENDATIONS

A. CONCLUSIONS

1. Laminar Flow Analysis

The heat transfer data collected proved reliable and accurate for comparison to future numerical models. The 33 mm and teardrop pin-fins in a set one configuration performed the best regarding heat transfer coefficients. This was predicted based on the increased heat transfer areas provided by these pins and configurations. With the Nusselt number directly proportional to the heat transfer coefficient it was expected that the same pins would lead this number as well. This was not the case since two results happen when increasing pin size. The open volume of the system decreases as the flow area increases. Since the open volume decreased the hydraulic diameter of the system decreased as well. This can be seen in figure (82) under the configuration "1" data. This decrease in hydraulic diameter outweighed the increase in the heat transfer coefficient associated with larger pins. Therefore when switching from a smaller to a larger pin size the Nusselt number, based on hydraulic diameter, will decrease. This same principal applies to switching configurations. Whenever switching from a full set one configuration to a configuration with fewer pins the hydraulic diameter increases and the heat transfer coefficient decreases (figure 82). The effect of an increasing hydraulic diameter is nearly four times larger in the 33 mm, 66 mm, and teardrop pin-fins. The larger effect of the increasing hydraulic diameter outweighed the effects of the decreasing heat transfer coefficient. This resulted in the 33 mm, 66 mm, and teardrop pin-fin set three configurations to become more dominant in their group. This conclusion shows how smaller or less pins maybe a better choice in the laminar flow region.

The results of the differential pressure analysis revealed some positive results. There is now new data especially in the laminar range where the Reynolds number is greater than 800 that can be used to help develop future numerical models. However, design of the CHE will have to change to provide a more accurate measure of differential pressure in the lower laminar range.
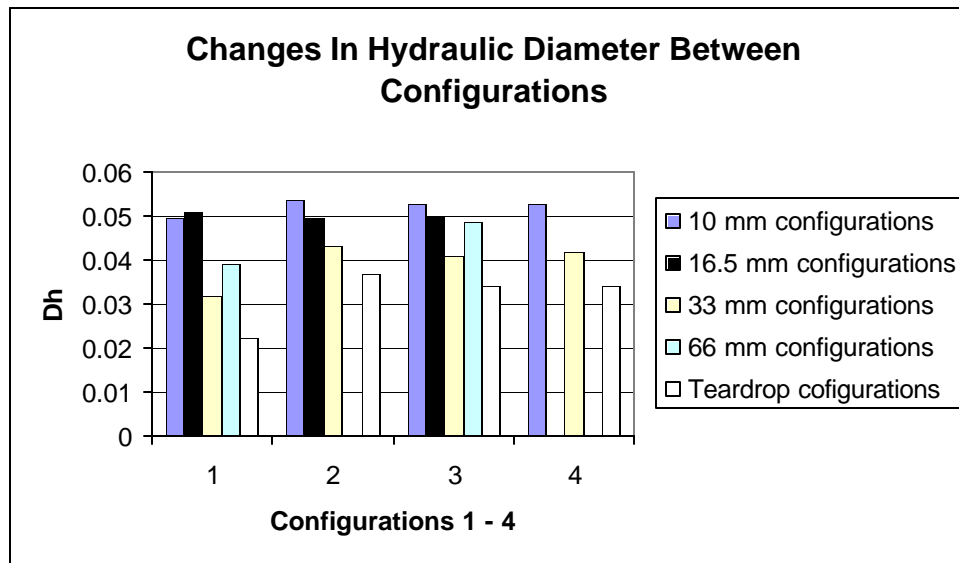
Figure 82.   Hydraulic diameter for each pin shape and configuration

The best performing pins regarding friction factor were the 10 mm and 16.5 mm pin-fins. This was expected since their geometry facilitated a smaller pressure drop. The heat transfer coefficient versus fluid power expenditure analysis resulted in the set one 10 mm pin-fin configuration to be the best performer in the laminar range. Other pin-fin configurations could achieve 10-15% higher however requiring a large increase in fluid power expenditure. Therefore based on the experimental data obtained the set one 10 mm pin-fin configuration was the top overall performer.

2.   Turbulent Flow Analysis

The turbulent data obtained in this research agreed well with previous numerical and experimental research conducted on the same CHE. The heat transfer characteristics showed similar trends as discussed in the laminar flow section. The heat transfer coefficient was dominated by total pin heat transfer surface area. The top pin-fin in this area was the teardrop in a set one configuration. The trends in the Nusselt number behaved similar to the pins in the laminar flow section. The top pin-fin in this area was the set three 33 mm configuration. If the set three teardrop configuration had been tested it probably would have been number one. In the turbulent region the increase in the heat transfer coefficient outweighs the decrease in hydraulic diameter when switching to larger pin sizes. This allowed the set three 33 mm pins to catch the set one 10 mm pins in the Nusselt versus Reynolds number category.

It was found in the differential pressure analysis that the trend in friction factor agreed with past numerical and experimental data. The region of agreement were for Reynolds numbers greater than 10,000. Some of the experimental data obtained by this research was invalid for Reynolds numbers equaling 2500 – 7500. The installed high capacity blower drawing air through a system possessing a 0.5-inch inlet throttle valve caused this. The system configuration resulted in large pressure drops that caused system leakage and masked the true CHE differential pressure. The challenge will be addressed further in the recommendations portion of this paper. Appendix D provides an uncertainty analysis for all calculations including the errors associated with the differential pressure measurement in the low laminar range.

The top performing pin-fins regarding friction factor were 10 mm pins in a set four configuration. Again this was expected since this configuration hosted the least resistance to airflow. In the heat transfer coefficient versus fluid power expenditure analysis the set one teardrop configuration performed the best. It provided the maximum heat transfer for a given pressure drop. For this reason it was selected as the number one performer of the turbulent region. Experimental data from the teardrop pin-fin was incorporated from Boulares (2003) research.

B.   RECOMMENDATIONS
1.   Differential Pressure Analysis

For an accurate laminar flow analysis, especially in the low Reynolds number spectrum, a change in the CHE design is required. The current inclined manometer can be read with an accuracy of plus or minus 0.001 inches of water (0.249 Pa). With flow rates that can be as low as 0.8 SCFM the differential pressure can be very difficult to distinguish. Required is a digital differential pressure detector capable of reading changes on the order of 0.0001 inches of water (0.0249 Pa). Since this is an unrealistic measurement further research in the lower Reynolds number region would require a larger CHE that exhibited proportionally larger differential pressures.

Placing filters or valves on the duct inlet to control system volumetric flow rate is not conducive to obtaining accurate data. It promotes system leakage and can causing

masking of true CHE differential pressure. These devices were needed because of the current system configuration. The system blower is powerful and without filters or a throttle valve on the system inlet lower turbulent flow regions would be impossible to achieve. To correct this deficiency a less powerful blower could be purchased or a more practical solution is to place a 2.5" throttle valve between the Omega FTB-940 turbine meter and exit duct bypass valves. This would significantly reduce any system leakage and provide more accurate differential pressure readings.

C.   FUTURE OF WORK

There are still many different pin geometries and configurations that could be tested. The amount of time required to disassemble, change pin configurations, and perform a full run takes about 12-14 hours. Therefore coordination between the numerical model makers and the person running the experiments is important. The flexibility of the numerical models is tremendous however should focus on the capabilities of the CHE. More applicable numerical data is needed in the turbulent range as well as the laminar. This will provide more comparable data to help improve both the quality of the models as well as the experiments.

APPENDIX A

A. NOMENCLATURE

$\bar{A}$	Average flow area (m^2)
A_{duct}	Duct area (m^2)
A_{wf}	Wetted area for flow (includes end walls) (m^2)
A_{wh}	Wetted area for heat (no end walls) (m^2)
CHE	Compact Heat Exchanger
Cp	Specific heat capacity (J/kg-K)
D, d	Pin diameter (m)
D_h	Hydraulic diameter (m)
E	Fluid friction power per unit surface area (W/m^2)
f	Friction factor
h	Heat transfer coefficient (W/m^2 -K)
$\bar{h}$	Average heat transfer coefficient (W/m^2 -K)
H	Pin height (m)
k	Thermal conductivity (W/m-K)
L	Length of CHE
$\dot{m}$	System mass flow rate (kg/sec)
N_p	Number of pins installed
Nu_{Dh}	Nusselt number based on hydraulic diameter
P_{dens}	Pressure for density (Pa)
P_{in}	Heat exchanger inlet pressure (Pa)
P_{man}	Manometer pressure (inch H$_2$0)
P_{NOAA}	Reference pressure from NOAA (inch H$_2$0)
P_{off}	Reference offset pressure (Pa)
P_{turb}	Heat Exchanger outlet pressure (Pa)
P_{vdc}	Voltage output of differential pressure transmitter (VDC)
$\Delta P, dp$	Heat exchanger differential pressure or pressure drop (Pa)
q	heat transfer rate (W)
$\dot{Q}$	Volumetric flow rate (m^3/s)
R	Gas constant (J/kg-K)
Re_{Dh}	Reynolds number based on hydraulic diameter
S	Span wise spacing (m)
T_{ave}	Average heat exchanger outlet temperature (K)
T_{in}	Heat exchanger inlet temperature (K)
T_{out}	Heat exchanger outlet temperature (K)
T_{wall}	End wall temperature (K)
ΔT	Temperature change across CHE (K)
ΔT_{lm}	Log mean bulk differential temperature (K)
$\bar{U}$	Average fluid velocity (m/sec)
V_{off}	Reference offset voltage, flow (VDC)
V_{open}	Open fluid volume in CHE
X	Stream wise spacing (m)

W	Width of CHE (m)
r	density (kg/m^3)
m	dynamic viscosity (Pa-s)

APPENDIX B

A.   PIN CONFIGURATIONS

(For all cases flow is left to right)

1.   10 mm Pin Data

Figures (83-86) show the various configurations tested for the 10 mm pin-fins.
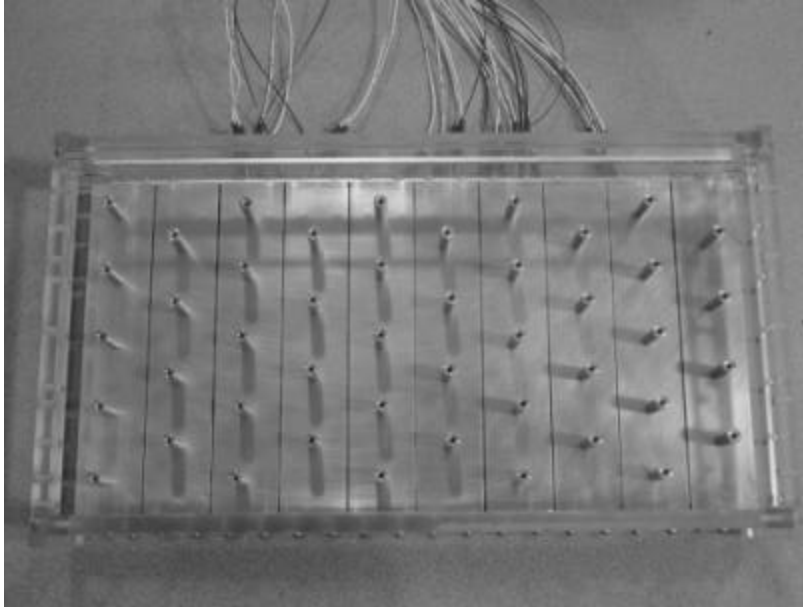
Figure 83.   10 mm set #1, S/D = 5.0 X/D = 5.0 H/D = 3.3
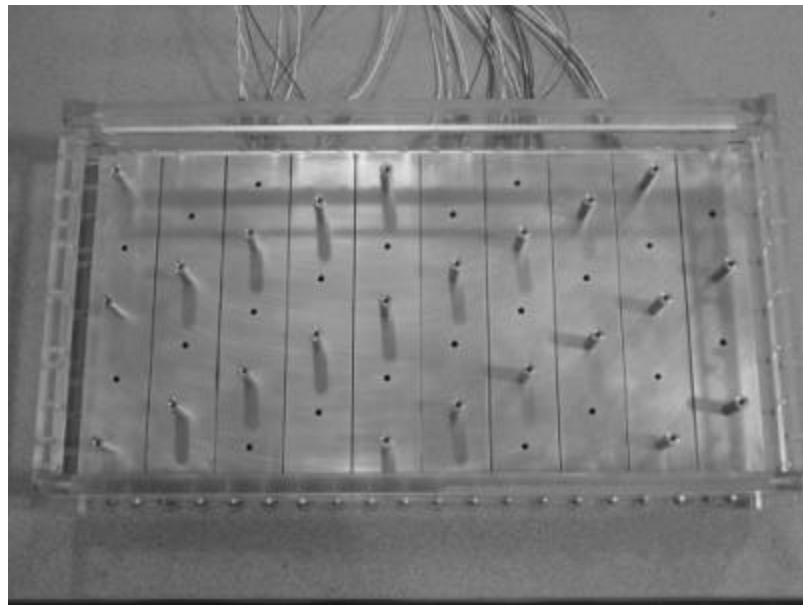
Figure 84.   10 mm set #2, S/D = 10.0 X/D = 10.0 H/D = 3.3
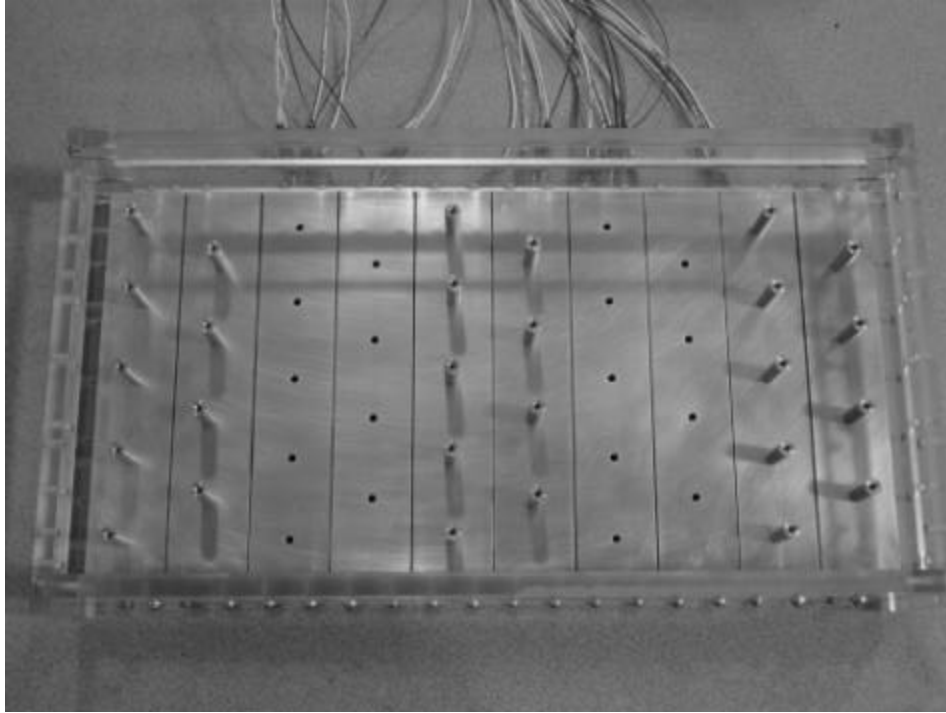
Figure 85.   10 mm set #3, S/D = 5.0 X/D = 10.0 H/D = 3.3
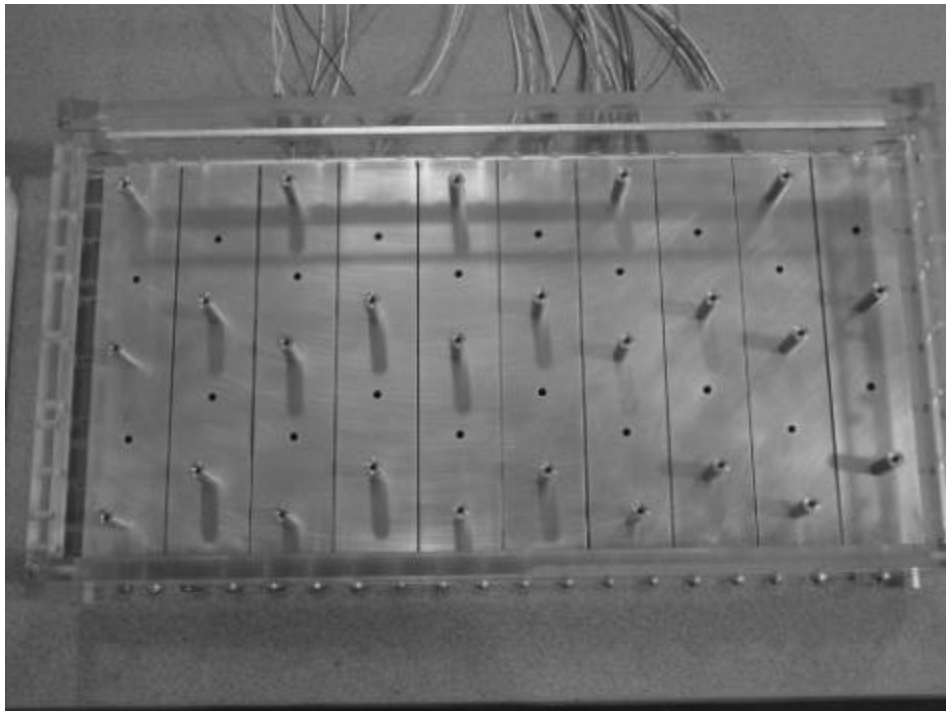
Figure 86.   10 mm set #4, S/D = 10.0 X/D = 5.0 H/D = 3.3

2. 16.5 mm Pin Data

Figures (87-90) show the various configurations tested for the 16.5 mm pin-fins.
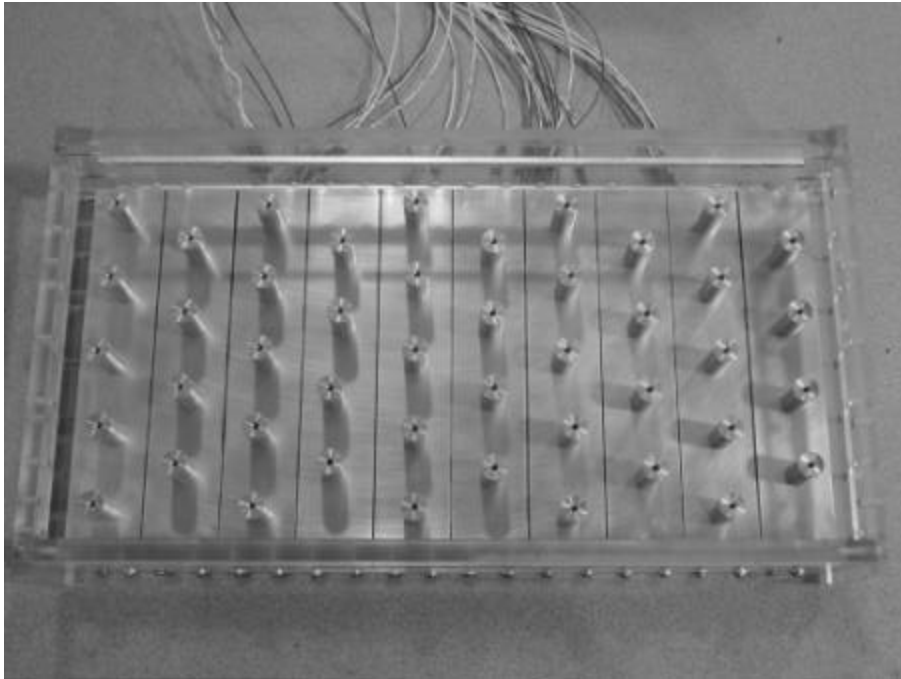
Figure 87. 16.5 mm set #1, S/D = 3.0 X/D = 3.0 H/D = 2.0
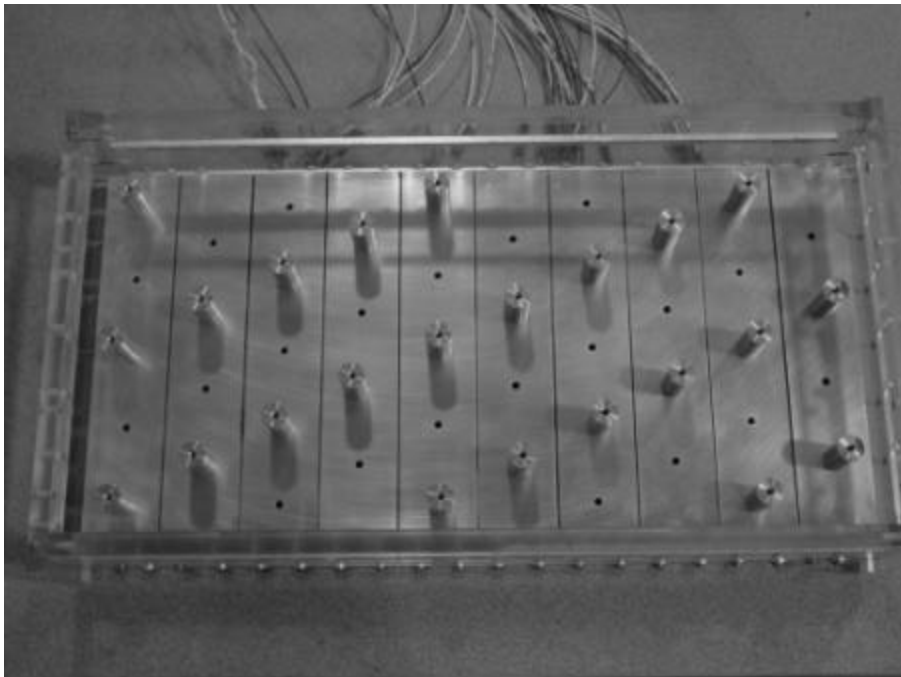
Figure 88. 16.5 mm set #2, S/D = 6.1 X/D = 6.0 H/D = 2.0
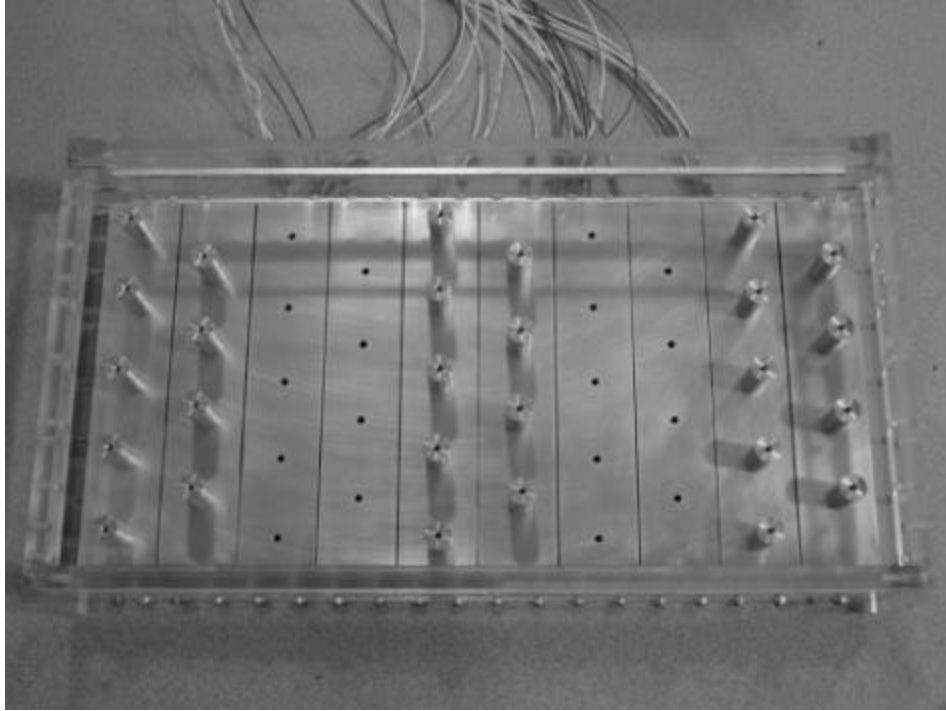
Figure 89.   16.5 mm set #3, S/D = 3.0 X/D = 6.1 H/D = 2.0
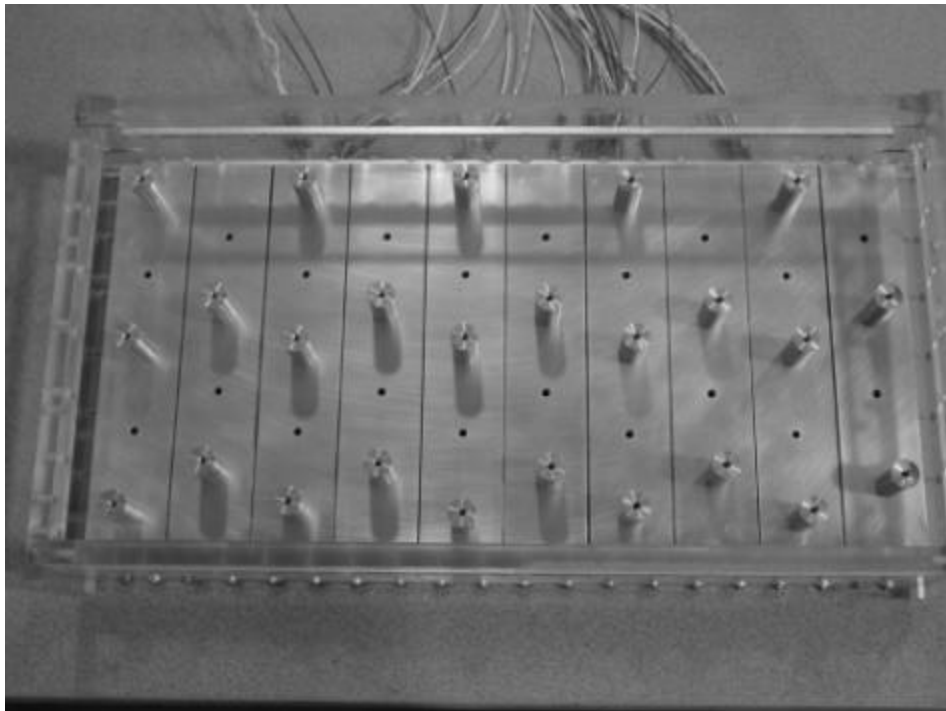
Figure 90.   16.5 mm set #4, S/D = 6.1 X/D = 3.0 H/D = 2.0

3. 33 mm Pin Data

Figures (91-94) show the various configurations tested for the 33 mm pin-fins.
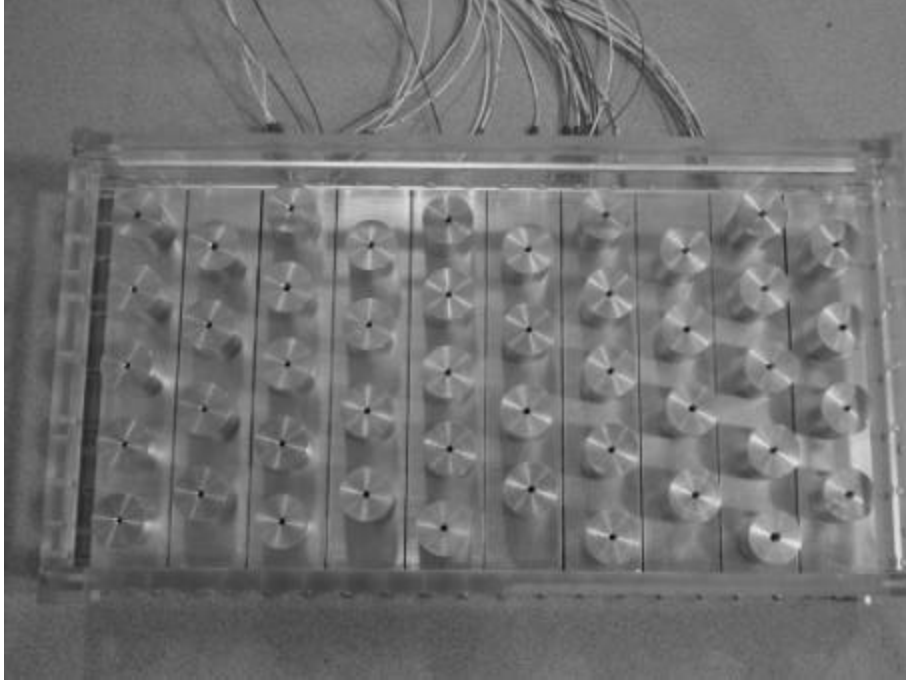
Figure 91.   33 mm set #1, S/D = 1.5 X/D = 1.5 H/D = 1.0
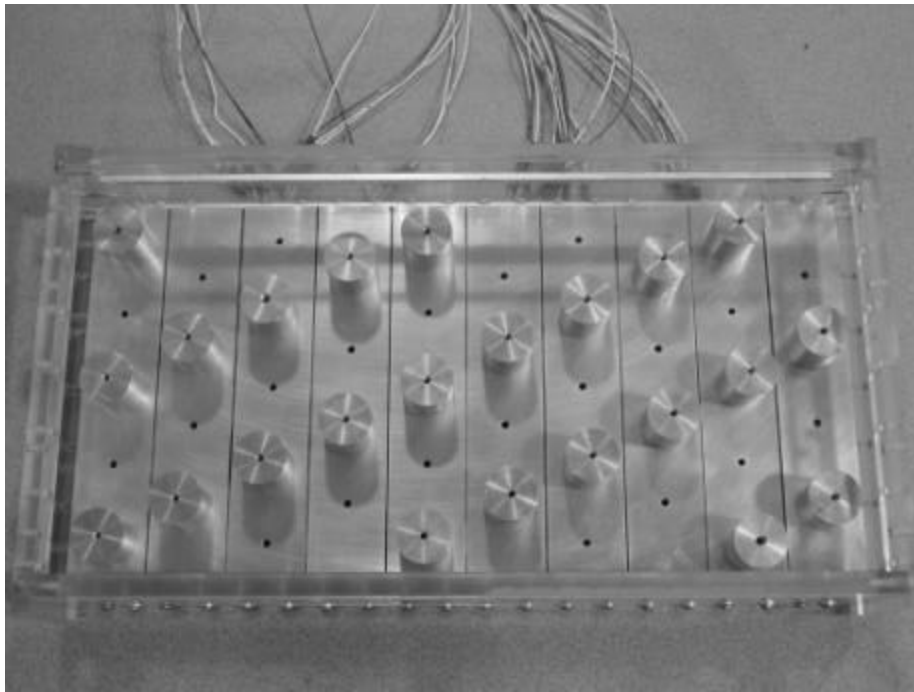
Figure 92.   33 mm set #2, S/D = 3.0 X/D = 3.0 H/D = 1.0
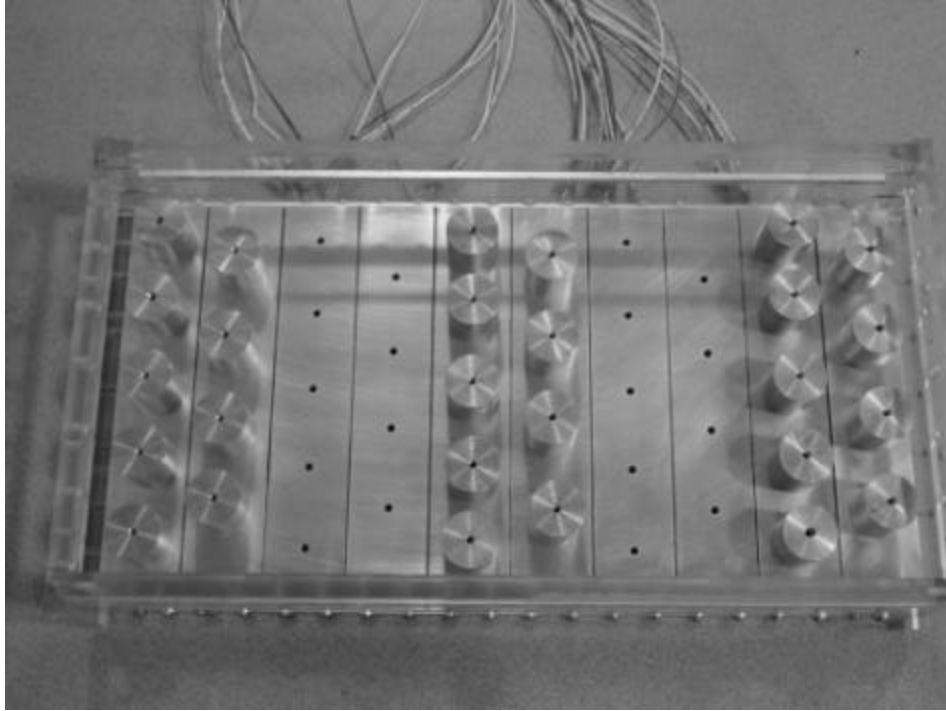
Figure 93.   33 mm set #3, S/D = 1.5 X/D = 3.0 H/D = 1.0
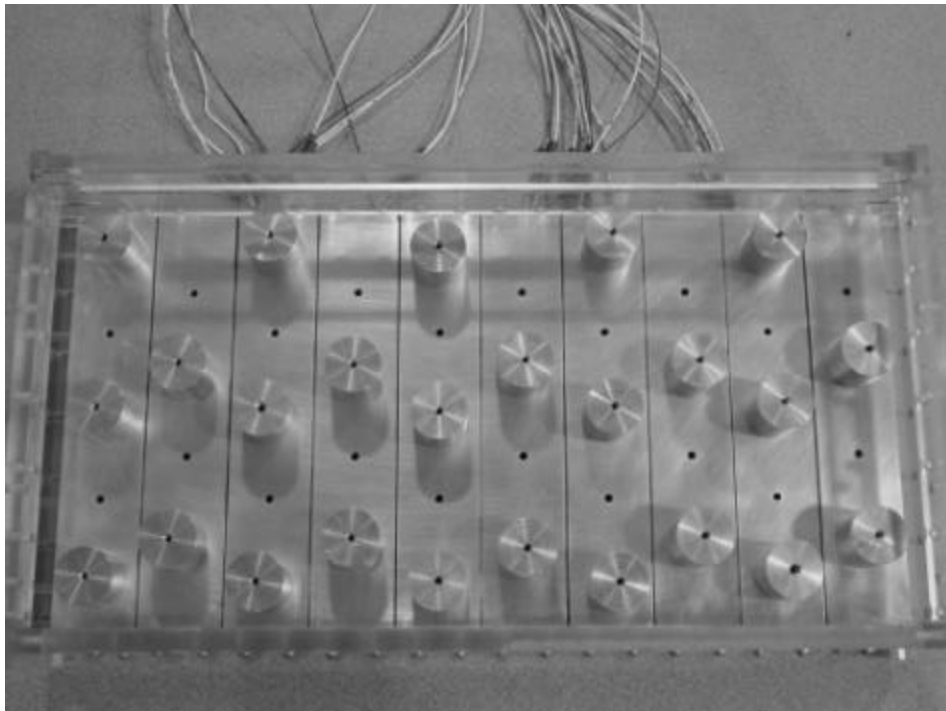
Figure 94.   33 mm set #4, S/D = 3.0 X/D = 1.5 H/D = 1.0

4.   66 mm Pin Data

Figures (95-96) show the various configurations tested for the 10 mm pin-fins. Only set numbers one and three were completed due to physical size constraints of pins and CHE.
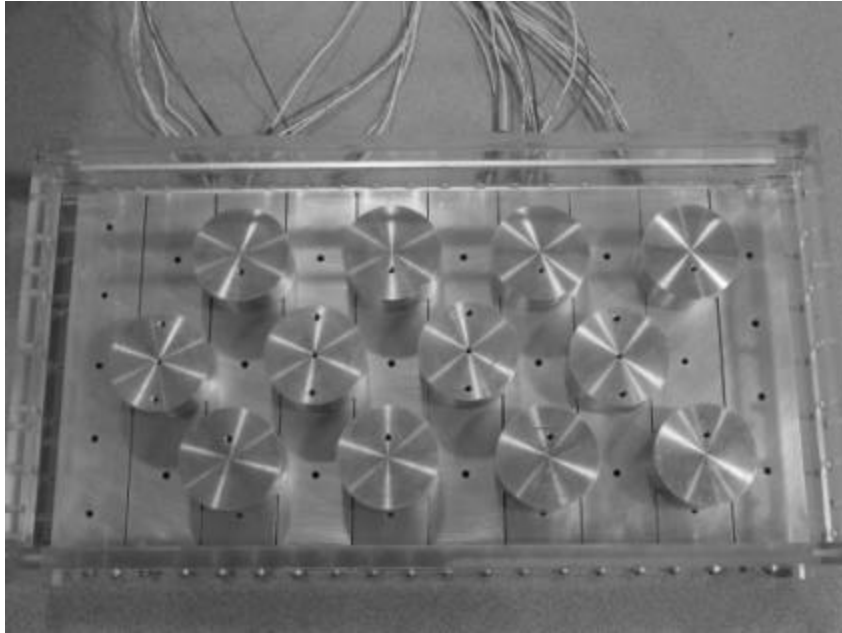
Figure 95.   66 mm set #1, S/D = 1.89 X/D = 0.76 H/D = 0.5
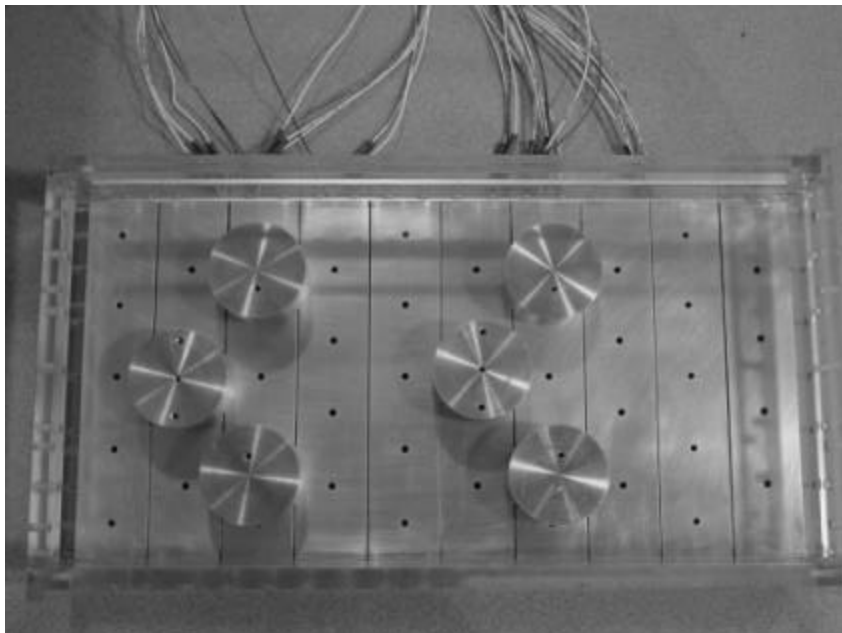
Figure 96.   66 mm set #3, S/D = 1.89 X/D = 1.52 H/D = 0.5

5. Teardrop Shape Pin Data

Figures (97-100) show the various configurations tested for the teardrop shaped pin-fins. The last row is filled with 33 mm cylindrical pin fins due to prevent pins from extending out of CHE and into the exit duct.
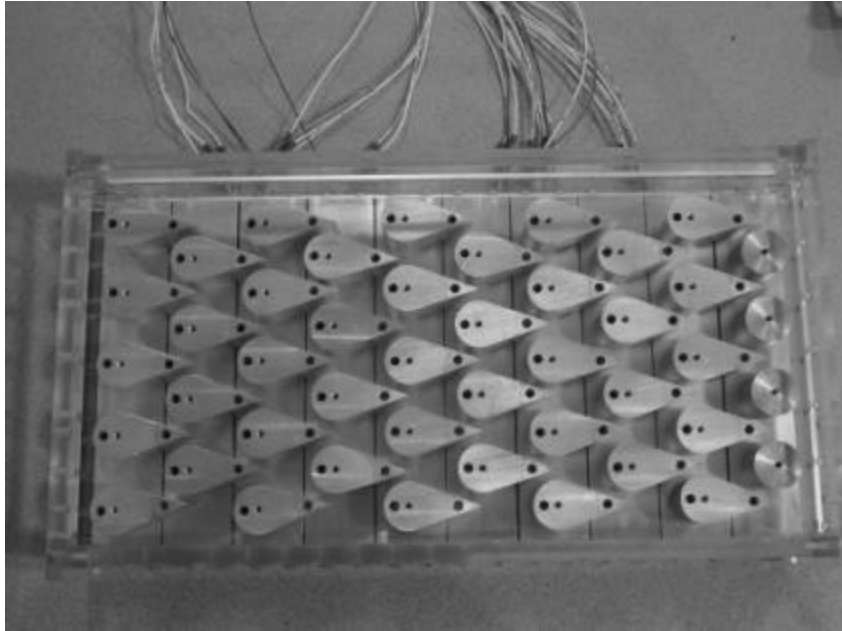
Figure 97.　　　Teardrop set #1, S/D = 1.5 X/D = 1.5 H/D = 1.0
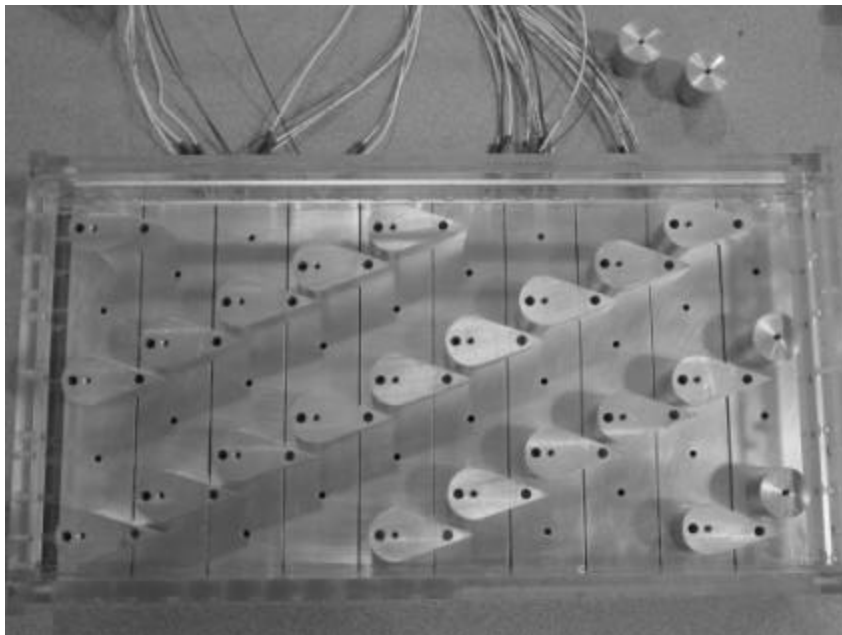
Figure 98.　　　Teardrop set #2, S/D = 3.0 X/D = 3.0 H/D = 1.0
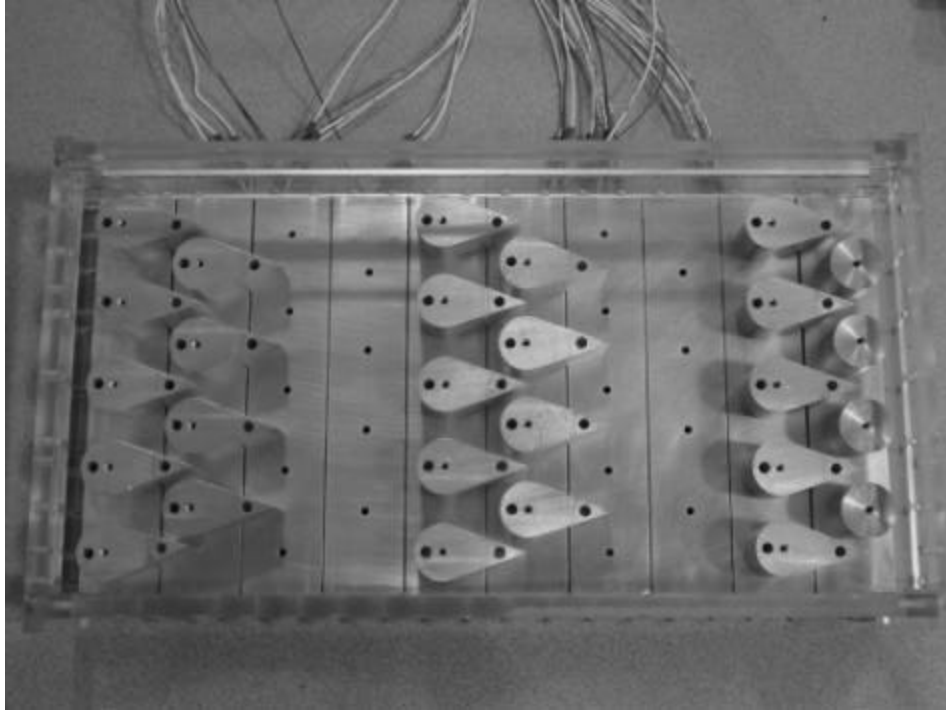
Figure 99.   Teardrop set #3, S/D = 1.5 X/D = 3.0 H/D = 1.0
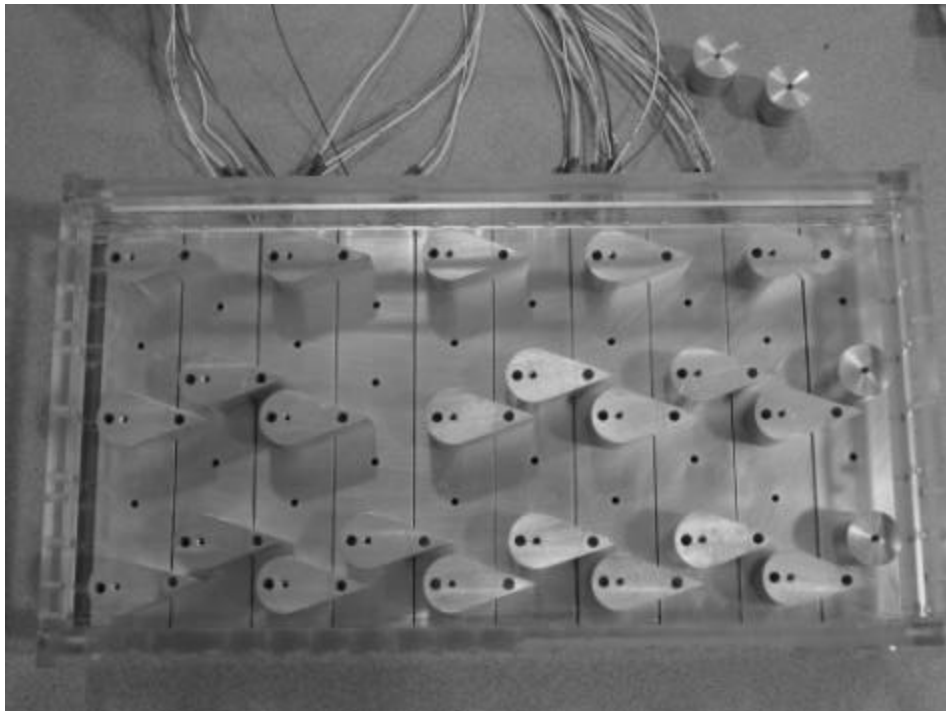
Figure 100.   Teardrop set #4, S/D = 3.0 X/D = 1.5 H/D = 1.0

THIS PAGE INTENTIONALLY LEFT BLANK

APPENDIX C

A.   EQUATIONS

1.   Conversions

a.   Volumetric flow - VDC to M³/sec:

$$\dot{Q}\left[\frac{m^3}{s}\right] = (\dot{Q}_{VDC}[VDC] - \dot{Q}off\,[VDC])0.0204\left[\frac{m^3}{sec-VDC}\right]$$

b.   Volumetric flow – SLPM to M³/sec:

$$\dot{Q}[\frac{m^3}{sec}] = (\dot{Q}[\frac{Liters}{min}])(\frac{1\min}{60sec})(0.001\frac{m^3}{Liter})$$

c.   Pressure – VDC to Pascals:

$$P[Pa] = (P_{VDC}[VDC] - P_{off[VDC]})(248.84[\frac{Pa}{inH_2O}])(6.25[\frac{inH2O]}{VDC}])$$

d.   Pressure - Inches of water to Pascals:

$$P[Pa] = (P_{inH_2O})(248.84[\frac{Pa}{inH_2O}])$$

e.   Pressure – Inches of Mercury to Pascals:

$$P[Pa] = (P_{inHg})(3386.388[\frac{Pa}{inHg}])$$

2.   Reynolds Number (Re$_{Dh)}$

a.   Reynolds number based on hydraulic diameter:

$$\mathrm{Re}_{D_h} = \frac{r\bar{U}D_h}{m}$$

b.   Hydraulic diameter:

$$D_h[m] = \frac{4V_{open}}{A_{wf}}$$

c.   Average fluid velocity:

$$\bar{U}[\frac{m}{\sec}] = \frac{\dot{m}}{\bar{\bar{r}}\bar{A}}$$

d.   Dynamic viscosity using Sutherland Law:

$$\boldsymbol{m}[Pa - \sec] = \boldsymbol{m_0}\left(\frac{T}{T_0}\right)^{\frac{3}{2}}\left(\frac{T_0 + S}{T + S}\right)$$

where: $T_0 = 273K$, $S_{air} = 110.4K$, $\boldsymbol{m_0} = 1.71E - 5 \; \dfrac{kg}{m \bullet s}$

e.   Density taken at exit of CHE:

$$\boldsymbol{r}[\frac{kg}{m^3}] = (\frac{P_{dens}}{RT})$$

f.   Open fluid volume of CHE:

$$V_{open}[m^3] = (LWH) - (\frac{N_p \boldsymbol{p} D_{pin}^2 H}{4})$$

     * This equation is for the cylindrical shaped pins.

$$V_{open}[m^3] = (LWH) - N_p[(\frac{\boldsymbol{p} D_{pin}^2 H}{8}) + (\frac{0.05 * DH}{2})]$$

     * This equation is for the teardrop shaped pins.

g.   Wetted area for flow (includes end walls):

$$A_{wf}[m^2] = 2\left(LW + HL - \frac{45\boldsymbol{p} D^2}{4}\right) + 45\boldsymbol{p} DH$$

     * This equation is for the cylindrical shaped pins.

$$A_{wf}[m^2] = 2\left(LW + HL - N_p[(\frac{\boldsymbol{p} D^2}{8}) - (\frac{0.05D}{2})]\right) + N_p[(\frac{\boldsymbol{p} DH}{2}) + (2H(0.5^2 * 0.0165^2)^{0.5})]$$

     * This equation is for the teardrop shaped pins.

h.   System mass flow rate:

$$\dot{m}[\frac{kg}{\sec}] = \dot{Q}_{measured}\boldsymbol{r}$$

i. Average flow area:

$$\bar{A}[m^2] = \frac{V_{open}}{L}$$

j. Final Reynolds number after substitution:

$$\mathrm{Re}_{D_h} = \frac{P_{turb}\dot{Q}_{measured}D_h}{RT\bar{A}\boldsymbol{m}}$$

3. Heat Transfer Coefficient (h)

a. Heat transfer coefficient:

$$h[\frac{W}{m^2-K}] = \frac{q}{(\Delta T_{lm})(A_{wh})}$$

b. Heat transfer rate:

$$q[Watts] = \dot{m}C_p(T_{outave} - T_{in})$$

c. Log mean bulk differential temperature:

$$\Delta T_{lm}[K] = \frac{(T_{wall} - T_{in}) - (T_{wall} - T_{out})}{\ln\left(\dfrac{T_{wall} - T_{in}}{T_{wall} - T_{out}}\right)}$$

d. Wetted area for heat calculations (no end walls):

$$A_{wh}[m^2] = 2\left(LW - \frac{N_p\boldsymbol{p}D^2}{4}\right) + N_p\boldsymbol{p}DH$$

* This equation is for the cylindrical shaped pins.

$$A_{wh}[m^2] = 2\left(LW - N_p[(\frac{\boldsymbol{p}D^2}{8}) + (\frac{0.05D}{2})]\right) + N_p[(\frac{\boldsymbol{p}DH}{2}) + (2H(0.5^2 * 0.0165^2)^{0.5})]$$

* This equation is for the teardrop shaped pins.

e. System mass flow rate:

$$\dot{m}[\frac{kg}{\sec}] = \dot{Q}_{measured}\boldsymbol{r}$$

4. Nusselt Number (Nu_{Dh})

a. Nusselt number based on hydraulic diameter

$$Nu_{D_h} = \frac{\overline{h}_{array} D_h}{k}$$

b. Average heat transfer coefficient for the CHE array:

$$\overline{h}_{array}[\frac{watts}{m^2 - K}] = \frac{q}{A_{wh}\Delta T_{lm}}$$

c. Hydraulic diameter, D_h, is the same as for Reynolds number:

$$D_h[m] = \frac{4V_{open}}{A_{wf}}$$

d. Open fluid volume of CHE:

$$V_{open}[m^3] = (LWH) - (\frac{N_p \boldsymbol{p} D^2_{pin} H}{4})$$

* This equation is for the cylindrical shaped pins.

$$V_{open}[m^3] = (LWH) - N_p[(\frac{\boldsymbol{p} D^2_{pin} H}{8}) + (\frac{0.05 * DH}{2})]$$

* This equation is for the teardrop pins.

e. Wetted area for flow (includes end walls):

$$A_{wf}[m^2] = 2\left(LW + HL - \frac{45\boldsymbol{p} D^2}{4}\right) + 45\boldsymbol{p} DH$$

* This equation is for the cylindrical shaped pins.

$$A_{wf}[m^2] = 2\left(LW + HL - N_p[(\frac{\boldsymbol{p} D^2}{8}) + (\frac{0.05D}{2})]\right) + N_p[(\frac{\boldsymbol{p} DH}{2}) + (2H(0.5^2 * 0.0165^2)^{0.5})]$$

* This equation is for the teardrop shaped pins.

f. Log mean bulk differential temperature:

$$\Delta T_{lm}[K] = \frac{(T_{wall} - T_{in}) - (T_{wall} - T_{out})}{\ln\left(\frac{T_{wall} - T_{in}}{T_{wall} - T_{out}}\right)}$$

g.   Wetted area for heat calculations (no end walls):

$$A_{wh}[m^2] = 2\left(LW - \frac{N_p \boldsymbol{p} D^2}{4} \right) + N_p \boldsymbol{p} DH$$

* This equation is for the cylindrical shaped pins.

$$A_{wh}[m^2] = 2\left(LW - N_p[(\frac{\boldsymbol{p} D^2}{8}) + (\frac{0.05D}{2})] \right) + N_p[(\frac{\boldsymbol{p} DH}{2}) + (2H(0.5^2 * 0.0165^2)^{0.5})]$$

* This equation is for the teardrop shaped pins.

h.   System mass flow rate:

$$\dot{m}[\frac{kg}{\sec}] = \dot{Q}_{measured} \, \boldsymbol{r}$$

5.   **Friction Factor (f)**

a.   Friction factor:

$$f = \frac{\Delta P_{CHE} D_h}{\frac{1}{2} \boldsymbol{r} \bar{U}^2 L}$$

b.   Differential pressure across CHE:

$$\Delta P_{CHE} = \Delta P_{measured} - P_{off}$$

c.   Hydraulic diameter, D_h, is the same as for Reynolds number:

$$D_h[m] = \frac{4V_{open}}{A_{wf}}$$

d.   Open fluid volume of CHE:

$$V_{open}[m^3] = (LWH) - (\frac{N_p \boldsymbol{p} D_{pin}^2 H}{4})$$

* This equation is for the cylindrical shaped pins.

$$V_{open}[m^3] = (LWH) - N_p[(\frac{\boldsymbol{p} D_{pin}^2 H}{8}) + (\frac{0.05 * DH}{2})]$$

* This equation is for the teardrop pins.

e. Wetted area for flow (includes end walls):

$$A_{wf}[m^2] = 2\left(LW + HL - \frac{45\mathbf{p}D^2}{4}\right) + 45\mathbf{p}\,DH$$

* This equation is for the cylindrical shaped pins.

$$A_{wf}[m^2] = 2\left(LW + HL - N_p[(\frac{\mathbf{p}D^2}{8}) + (\frac{0.05D}{2})]\right) + N_p[(\frac{\mathbf{p}DH}{2}) + (2H(0.5^2 * 0.0165^2)^{0.5})]$$

* This equation is for the teardrop shaped pins.

f. Density taken at exit of CHE:

$$\mathbf{r}[\frac{kg}{m^3}] = (\frac{P_{dens}}{RT})$$

g. Average fluid velocity:

$$\bar{U}[\frac{m}{sec}] = \frac{\dot{m}}{\mathbf{r}\bar{A}}$$

h. System mass flow rate:

$$\dot{m}[\frac{kg}{sec}] = \dot{Q}_{measured}\,\mathbf{r}$$

i. Average flow area:

$$\bar{A}[m^2] = \frac{V_{open}}{L}$$

6.   Frictional Power Expenditure (E)

a. Frictional power expenditure:

$$E[\frac{watts}{m^2}] = \frac{\dot{Q}_{measured}\Delta P_{CHE}}{A_{wf}}$$

b. Differential pressure across CHE:

$$\Delta P_{CHE} = \Delta P_{measured} - P_{off}$$

c.   Wetted area for flow (includes end walls):

$$A_{wf}[m^2] = 2\left(LW + HL - \frac{45\boldsymbol{p}D^2}{4}\right) + 45\boldsymbol{p}DH$$

* This equation is for the cylindrical shaped pins.

$$A_{wf}[m^2] = 2\left(LW + HL - N_p[(\frac{\boldsymbol{p}D^2}{8}) - (\frac{0.05D}{2})]\right) + N_p[(\frac{\boldsymbol{p}DH}{2}) + (2H(0.5^2 * 0.0165^2)^{0.5})] *$$

* This equation is for the teardrop shaped pins.

83

THIS PAGE INTENTIONALLY LEFT BLANK

APPENDIX D

A.   UNCERTAINTY ANALYSIS

The method of determining the uncertainty analysis came from Kline and McClintock (1953). The analysis will be calculated for the Reynolds number, Nusselt number, and friction factor. The governing equation is as follows:

$$W_R = \left[\left(\frac{\partial R}{\partial x_1} W_1\right)^2 + \left(\frac{\partial R}{\partial x_2} W_2\right)^2 + \cdots + \left(\frac{\partial R}{\partial x_n} W_n\right)^2\right]^{1/2}$$

Where:

R is a given function of the independent variables $x_1, x_2, \ldots x_n$.

W_R is the uncertainty.

1. Reynolds Number

$$\text{Re}_{D_h} = \frac{r\bar{U}D_h}{m}$$

$$\frac{W\,\text{Re}_{D_h}}{\text{Re}_{D_h}} = \sqrt{\left(\frac{W_r}{r}\right)^2 + \left(\frac{W_{Dh}}{D_h}\right)^2 + \left(\frac{W_{\bar{U}}}{\bar{U}}\right)^2}$$

The uncertainty associated with the Reynolds number is base on density, average fluid velocity, hydraulic diameter, and dynamic viscosity. The dynamic viscosity will be treated as a constant and three variables will be analyzed.

a.   *Density*

$$\frac{W_r}{r} = \left[\left(\frac{W_p}{p}\right)^2 + \left(\frac{W_T}{T}\right)^2\right]^{1/2} = \left[\left(\frac{1.0025}{101325}\right)^2 + \left(\frac{0.5}{312}\right)^2\right]^{1/2} = 0.0016$$

- 1.0025 represents the 0.25% error associated with the pressure transducer.

85

- 0.5 K represents the error associated with the thermocouples.

- 101325 Pascals represents maximum pressure .

- 312 K represents max heater temperature.

b. *Hydraulic Diameter*

$$\frac{W_{Dh}}{D_h} = \left[\left(\frac{W_{Vopen}}{V_{open}}\right)^2 + \left(\frac{W_{Aw}}{A_w}\right)^2\right]^{1/2}$$

Where,

$$\frac{W_{Vopen}}{V_{open}} = \left[\left(\frac{W_x}{x}\right)^2 + \left(\frac{W_y}{y}\right)^2 + \left(\frac{W_z}{z}\right)^2\right]^{1/2} = \left[\left(\frac{3}{500}\right)^2 + \left(\frac{1}{250}\right)^2 + \left(\frac{0.5}{33}\right)^2\right]^{1/2} = 0.017$$

and

$$\frac{W_{Aw}}{A_w} = \left[\left(\frac{W_x}{x}\right)^2 + \left(\frac{W_y}{y}\right)^2\right]^{1/2} = \left[\left(\frac{3}{500}\right)^2 + \left(\frac{1}{250}\right)^2\right]^{1/2} = 0.007$$

therefore,

$$\frac{W_{Dh}}{D_h} = \left[\left(\frac{W_{Vopen}}{V_{open}}\right)^2 + \left(\frac{W_{Aw}}{A_w}\right)^2\right]^{1/2} = 0.018$$

- 3mm/500mm represents the uncertainty in length in the X-direction.

- 1mm/250mm represents the uncertainty in length in the Y-direction.

- 0.5mm/33mm represents the uncertainty in length in the Z-direction.

c. *Average Fluid Velocity*

This value had to be calculated twice since two separate meters were used for laminar and pressure calculations.

(1). Laminar

$$\frac{W_{\bar{U}}}{\bar{U}} = \left[\left(\frac{W_{\dot{Q}}}{\dot{Q}}\right)^2 + \left(\frac{W_{\bar{A}}}{\bar{A}}\right)^2\right]^{1/2}$$

where,

$$\frac{W_{\dot{Q}}}{\dot{Q}} = \left[\left(\frac{W_V}{V_f}\right)^2\right]^{1/2} = \left[\left(\frac{0.015}{300}\right)^2\right]^{1/2} = 0.00005$$

and

$$\frac{W_{\bar{A}}}{\bar{A}} = \left[\left(\frac{W_{Vopen}}{V_{open}}\right)^2 + \left(\frac{W_L}{L}\right)^2\right]^{1/2} = \left[(0.017)^2 + (0.006)^2\right]^{1/2} = 0.018$$

therefore,

$$\frac{W_{\bar{U}}}{\bar{U}} = \left[\left(\frac{W_{\dot{Q}}}{\dot{Q}}\right)^2 + \left(\frac{W_{\bar{A}}}{\bar{A}}\right)^2\right]^{1/2} = \left[(0.00005)^2 + (0.018)^2\right]^{1/2} = 0.018$$

- 0.015 represent the 1.5% uncertainty associated with the Omega FMA-1844 mass flow meter.
- 0.017 represents the total uncertainty of the open volume.
- 0.018 represents the total uncertainty of the average flow area.

(2) Turbulent

$$\frac{W_{\dot{Q}}}{\dot{Q}} = \left[\left(\frac{W_V}{V_f}\right)^2\right]^{1/2} = \left[\left(\frac{0.03}{0.635VDC}\right)^2\right]^{1/2} = 0.0472$$

and

$$\frac{W_{\bar{A}}}{\bar{A}} = \left[\left(\frac{W_{Vopen}}{V_{open}}\right)^2 + \left(\frac{W_L}{L}\right)^2\right]^{1/2} = \left[(0.017)^2 + (0.006)^2\right]^{1/2} = 0.018$$

therefore,

$$\frac{W_{\bar{U}}}{\bar{U}} = \left[\left(\frac{W_{\dot{Q}}}{\dot{Q}} \right)^2 + \left(\frac{W_{\bar{A}}}{\bar{A}} \right)^2 \right]^{1/2} = \left[(0.0472)^2 + (0.018)^2 \right]^{1/2} = 0.051$$

- 0.03 represent the 3.0% uncertainty associated with the Omega FTB-940 turbine mass flow meter.
- 0.017 represents the total uncertainty of the open volume.
- 0.018 represents the total uncertainty of the average flow area.

d. *Reynolds Number Uncertainty*

(1) Laminar

$$\frac{W_{Re_{Dh}}}{Re_{Dh}} = \left[\left(\frac{W_r}{r} \right)^2 + \left(\frac{W_{Dh}}{D_h} \right)^2 + \left(\frac{W_{\bar{U}}}{\bar{U}} \right)^2 \right]^{1/2} = \left[(0.0016)^2 + (0.018)^2 + (0.018)^2 \right]^{1/2} = 0.0255$$

- Based on maximum flow the max uncertainty is 2.55%. This number would decrease as flow decreased.

(2) Turbulent

$$\frac{W_{Re_{Dh}}}{Re_{Dh}} = \left[\left(\frac{W_r}{r} \right)^2 + \left(\frac{W_{Dh}}{D_h} \right)^2 + \left(\frac{W_{\bar{U}}}{\bar{U}} \right)^2 \right]^{1/2} = \left[(0.0016)^2 + (0.051)^2 + (0.018)^2 \right]^{1/2} = 0.054$$

- Based on maximum flow the max uncertainty is 5.4%. This number would decrease as flow decreased.

2. Nusselt Number

$$Nu_{Dh} = \frac{hD_h}{k},$$

Where,

$$h = \frac{q}{A_w \Delta T_{lm}}$$

therefore,

$$\frac{W_{Nu_{Dh}}}{Nu_{Dh}} = \left[\left(\frac{W_h}{h} \right)^2 + \left(\frac{W_{Dh}}{D_h} \right)^2 \right]^{1/2}$$

88

and

$$\frac{W_h}{h} = \left[\left(\frac{W_q}{q}\right)^2 + \left(\frac{W_{Aw}}{A_w}\right)^2 + \left(\frac{W_{\Delta T_{lm}}}{\Delta T_{lm}}\right)^2\right]^{1/2}$$

The uncertainties for hydraulic diameter, heat transfer rate, wetted surface area and bulk log mean differential temperature must be determined. Thermal conductivity will be assumed constant and the values of hydraulic diameter and wetted surface area will be the same as for the Reynolds number.

$$\frac{W_{Dh}}{D_h} = \left[\left(\frac{W_{Vopen}}{V_{open}}\right)^2 + \left(\frac{W_{Aw}}{A_w}\right)^2\right]^{1/2} = 0.018$$

and

$$\frac{W_{Aw}}{A_w} = \left[\left(\frac{W_x}{x}\right)^2 + \left(\frac{W_y}{y}\right)^2\right]^{1/2} = \left[\left(\frac{3}{500}\right)^2 + \left(\frac{1}{250}\right)^2\right]^{1/2} = 0.007$$

a. ***Heat Transfer Rate***

$$\frac{W_q}{q} = \left[\left(\frac{W_q}{q}\right)^2\right]^{1/2} = \frac{8.387}{1200} = 0.007$$

- 8.387 is based on how long each heater is on during a given cycle. The total run time is 20 minutes or 1200 seconds.

b. ***Bulk Differential Log Mean Temperature***

$$\frac{W_{\Delta T_{lm}}}{\Delta T_{lm}} = \frac{0.5K}{9.5} = 0.0526$$

- 0.5 (k) represents the uncertainty of each thermocouple and the max bulk differential temperature observed was approximately 9.5K.

89

c. *Nusselt Number Uncertainty*

$$\frac{W_{Nu_{Dh}}}{Nu_{Dh}} = \left[\left(\frac{W_q}{q}\right)^2 + \left(\frac{W_{Aw}}{A_w}\right)^2 + \left(\frac{W_{\Delta T_{lm}}}{\Delta T_{lm}}\right)^2 + \left(\frac{W_{Dh}}{D_h}\right)^2\right]^{1/2} =$$

$$\left[(0.007)^2 + (0.007)^2 + (0.0526)^2 + (0.018)^2\right]^{1/2} = 0.0564$$

- The overall uncertainty for the Nusselt number is 5.64%. This number can increase as the bulk differential mean temperature decreases.

3. Friction Factor

$$f = \frac{2\Delta p D_h}{r\bar{U}^2 L},$$

$$\frac{W_f}{f} = \left[\left(\frac{W_{\Delta p}}{\Delta p}\right)^2 + \left(\frac{W_{Dh}}{D_h}\right)^2 + \left(\frac{W_r}{r}\right)^2 + \left(\frac{W_L}{L}\right)^2\right]^{1/2}$$

The uncertainty of friction factor is based on CHE differential pressure, hydraulic diameter, density, CHE length, and average fluid velocity. All except the differential pressure have been determined and are as follows:

$$\frac{W_{Dh}}{D_h} = \left[\left(\frac{W_{Vopen}}{V_{open}}\right)^2 + \left(\frac{W_{Aw}}{A_w}\right)^2\right]^{1/2} = 0.018$$

$$\frac{W_r}{r} = \left[\left(\frac{W_p}{p}\right)^2 + \left(\frac{W_T}{T}\right)^2\right]^{1/2} = \left[\left(\frac{1.0025}{101325}\right)^2 + \left(\frac{0.5}{312}\right)^2\right]^{1/2} = 0.0016$$

$$\frac{W_L}{L_x} = \left[\left(\frac{W_x}{x}\right)^2\right]^{1/2} = \left[\left(\frac{3}{500}\right)^2\right]^{1/2} = 0.006$$

For laminar:

$$\frac{W_{\bar{U}}}{\bar{U}} = \left[\left(\frac{W_{\dot{Q}}}{\dot{Q}}\right)^2 + \left(\frac{W_{\bar{A}}}{\bar{A}}\right)^2\right]^{1/2} = \left[(0.00005)^2 + (0.018)^2\right]^{1/2} = 0.018$$

For turbulent:

$$\frac{W_{\bar{U}}}{\bar{U}} = \left[\left(\frac{W_{\dot{Q}}}{\dot{Q}}\right)^2 + \left(\frac{W_{\bar{A}}}{\bar{A}}\right)^2\right]^{1/2} = \left[(0.0472)^2 + (0.018)^2\right]^{1/2} = 0.051$$

$$\frac{W_{Aw}}{A_w} = \left[\left(\frac{W_x}{x}\right)^2\right]^{1/2} = \left[\left(\frac{3}{500}\right)^2\right]^{1/2} = 0.006$$

a.   *Differential Pressure*

$$\frac{W_{\Delta p}}{\Delta p} = \left[\left(\frac{0.498 Pa}{\Delta p}\right)^2\right]^{1/2} = \frac{0.498 Pa}{\Delta p}$$

b.   *Friction Factor Uncertainty*

(1)   Laminar

$$\frac{W_f}{f} = \left[\left(\frac{W_{\Delta p}}{\Delta p}\right)^2 + \left(\frac{W_{Dh}}{D_h}\right)^2 + \left(\frac{W_r}{r}\right)^2 + \left(\frac{W_L}{L}\right)^2 + \frac{W_{\bar{U}}}{\bar{U}}\right]^{1/2} =$$

$$\left[\left(\frac{0.498 Pa}{\Delta p}\right)^2 + (0.018)^2 + (0.0016)^2 + (0.006)^2 + (0.018)^2\right]^{1/2}$$

$$= 0.0628 - 3.984$$

- The uncertainty for friction factor in the laminar range can be from 6.28% at the high end to 398.4% at the low end of the laminar range.

(2)   Turbulent

$$\frac{W_f}{f} = \left[\left(\frac{W_{\Delta p}}{\Delta p}\right)^2 + \left(\frac{W_{Dh}}{D_h}\right)^2 + \left(\frac{W_r}{r}\right)^2 + \left(\frac{W_L}{L}\right)^2 + \frac{W_{\bar{U}}}{\bar{U}}\right]^{1/2} =$$

$$\left[\left(\frac{0.498 Pa}{\Delta p}\right)^2 + (0.018)^2 + (0.0016)^2 + (0.051)^2 + (0.018)^2\right]^{1/2}$$

$$= 0.057$$

- The uncertainty for friction factor in the turbulent range is 5.7%.

THIS PAGE INTENTIONALLY LEFT BLANK

APPENDIX E

A.   EQUIPMENT LIST

1) Omega differential pressure transducer, model PX653-25D5V

2) Omega turbine flow meter, model FTB-940

3) Omega 0-5 VDC transmitter for FTB-940, model FLSC-61

4) Omega mass flow meter, model FMA-1844 with attached LCD display

5) Pentium III IBM compatible computer with Microsoft Windows 2000 based operating system

6) PC to HP 3852A interface card

7) Hewlett Packard 3852A data acquisition unit

8) HP3852A control modules

9) G Relay board and Relays by Grayhill; 24 channel rack, # 70GRCQ24 and G5 Modules, #70G-OAC5

10) HP interface ribbon cable for relay board

11) SOLA Electric 120VAC constant voltage power supply, model LR 44590

12) Brand Electric power meter

13) Bush Samos 10 hp, 388 cfm regenerative blower, model FBC3388.6

14) The Merriam Instrument Company 0-4" inclined manometer, model 40HA10

15) The Merriam Instrument Company 0-50" vertical manometer, model M-103

16) National Instruments LabVIEW software

17) Omega precision Type E fine wire thermocouples

18) Watlow 120 VAC 50 Watt heaters, part number 0241C-14

19) Digital power meter by Brand Electronics, Model 20-1850/CI

20) Omegabond highly conductive epoxy adhesive, OB-101-1/2

21) 6061 T6 aluminum metal for plates and pin construction

22) Plexiglass ducting

23) PVC piping and transition pieces (0.5" to 2.5")

24) Stainless steel piping and fittings (0.5")

25) 3/16 inch non-fluted wooden dowel

THIS PAGE INTENTIONALLY LEFT BLANK

APPENDIX F

A.   EQUIPMENT SPECIFICATIONS AND CALIBRATION DATA

1. Blower

The Busch Samos Regenerative Blower was a model FBC 3388.6 and is shown in figure (101). The normal operating parameters are 450 VAC, 10 amps, and 0 hp with a max capacity of 388 CFM. Figure (102) shows the pump curve used for this research.

Figure 101.   Typical Samos regenerative blower
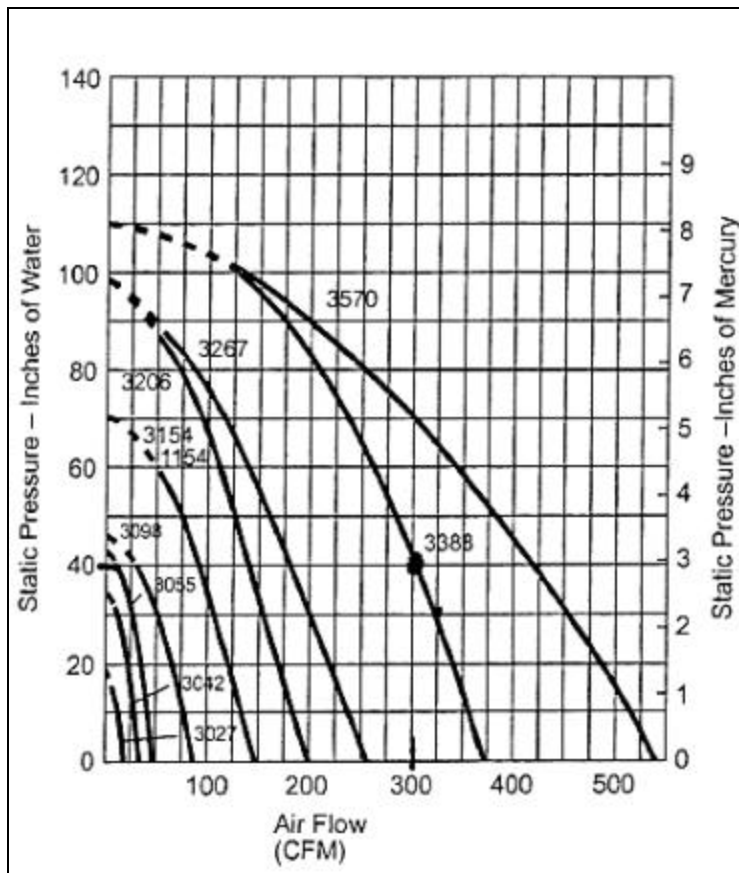
Figure 102.   Blower pump curve, manufacturer data

2. Mass Flow meter: Omega FTB-940

The normal range of operation is 25 - 450 ACFM. As seen in figure (103) the FLSC-61 attaches to the turbine meter to convert a frequency to VDC output that is sent to LabVIEW.

Figure 103.   Typical turbine mass flow meter with attached transmitter.

The calibration data shown in tables (5) and (6) were provided the manufacturer, Omega Engineering.   The calibration was verified locally using an air velocity transducer. The results were exact to that of Omega Engineering.

Table 5.   Manufacturer calibration data for flow meter –Volumetric flow rate to frequency

Calibration Data			Conversions	
Pulses/sec	K [pulses/acf]	Q [acf/sec]	Q [acf/min]	Q[m^3/s]
1027.4236	131.52994	7.811328736	468.6797242	0.221192198
917.7682	131.53099	6.977581481	418.6548889	0.197583104
812.3649	132.46224	6.132803582	367.9682149	0.173661658
695.9073	131.84075	5.278393061	316.7035837	0.149467447
592.1823	132.14931	4.481160742	268.8696445	0.126892341
480.793	132.77132	3.621211268	217.2726761	0.102541284
374.4457	132.45919	2.826875961	169.6125576	0.080048213
268.4616	132.45945	2.026745544	121.6047326	0.057391043
159.7085	131.52611	1.214272208	72.85633248	0.03438436
46.8041	131.20926	0.356713391	21.40280343	0.010100998

Table 6.   Manufacturer calibration data for flow meter – Frequency to VDC output

Calibration Data	
Input Frequency	Output Voltage [VDC]
0	0
237.5	2.532
475	5.03
712.5	7.53
950	10

With the data provided from tables (5) and (6), curves were created using excel to convert DC output to a volumetric flow rate. The relationships were linear and the slopes are displayed in figures (104) and (105).
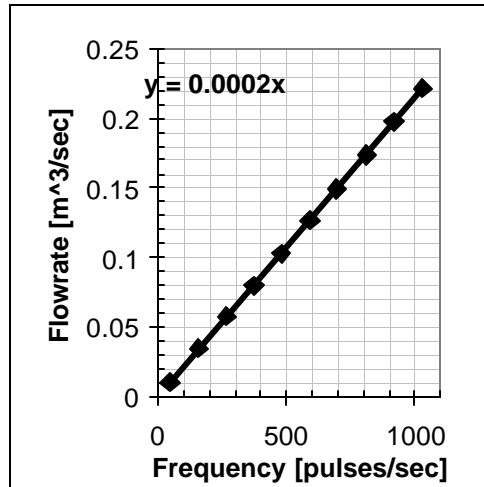
Figure 104.   Linear fit to flow meter calibration data
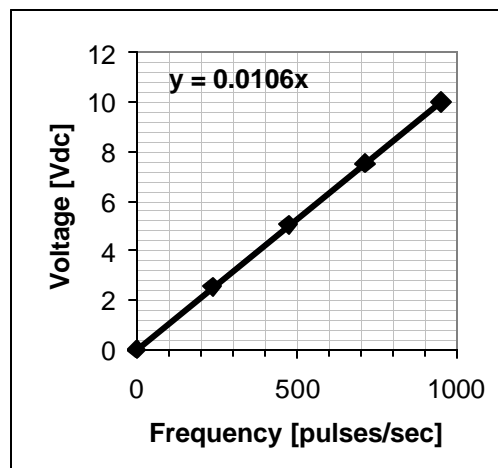
Figure 105.   Linear fit to transmitter calibration data

3. Mass Flow Meter: Omega FMA-1844

The normal range of operation is 0 – 500 SLPM or 0 – 17.657 SCFM. The meter operated on a 12 VDC power supply and is accurate to 1.5 percent of full scale. Data was read directly off of the LCD display mounted on the flow meter (figure 106). Omega Engineering performed the initial calibration. The calibration was verified locally using an inline pitot/static tube arrangement.

Figure 106.   Typical Omega FMA-1800 series flow meter with LCD display

4. Differential Pressure Transmitter: Omega PX653-25D5V

The differential pressure transducer shown in figure (107) operates on a 24 VDC power supply and has an accuracy of 0.25 percent full scale. Omega Engineering performed the initial calibration and for redundancy purposes it was performed locally using an inclined manometer. Figure (108) shows the relationship between differential pressure measured (inches of water) and the differential pressure transducer output (VDC).

Figure 107.   Omega PX653-25D5V differential pressure transducer
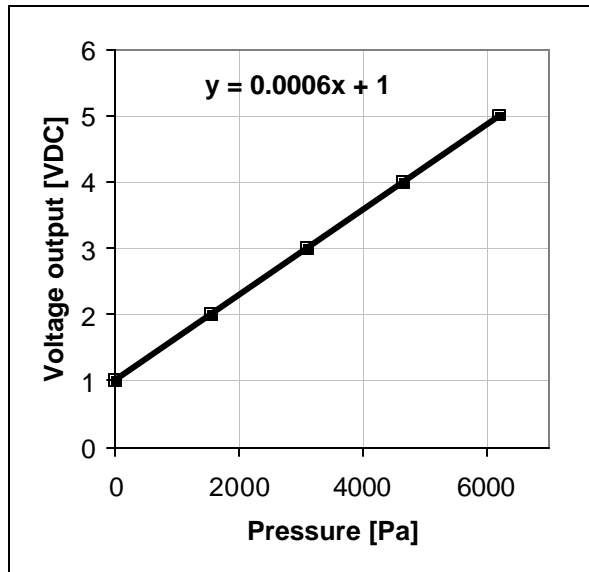
Figure 108.   Plot of calibration data for differential pressure transducer

5. Thermocouples, Heaters, and digital power meter

There were a total of 20 heaters used for the CHE. Watlow was the manufacturer for each 50-watt heater. Each heater was calibrated separately and then as a unit against a power meter made by Brand Electronics. The power meter (figure 109) monitored the power supply to the heater assembly and showed that each heater actually did use 50 watts of power and when all were energized then 1000 watts were consumed.

Figure 109.   Digital power meter by Brand Electronics

The most efficient way to measure the accuracy of the thermocouple, heaters (figure 110), and relays was to gather the empirical data of various sub-runs and calculate the heat rate based on mass flow rate, specific heat capacity, and differential temperature across the heat exchanger. The heat rate (watts) measured should equal the heat rate

measured by the digital power meter. In order to compare the two numbers a no-flow sub-run was performed to determine the losses to ambient. Once the losses were determined then the no-flow number was subtracted from the power meter and compared
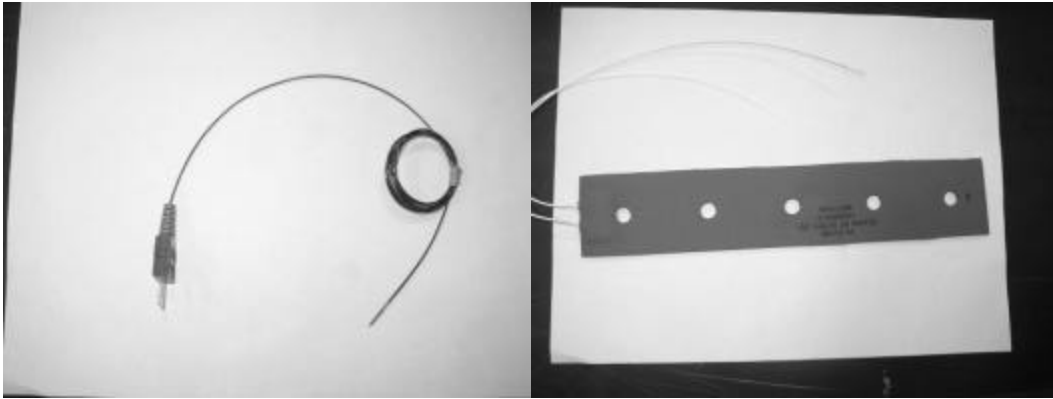
Figure 110. Omega type E thermocouple (left) and Watlow 50-watt heater (Right)

to the calculated heat rate. A third way of measuring heat rate was analyzing how long each heater was on for each sub-run. LabVIEW records which heaters are on and for how long. By multiplying the average time each heater was on by the number of times each heater was on for a given sub-run, then dividing by the length of the sub-run (seconds), the heat rate could be determined. On the vast majority all three methods agreed within ten percent, which was acceptable. Table (7) shows results from a data run using 33-mm pins in configuration set number one. The agreement gives confidence to the overall system performance as well as the heat transfer characteristics derived.

Table 7. Comparison of heat rate from three methods for 33 mm pins, set #1

Ch. 20 Tin K	Ch. 21-24 Tout Average K	Cp j/kg-K	$\dot{m}$ kg/sec	Calc Heat rate net watts	Heat rate 0 Flow electric watts	Total Calc Heat rate watts	Heat rate electric watts	Heat rate Power Meter watts
						#1	#2	#3
296.7443	303.7609	1005	0.000487	3.431907	42.41426	45.846167	45.87461	45.86
297.6849	305.5696	1005	0.001461	11.57774	42.41426	53.992	53.86861	53.81
297.6765	306.6153	1005	0.00241	21.6494	42.41426	64.06366	64.85279	64.80
297.6546	306.6604	1005	0.003382	30.60838	42.41426	73.02264	73.95968	74.01
297.42	306.5361	1005	0.004289	39.29537	42.41426	81.70963	82.8927	82.92
297.2251	306.3094	1005	0.005324	48.60875	42.41426	101.02301	94.42176	94.39

LIST OF REFERENCES

Adametz, D.S., *Numerical Analysis of Heat Exchanger Performance for a Staggered Short Pin-Fin Array*, Naval Postgraduate School, Monterey, California, 2001.

Al Dabagh, A. M., and Andrews, G.E., "Pin-Fin Heat Transfer: Contributions of the Wall and the Pin to the Overall Heat Transfer," ASME Paper No. 92-GT-242, 1992.

Arora, S.C., and Abdel-Messeh, W., Pressure Drop and Heat Transfer Characteristics of Circular and Oblong Low Aspect Ratio Pin Fins, AGARD Conference Proceedings, pp.4-1-4-15, 1985.

Avallone, E. A. and Baumeister III, T., editors, *Marks' Standard Handbook for Mechanical Engineers*, McGraw-Hill, Inc., 10th Ed., 1996.

Boulares, J., *Numerical And Experimental Study Of The Performance Of A Drop-Shaped Pin Fin Heat Exchanger*, Naval Postgraduate School, Monterey, California, 2003.

Chen, Z., Li, Q., Meier, D., and Warnecke, H.J., "Convective heat transfer and pressure loss in rectangular ducts with drop-shaped pin fins," *Heat and Mass transfer*, Vol. 33, pp. 219 - 224, 1997.

Chyu, M.K., "Heat Transfer and Pressure Drop for Short Pin-Fin Arrays with Pin-Endwall Fillet," ASME *J. of Heat Transfer*, Vol. 112, pp. 926-932, 1990.

Chyu, M.K., Hsing, Y.C., Shih, T. I.-P., and Natarajan, V., "Heat Transfer Contributions of Pins and Endwall in Pin-Fin Arrays: Effects of Thermal Boundary Condition Modeling," *ASME J. of Turbomachinery*, Vol. 121, pp. 257-263, 1998.

Chyu, M. K., *Effects of Perpendicular Flow Entry on Convective Heat/Mass Transfer from Pin-Fin Arrays*, ASME Journal of Heat Transfer, Vol. 121, 1999, pp. 668-674.

Donahoo, E.E., Camci, C., Kulkarni, A.K., and Belegundu, A.D., "Determination of Optimal Row Spacing for a Staggered Cross-Pin Array in a Turbine Blade Cooling Passage," *Enhanced Heat Transfer*, Vol. 8, pp. 41-53, 2001.

Hamilton, L.J., *Numerical Analysis of the Performance of a Staggered Cross-Pin Array Heat exchanger*, Naval Postgraduate School, Monterey, California, 2003.

Han, J.C., Dutta, S., and Ekkad, S., *Gas Turbine Heat Transfer and Cooling Technology*, Taylor and Francis, 2000.

Holman, J. P., *Experimental Methods For Engineers*, McGraw-Hill, Inc., 6th Ed., 1994.

Incropera, F.P. and DeWitt, D.P., *Introduction to Heat Transfer*, 3rd Ed., Wiley, New York, 1996.

Jubran, B.A., Hamdan, M.A., Abdualh, R.M., "Enhanced Heat Transfer, Missing Pin, and Optimization for Cylindrical Pin Fin Arrays", ASME *J. of Heat Transfer*, Vol. 115, pp. 576-583, 1993.

Kays, W. M. and London, A. L., *Compact Heat Exchangers*, McGraw-Hill, Inc., 3rd Ed., 1984.

Kline, S.J. and McClintock, F.A., "Describing Uncertainties in Single Sample Experiments," *Mechanical Engineering*, Vol. 75, pp. 3 - 8, 1953.

Li, Q., Chen, Z., Flechtner, U., Warnecke, H.-J., "Heat Transfer and Pressure Drop Characteristics in Rectangular Channels with Elliptic Pin Fins," *Int. J. of Heat and Fluid Flow*, Vol 19, pp. 245-250, 1998.

Metzger, D.E., *Developing Heat Transfer in Rectangular Ducts With Staggered Arrays of Short Pin Fins*, ASME Journal of Heat Transfer, Vol. 104, 1982, pp. 700-706.

Metzger, D.E., Berry, R.A., Bronson, J.P., "Developing Heat Transfer in Rectangular Ducts With Staggered Arrays of Short Pin Fins", ASME *J. of Heat Transfer*, Vol. 104, pp. 700-706, 1982.

Metzger, D.E., Fan, C.S., and Haley, S. W., "Effects of Pin Shape and Array Orientation on Heat Transfer and Pressure Loss in Pin Fin Arrays," *ASME J. of Engineering for Gas Turbines and Power*, Vol. 106, pp. 252-257, 1984.

Ramthun, D., *An Experimental Study of a Pin-Fin Heat Exchanger, Naval Postgraduate School, Monterey*, California, 2003.

Shah, R. K., *Progress in the Numerical Analysis of Compact Heat Exchanger Surfaces*, Advances in Heat Transfer, Vol. 34, Academic Press, 2001, pp. 363-443.

Sparrow, E.M., Stahl, T.J., and Traub, P., "Heat Transfer Adjacent to the attached end of a Cylinder in Crossflow," *Int. J. of Heat and Mass Transfer*, Vol. 25, pp. 233-242, 1984

Van Fossen, G.J., "Heat Transfer Coefficient for Staggered Arrays of Short Pin Fins," ASME *J. of Engineering for Power*, Vol. 104, pp. 268-274, 1982.

Weills, N. D. and Ryder, E. A., *Thermal Resistance Measurements of Joints Formed Between Stationary Metal Surfaces*, Transactions of the ASME, April 1949, pp. 259-267.

White, F. M., *Fluid Mechanics*, McGraw-Hill, Inc., 4th Ed., 1999.

INITIAL DISTRIBUTION LIST

1. Defense Technical Information Center
   Ft. Belvoir, Virginia

2. Dudley Knox Library
   Naval Postgraduate School
   Monterey, California

3. Professor Ashok Gopinath
   Naval Postgraduate School
   Monterey, California

4. LT Jeffrey W. Summers
   Naval Postgraduate School
   Monterey, California